PAUL SCHERRER INSTITUT

PSI

u^b

UNIVERSITÄT BERN

LABOR FÜR RADIO- UND UMWELTCHEMIE
DER UNIVERSITÄT BERN UND
DES PAUL SCHERRER INSTITUTS

$$\sigma \ {}^{60}Fe(n,\gamma){}^{61}Fe$$

Annual Report 2007

January 2008

Cover page

First measurement of the neutron capture cross section of ^{60}Fe at stellar neutron energies in 2007 at the Karlsruhe Van de Graaff accelerator (FZK, Germany)
This nuclear reaction plays a key role in tracing the history of the early Solar System. ^{60}Fe (together with ^{107}Pd, ^{41}Ca, ^{36}Cl, ^{26}Al, and ^{10}Be) must be considered as a late addition to the protosolar nebula. Whether this material stems from a supernova or a nearby asymptotic giant branch (AGB) star is still an open question. The measurement became possible because - for preparing the target - 6 μg of the extremely rare isotope ^{60}Fe could be separated from a copper beam dump of the PSI accelerator facilities (see contribution on page 46).
The background picture shows the remnant of the Supernovae explosion in 1604, known as "Keplers Star". The right picture describes the location of this Supernova (in the foot of Ophiuchus, marked with an *N*) in Johannes Keplers book *De Stella nova in pede Serpentarii* (*On the New Star in Ophiuchus's Foot*) (1604). The photo in the lower left shows a part of the copper beam dump.

TABLE OF CONTENTS

Analytical Chemistry

Radwaste Analytics

Proton Irradiation Facility

Radiochemistry Universität Bern

EDITORIAL

The previous year was full of partly unexpected changes. The PSI director was elected president of ETH Zürich which left our institute since September 2007 in a transition state with Martin Jermann filling currently the position of a director *ad interim*. At the same time I did step back from the position of a deputy director. These changes, fortunately, were of no impact concerning the decision on a continuation of a joint laboratory on Radiochemistry and Environmental Chemistry between Bern University and PSI after my retirement in summer 2009. The contract was signed in early summer by the rector of Bern University and the PSI director.

Based on this contract, the position of a new head of the laboratory being also full professor at the Department of Chemistry and Biochemistry at Bern University was announced in the press. Candidates are currently being valuated by a joint commission including members from PSI, Bern University and representatives from the Universities of Fribourg and Neuchatel, respectively.

During the last summer an unprecedented high number of six students were visiting our laboratory for two to four month in order to participate in our research. These summer practical courses have meanwhile been accepted at Bern University as part of the Master Courses in Chemistry with allocated ECTS points (two per month).

The participation of members of our laboratory in teaching duties at Bern University increased again. Currently five persons are involved in education at the Bachelor or the Master level. In addition, the Laboratory Course on Radiochemistry - part of the Master program - benefited from the support of Max Doebeli from ETH Zürich (introduction to nuclear analytics with proton beams) and Jürg Jourdan from Basel University (introduction to neutron activation analysis). These external courses were much appreciated by the students.

It is with great pleasure to announce that the topic *chemistry in liquid metal targets* (e.g. for the project MEGAPIE) became a fully supported R&D task of our radiochemistry laboratory. As a consequence, the assigned permanent position could be filled by Jörg Neuhausen, a specialist in the field.

The prominent event of the year was the Third International Conference on Transactinides TAN'07 from 23–28 Sept. in Davos. This conference was attended by roughly 100 participants from all over the world. In a pre-conference session, Darleane C. Hoffman from Berkeley presented an address honoring the seminal scientific contributions of Hans Rudolf von Gunten to the field of heavy element sciences.

Two social events (snowshoeing and visit of the Schnidejoch) offered excellent opportunities for mutual discussions in a relaxed atmosphere, though some of the students were challenged by the alpine environment around the Schnidejoch!

Heinz W. Gäggeler

I. ADSORPTION PROPERTIES OF ELEMENT 112 ON GOLD

*R. Eichler, H. W. Gäggeler, F. Haenssler, A. A. Serov (Univ. Bern & PSI), R. Dressler, A. Laube, D. Piguet,
P. Rasmussen (PSI), N. V. Aksenov, A. V. Belozerov, G. A. Bozhikov, V. I. Chepigin, S. N. Dmitriev, A. V. Gorshkov,
M. G. Itkis, V. Ya. Lebedev, O. N. Malyshev, Yu. Ts. Oganessian, O. V. Petrushkin, A. G. Popeko, S. V. Shishkin,
A. V. Shutov, A. I. Svirikhin, E. E. Tereshatov, G. K. Vostokin, A.V. Yeremin (FLNR), M. Wegrzecki (ITE)*

*The production of $^{283}112$ in the nuclear fusion reaction of ^{48}Ca with Pu-242 was confirmed and the adsorption
properties of element 112 on gold surfaces were validated in an additional experiment series.*

First unambiguous experimental results from chemical investigations of element 112 were obtained in 2006 at FLNR, Dubna, Russia [1]. $^{283}112$ was produced indirectly in the nuclear fusion reaction:

^{242}Pu$(^{48}$Ca,3n$)^{287}114(T_{1/2}$=0.48 s,E_α=10.02 MeV)$\rightarrow$ $^{283}112$.

It decays with a half-life of about 3.8 s by alpha-particle emission (E_α=9.54 MeV) to ^{279}Ds, that undergoes spontane-ous-fission (SF) decay with a half-life of 200 ms [2]. These decay properties of the isotope $^{283}112$ were confirmed using the same nuclear reaction in 2007 with SHIP separator at the GSI Darmstadt, Germany [3]. The chemical setup applied in the experiments was based on the thermochroma-tographic In situ Volatilization and On-line detection technique (IVO) in combination with the Cryo-On-Line Detector (COLD) (for experimental details see [1]). Two atoms of $^{283}112$ were detected during this experiment (Fig. 1, chain 1 and 2). The observed thermochromatographic deposition pattern for ^{185}Hg, ^{219}Rn, and $^{283}112$ at varied experimental conditions are depicted in Figure 2, panels a) and b). The two observed atoms of element 112 revealed evidence for a high volatility and a metallic character in its adsorption interaction with the stationary gold surface comparable to its lighter homologue Hg [1].
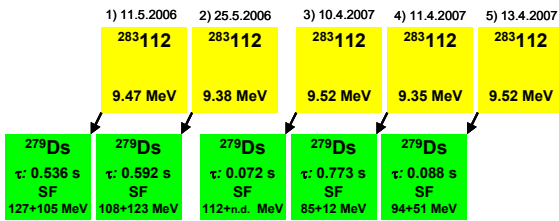
Fig.1: Detected decay chains assigned to the isotope $^{283}112$.

In a second experiment series in 2007 [4] we were able to increase the overall efficiency by almost a factor 3 by shortening the transport time and by increasing the transmission of the target grid. The faster carrier gas flow broadened significantly the chromatographic depositions of ^{185}Hg and ^{119}Rn (Fig. 2, panel c) and transported the three detected atoms of $^{283}112$ (Fig. 1, chains 3-5) further down to lower temperatures. Two of them deposited on the detectors 11 (chain 3, −21°C) and 14 (chain 5, −39°C). The third atom was even deposited on the detector 26 (chain 4, −124°C).

From the dew point measurements in the carrier gas we conclude that overall four atoms of element 112 clearly adsorbed on the gold surface and one atom of element 112 deposited on ice. The expected number of randomly correlated decay chains of the observed type $\alpha_{9.5\pm0.2\ MeV}$ SF$_{E>50MeV}$ during the entire experiment was calculated as 0.05. A Monte-Carlo based microscopic kinetic model of gas chromatography [5] was applied to evaluate the most

probable standard adsorption enthalpy on gold surfaces $(-\Delta H_{ads}{}^{Au})$ from the chromatographic depositions: ^{185}Hg (grey dashed lines): $\Delta H_{ads}{}^{Au}(Hg)$>65 kJ/mol; ^{219}Rn (grey solid lines): $-\Delta H_{ads}{}^{ice}(Rn)$=19±2 kJ/mol; $^{283}112$ (red lines): $-\Delta H_{ads}{}^{Au}(112)$=52$^{+4}_{-3}$ kJ/mol. The error bars represent 68% c.i. Our observation bolsters the discovery of elements 114 and 116 in ^{48}Ca induced nuclear fusion reactions with ^{242}Pu and ^{248}Cm targets at FLNR Dubna [2]. For chemical implications see part II of this report [6].
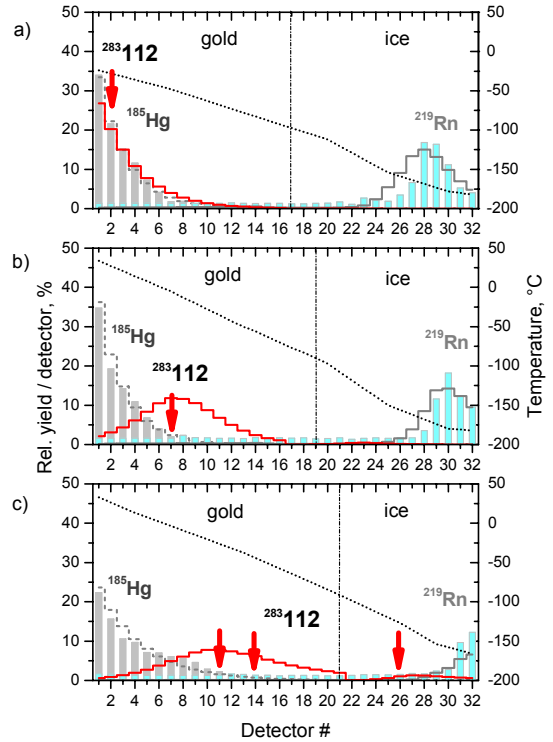
Fig. 2: Deposition patterns ^{185}Hg, ^{219}Rn, and $^{283}112$ in the COLD dependent on experimental parameters. ^{185}Hg (grey bars), ^{219}Rn (cyan bars) and $^{283}112$ (red arrows); Experimental parameters: a) gas flow 860 ml/min, temperature gradient from -24°C to -184°C (black dashed line, right hand axis); b) gas flow 890 ml/min, temperature gradient from 35°C to -180°C; c) gas flow 1500 ml/min, temperature gradient from 32°C to -164°C. The beginning ice coverage of the detectors at -95°C is indicated by vertical dash-dotted line.

REFERENCES

[1] R. Eichler et al. Nature, **83,** 487 (2007).
[2] Y. T. Oganessian et al., Phys. Rev. C **70,** 64609 (2004).
[3] S. Hofmann et al., Eur. Phys. J. A **32,** 251 (2007).
[4] R. Eichler et al., Angew. Chem. (2007) accepted.
[5] I. Zvara, Radiochim. Acta **38,** 95 (1985).
[6] R. Eichler et al., see this report Part II, p. 4.

II. CHEMICAL PROPERTIES OF ELEMENT 112

R. Eichler, H. W. Gäggeler, F. Haenssler, A. A. Serov (Univ. Bern & PSI), R. Dressler, A. Laube, D. Piguet,
P. Rasmussen (PSI), N. V. Aksenov, A. V. Belozerov, G. A. Bozhikov, V. I. Chepigin, S. N. Dmitriev, A. V. Gorshkov,
M. G. Itkis, V. Ya. Lebedev, O. N. Malyshev, Yu. Ts. Oganessian, O. V. Petrushkin, A. G. Popeko, S. V. Shishkin,
A. V. Shutov, A. I. Svirikhin, E. E. Tereshatov, G. K. Vostokin, A.V. Yeremin (FLNR), M. Wegrzecki (ITE)

The experimentally determined adsorption enthalpy of element 112 on gold is used to assess macroscopic thermodynamic and physical data related to the volatility of element 112.

Element 112, a representative of group 12 of the periodic table has a predicted closed-shell electronic ground state configuration $[Rn]5f^{14}6d^{10}7s^2$, rendering this element one of the key elements regarding relativistic effects in the electronic structure [1-3]. For element 112 a noble metallic character was predicted from empirical extrapolations [4,5]. Atomic Dirac–Fock calculations revealed a contraction of the spherical 7s orbitals leading for element 112 to the prediction of an enhanced stability of the elemental atomic state. Accordingly, a noble-gas like behavior was postulated [6]. Modern calculation methods confirmed a stronger binding of the 7s orbitals. However, the spin-orbit coupling of the 6d orbitals is predicted to lead to an electronic ground state configuration with the $6d^{5/2}$ orbital in close energetic and spatial vicinity to the 7s orbital, rendering element 112 to be a noble transition metal [7,8] or even a semiconductor [9]. The energy content of the adsorption bond between element 112 and a metallic stationary phase, the standard adsorption enthalpy at zero surface coverage (ΔH_{ads}^{Au}) differentiates between metal bond formation or weak van der Waals physisorption interaction. The semi-empirical macroscopic adsorption model based on the Miedema approach predicts in comparison to Hg a weaker metallic interaction of element 112 with gold [5]. Relativistic calculations employing the interaction of atomic element 112 with gold clusters also point to a metallic interaction [8]. An adhesion model for noble gases on metals was extended to estimate the physisorption interaction of a noble-gas like element 112 with gold [9].

From the thermochromatographic deposition behavior of 5 atoms of element 112 its adsorption enthalpy on gold was determined as $-H_{ads}^{Au}(112)=52^{+4}_{-3}$ kJ/mol (68% c.i.) [10,11]. This adsorption enthalpy reveals a significantly weaker metallic bond character involved in the adsorption interaction between element 112 and gold compared to Hg. However, if compared to the predicted adsorption enthalpy using a physisorption model [12] the observation clearly distinguishes element 112 from the noble gases. The calculations of the 112-Au interaction potential using density functional methods [8] and the macroscopic semi-empirical Eichler-Miedema adsorption model [5] predict a metallic bond character, but seem to overestimate the energetic content of this metallic adsorption bond. However, element 112 is chemically not as inert as a noble gas as suggested by Pitzer in 1976 [6].

An empirical link between single atomic property ΔH_{ads}^{Au} ΔH_{ads} and the volatility of macroscopic amounts of an element determined by the standard sublimation enthalpy (ΔH_{subl}) was established [13] (equation 1).

$$-\Delta H_{ads}^{Au} = (1.08\pm0.05)\cdot\Delta H_{subl}+(10.3\pm6.4),\ kJ/mol \qquad (1)$$

Using this correlation the standard sublimation enthalpy of element 112 of $\Delta H_{subl}(112)=38^{+10}_{-12}$ kJ/mol can be estimated, which is in excellent agreement with predictions from [5]. Moreover, applying the estimated value for the sublimation entropy $\Delta S_{subl} = 106.5\pm2.0$ J/molK [5] element 112 can be presumed to have a boiling point of 357^{+112}_{-108} K. These values indicate that element 112 is considerably more volatile compared to its lighter homologues Zn, Cd, and Hg (see Figure 1) manifesting the preserved trend of increasing stabilization of the elemental atomic state due to relativistic effects in the electronic structure along group 12 of the periodic table up to element 112.
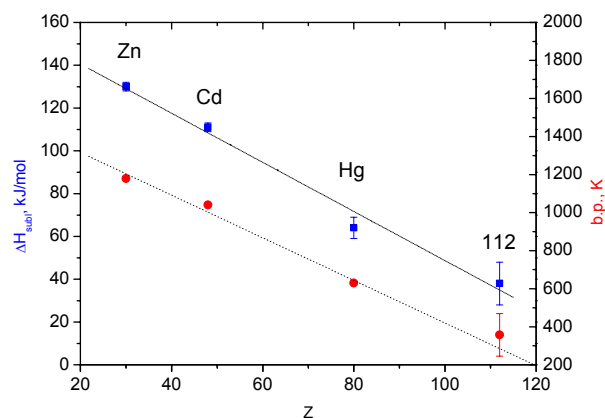
Fig. 1: Trends of volatility for group 12 elements of the periodic table. The standard sublimation enthalpy (ΔH_{subl}) (blue squares, left hand axis) and the boiling points b.p. of the elements (red circles, right-hand axis) are taken as a measure for elemental volatility. Data for Zn, Cd, and Hg are taken from [14].

REFERENCES

[1] P. Pyykkö, J.-P. Desclaux, Acc. Chem. Res. **12,** 276 (1979).
[2] B. Fricke, in Structure and Bonding, Vol. 21, Springer, Heidelberg, 1975, pp.89.
[3] P. Schwerdtfeger, M. Seth, in Encyclopedia of computational chemistry, Vol. 4, (Ed.: P. von Ragué Schleyer), Wiley, New York, 1998, pp. 2480.
[4] B. Eichler, Kernenergie, **19,** 307 (1976).
[5] B. Eichler, PSI Reports 00-09 and 03-01, ISSN 1019-0643.
[6] K.S. Pitzer, J. Chem. Phys. **63,** 1032 (1976).
[7] M. Seth et al., J. Chem. Phys. **106,** 3623 (1997).
[8] V. Pershina, T. Bastug, Chem. Phys. **311,** 139 (2005).
[9] N. Gaston et al. Angew. Chem. Int. Ed. **46,** 1663 (2007).
[10] R. Eichler et al., see this report Part I, p. 3.
[11] R. Eichler et al., Angew. Chem. (2007) accepted.
[12] R. Eichler et al. J. Phys. Chem. **B106,** 5413 (2002).
[13] R. Eichler, Radiochim. Acta **93,** 245 (2005).
[14] CRC Handbook of Chemistry and Physics, (Eds.: D. R. Lide), 87. ed. CRC Press, Boca Raton, 2006.

pureCOLD - STATUS

R. Dressler, P. Rasmussen (PSI), R. Eichler (Univ. Bern & PSI)

A status report on the development of fast pile-up rejection electronics for the COLD detector is given.

The unambiguous identification of isotopes of the heaviest elements is a very important prerequisite for the investigation of the chemical properties of these elements. The recording of consecutive decays of the investigated isotope as well as its descendents gives the highest possible confidence of assigning an observed event to the isotope of interest. However, the occurrence of unwanted by-products in the used nuclear reactions can lead to a large number of background events in energy regions where the decay of the investigated isotope or its daughter nuclei is expected. Especially the decay of ^{212}Bi and ^{212}Po can disturb the measurement due to the consecutive emission of high energetic β- and α-particles with a sum energy of more than 11 MeV within a very short time period of typically less then 1 ms. Conventional nuclear spectroscopy electronics is not able to resolve in time the consecutive hits of the β- and α-particle, which leads to a so called pile-up pulse height amplification.

A new detection electronic system was designed to distinguish pile-up signals from real α-events with energies higher than 8.9 MeV. We present here the results so far obtained with a prototype of such electronics using a 100 mm^2 PIN diode with an ^{232}U activity on a surface of the detector.

The discrimination of pile-up signals is based on the sampling of the leading edge of the fast amplifier signal using eight consecutive thresholds. The time stamps of passing through these thresholds are recorded with a resolution of 0.5 ns (see Fig. 1 for typical pile-up signals). In the case of a preceding β-particle the time difference between at least two of these time stamps exceeds 10 ns. This results in a clear separation of the pile-up events from pure α-events in a time versus energy plot as depicted in Fig. 2.
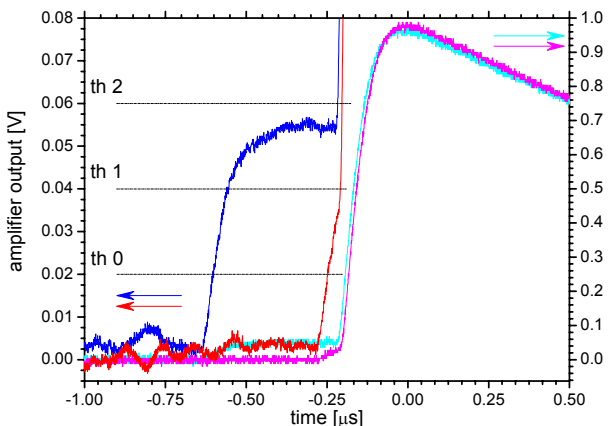
Fig. 1: Signal shapes of pile up events after timing amplifier (cyan/blue and magenta/red are identical events; blue, red – left hand axis; cyan, magenta – right hand axis; sampling rate 2.5 GHz;). The voltage of the first three thresholds is indicated, too.

The spectroscopic resolution of the prototype was determined to be 60 keV. In Fig. 3 an obtained α-spectrum to gether with a decomposition of the ^{212}Po peak into pure α-events and pile-up events is depicted.
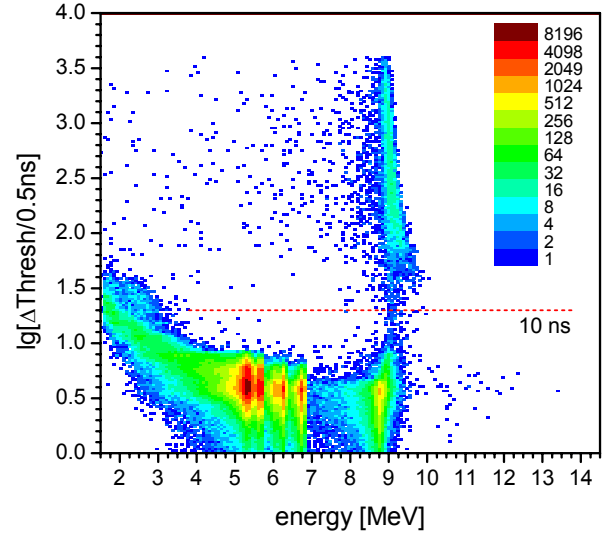
Fig. 2: Time difference between passing the first and second threshold versus α-particle energy. A gap from 4.5 ns to 20 ns separates the true α-events of ^{212}Po from the β-α pile-up events of the decay of ^{212}Bi and ^{212}Po.
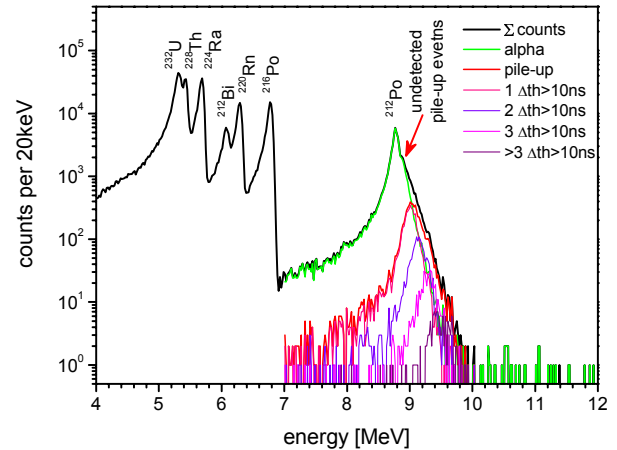
Fig. 3: α-spectra of ^{232}U and its descendents (black). True α-events within the ^{212}Po peak (green); all detected pile-up events (red); pile-up events with one, two, three, and more threshold passages (Δth) longer then 10ns (pink, violet, magenta, and purple). The red arrow indicates the position of so far undetected pile-up events above 8.785 MeV.

The system reaches promising pile-up separation factors in the energy region above 9.1 MeV. The work is ongoing to improve the separation also in the energy region between 8.8 and 9.0 MeV marked by the red arrow in Fig.3. Most important hardware construction areas are: 1) the signal-to-noise ratio; 2) the spectroscopic resolution; 3) the rise time of the leading edge of the signal. In the finalized system a thorough selection of the threshold levels is needed to reach best possible performance.

ISOTHERMAL VACUUM ADSORPTION CHROMATOGRAPHY (IVAC) FOR DETERMINATION OF CHEMICAL PROPERTIES OF SUPER HEAVY ELEMENTS

A. Serov, R. Eichler, H.W. Gäggeler (Univ. Bern & PSI), R. Dressler, D. Piguet (PSI)

Further developments towards isothermal vacuum adsorption chromatography are accomplished. A detector coverage absorbing IR- and visible light was evaluated.

INTRODUCTION

The discovery of isotopes of super heavy elements (SHE) with Z=112-118 in ^{48}Ca-induced nuclear fusion reactions with actinide targets at the Flerov Laboratory of Nuclear Reactions (FLNR) Dubna, Russia [1] paved the way for experiments aiming at the investigation of chemical properties of the SHE. The first experiments were based on the well-known Insitu-Volatilization and On-line detection setup (IVO) based on the gas thermochromatography method with the Cryo-On-Line Detector (COLD) [2], revealing a number of drawbacks: low spectroscopic resolution of detectors in gas atmosphere; limitation to temperature ranges between 35 and -180°C. The vacuum adsorption chromatographic method proposed here may help overcoming these drawbacks.

EXPERIMENTAL

For investigations of thermodynamic properties of less volatile SHE with short half-lives we designed an experimental set-up based upon the IVAC principle [3, 4].
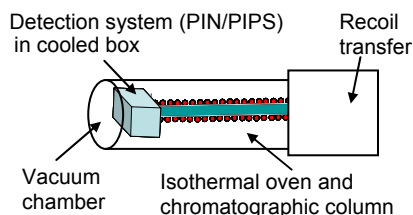
Fig. 1: Schematic view of IVAC

There are two important problems to be solved: A) Stopping of recoiling fusion reaction products and their transfer into vacuum; B) Design and construction of an appropriate detection system. We started the project working on a solution for problem B. It's well-known from experiments and literature that detectors, based on semiconductors can not be operated at elevated temperatures above 40°C. Another limitation is the sensitivity of semiconductor detectors to visible and also to infrared light. Hence, these detectors are not operational in the vicinity of elevated isothermal temperatures applicable in IVAC, because the chromatographic column heated up to temperatures >600°C emits a considerable amount of visible and infrared light. A possible solution could be a non-transparent coverage e.g. a thin metal layer. Therefore, we did a screening for possible materials and tested different layer thicknesses. Metals with relatively low Z, e.g. Al, Mg, Mn, Zn, Cu, and Ag were selected as possible materials for the protection of PIN diodes to keep the spectroscopic resolution reasonably. These metals were evaporated at vacuum conditions and deposited on the surface of the diodes. By controlling the temperature and

time of evaporation it was possible to reproducibly create coverages of the detectors by thin metal layers. For each metal the appropriate parameters were evaluated experimentally. Mg layers of 50-100 nm thickness turned out to protect the diodes best from VIS-IR irradiation. Hence, all further experiments were made with magnesium. The detector covered by Mg was placed 5 mm from the outlet of oven and was cooled from the back side by water (~10°C). The temperature of the oven was increased from room temperature up to 675°C. An ^{227}Ac source, from which ^{219}Rn emanates, was placed inside of the quartz tube. Online measurements of α–spectra were made at various isothermal temperatures of the chromatographic column.

RESULTS AND CONCLUSIONS

It was found that detectors covered by Mg can operate until an oven temperature T=625°C. The spectroscopic resolution of non-covered detectors was about 100 keV (Fig. 2), while covered show 120 keV [5]. Several diodes were successfully covered by Mg and ready for future investigations. However, the problem of low resolution of covered detectors should be solved by further optimizing the thickness of the Mg layers. Furthermore, the next steps of our project include the investigation of the IVAC behaviour at heavy ion beam irradiation conditions.
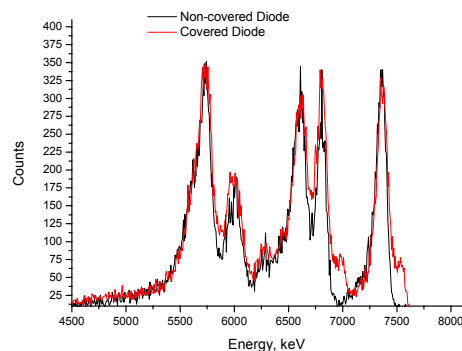
Fig. 2: Spectrum obtained from an ^{227}Ac source on non-covered and covered detectors at room temperature.

REFERENCES

[1] Yu. Ts. Oganessian et al., Phys. Rev. C **70**, 064609 (2004).
[2] R. Eichler et al., Nature **447**, 72-75 (2007).
[3] Qin Zhi et al., Ann. Rep. Labor Radio- & Umweltchemie, Univ. Bern & PSI (2003), p. 10.
[4] R. Eichler et al Ann. Rep. Labor Radio- & Umweltchemie, Univ. Bern & PSI (2005), p. 7.
[5] A. Serov et al., Abstract, TAN07, Davos (2007).

CHEMICAL INTERACTION OF [211]At WITH METALLIC SURFACES

A. Serov, R. Eichler, H.W. Gäggeler (Univ. Bern & PSI), R. Dressler, D, Piguet (PSI), B. Muther, D. Wittwer (Univ. Bern), N. V. Aksenov, G. A. Bozhikov, V. Ya. Lebedev, O. V. Petrushkin, S. V. Shishkin (FLNR), M. Wegrzecki (ITE)

The adsorption interaction of astatine on surface of Au, Ag, Pt, Pd, Ni, and Cu was investigated.

INTRODUCTION

The extension of the periodic table by the discovery of new elements in the Super Heavy Elements (SHE) region (see for review [1]) rose several questions about their chemical properties. Strong influence of relativistic effect is expected on the chemical behaviour of SHE. To prepare and design experiments with SHE, their lighter homologues have to be chemically investigated on a one-atom-at-a-time level. There are several methods available for those investigations comprising aqueous and gas-phase chemistry (see for review [2]). Recently, by using gas phase chemical methods, based on the well-known Insitu-Volatilization and On-line detection setup (IVO) with the Cryo-On-Line Detector (COLD), the chemical interaction of element 112 and its lighter homologue mercury with gold surface was investigated [3]. The present work aimed at the experimental determination of the standard adsorption enthalpy ($\Delta H_{ads.}$) of carrier-free [211]At on surfaces of Au, Ag, Pt, Pd, Ni, and Cu. This work represents a model study for the investigation of chemical properties for element 117.

EXPERIMENTAL

The schematic view of the experimental set-up is shown in figure 1. A target prepared by vacuum deposition of natural bismuth (~300 $\mu g/cm^2$) on a beryllium backing (12 μm) was irradiated by [40]Ar beam (energy 303 MeV, intensity 10 pnA). [211]At was produced in transfer reactions of the beam particles with the target material. [211]At was transferred through a Teflon capillary (length: 4 m, temperature: 70 ^0C) in a gas loop system with argon (flow rate 1-1.2 l/min) to the isothermal oven. The isothermal oven contained a steel tube with a quartz tube inlay. 20 cm of the middle section of the isothermal column was covered inside by a metal foil. Hence, a defined stationary metal phase was designed for chromatographic purposes. The isothermal temperature was adjustable between 1000°C and 25°C. A number of metal foils pre-treated (Ni, Cu. Ag in H_2 at 800°C followed by pure He at 800°C; Au, Pt, Pd heated up in He to 800°C) served in subsequent experiments as stationary phase to investigate their interaction with astatine. To measure the [211]At, able to pass the isothermal chromatography, the COLD was used with 4 pairs of PIN diodes, filling up of the other 28 empty detector positions with PTFE dummies.

RESULTS AND CONCLUSIONS

During this experiment chemical interaction of [211]At with different metal surfaces was investigated. The isothermal temperature was decreased from 600°C stepwise for each metal At each temperature the [211]At accumulation was measured during a ~1 h beam-on period. Subsequently the [211]At activity was measured in a ~15 min beam-off period again. Thus, the amount of [211]At passing the isothermal column was determined for each temperature. It was observed that trace amounts of oxygen present in the experimental set-up produced oxide layers on the surfaces of Pd, Ni, and Cu. Hence, a noticeable interaction of astatine with the metals was not observed. The introduction of 3-5% of hydrogen into the loop gas can be a possible solution of this problem in future experiments. The more inert Au, Ag, and Pt were stable against oxidation at experimental conditions. Due to accumulative grow-in and decay of the long-lived astatine in detectors during the experiment, the adsorption data evaluation is ongoing. However, the temperature intervals, where the retention starts, are clearly seen in the measured yield curves for [211]At (see Figure 2): Au:350-375°C; Ag: 325-350°C; Pt: 400-450°C.
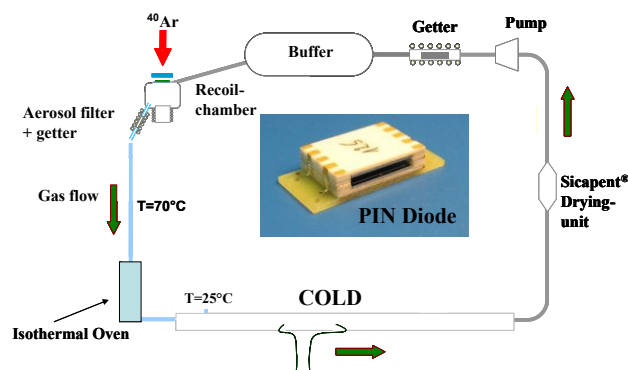
Fig.1: Experimental setup.
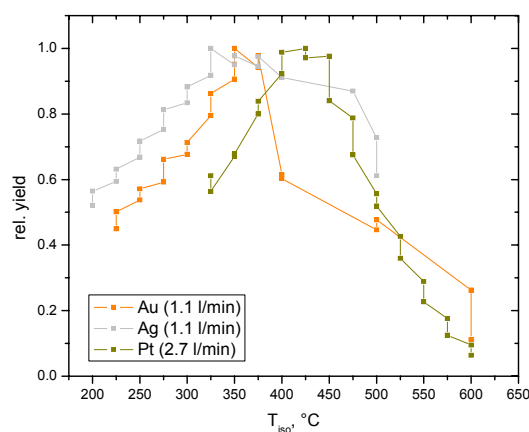
Fig. 2: The measured yield curves for [211]At with Au, Ag, and Pt. The gas flow is indicated. Each experiment was started at 600°C. As expected the activity increases for lower T_{iso} due to grow-in. At a certain temperature the retention of astatine on the chromatographic surface starts.

REFERENCES

[1] Yu. Ts. Oganessian et al., Phys. Rev. C **70**, 64609 (2004).

[2] Chemistry of Superheavy Elements. (ed. M. Schädel) Kluwer Academic Publishers, Dodrecht, 2003.

[3] R. Eichler et al., Nature **447**, 72 (2007).

PREPARATION OF CARRIER FREE $^{200\text{-}202}$Tl

D. Wittwer, B. Muther (Univ. Bern), S. Köchli, D. Piguet (PSI), R. Eichler (Univ. Bern & PSI)

A chemical separation was developed for carrier-free $^{200\text{-}202}$Tl from samples of PbO_2 /PbO irradiated with fast neutrons from the PSI-SINQ using the NAA rabbit system.

1   INTRODUCTION

The availability of carrier-free amounts of various elements of the 6-th row of the periodic table is crucial for performing model studies for the chemical investigation of the superheavy elements. Typically, the on-line preparation by heavy ion induced nuclear reactions using a heavy ion beam from a cyclotron is the method of choice. Here we present a method to prepare carrier free samples of Tl produced by the irradiation of PbO_2 and PbO with fast neutrons from SINQ using the PSI-NAA rabbit system. A Tl separation from PbO_2 was described already in [1,2]. There, no special measures have been undertaken to obtain carrier free amounts of the Tl isotopes.

2   EXPERIMENTAL

Samples of 1g of $^{nat}PbO_2$ p.a. (FLUKA) were heated up in various gas mixtures and in vacuum to temperatures of about 800°C using the setup depicted in Figure 1. After 3 h separation time the Tl content was measured in the remaining Pb sample and in the catcher material behind the oven by ICP-OES (see Table 1).
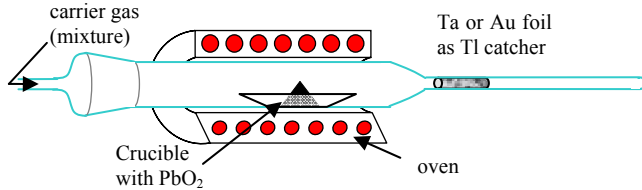
Fig. 1: Schematic setup used for the Tl separation

Table 1: Results of the ICP-OES analyses

Experimental	PbO_2	Catcher		
	Tl (µg/g)	Pb (µg/g)	Tl (µg/g)	Ratio Tl/Pb
He/Ta $_{crucible}$	<0.2	0.38	4.25	11.184
He/Ta $_{crucible}$	<0.2	0.65	3.64	5.600
He/Fe $_{crucible}$	<0.2	1.16	6.90	5.948
He/O_2/Fe $_{crucible}$	<0.2	0.51	9.28	18.196
He/O_2/H_2O/Fe $_{crucible}$	0.26	1.21	2.28	1.884
He/6%H_2/Fe $_{crucible}$	<0.2	1.95	6.78	3.477
He/6%H_2/H_2O/Fe $_{crucible}$	<0.2	3.65	5.15	1.411
Vacuum/Fe $_{crucible}$	<0.2	9.31	0.25	0.027

In the Ta-crucible a reduction of PbO_2 to metallic Pb is observed, which seems to support the release of elemental Tl. However, the formed Pb sticks to the crucible material and is therefore lost for further irradiations. Otherwise, the separation was best using a gas mixture of dry helium and oxygen and a steel crucible. There is a chemical reaction observed from the black PbO_2 to the yellow PbO, which obviously supports the Tl release too. Most probably the macroscopic amounts of Tl are released in the form of Tl_2O, which is not formed at carrier free conditions.

2 g of the original PbO_2 was irradiated in the PSI NAA rabbit system connected to the spallation neutron source SINQ at PSI. Based on the results described above after a decay time of two days the separation procedure of PbO_2 and Tl was performed. For 8 h the PbO_2 sample was heated in a dry He/O_2 mixture at 100 ml/min gas flow to 800°C. The long-lived thallium isotopes ^{200}Tl ($T_{1/2}$ = 26.1 h), ^{201}Tl ($T_{1/2}$ = 73.1 h), and ^{202}Tl ($T_{1/2}$ = 12.23 d) produced through the fast neutron activation of the lead served as a separation monitor. Indeed a very good Pb/Tl separation could be achieved, indicating that also macroscopic amounts of Tl were released from the initial Pb sample. ^{206}Bi is observed due to traces of Bi in $^{nat}PbO_2$ p.a. (see Fig. 2, panel A).
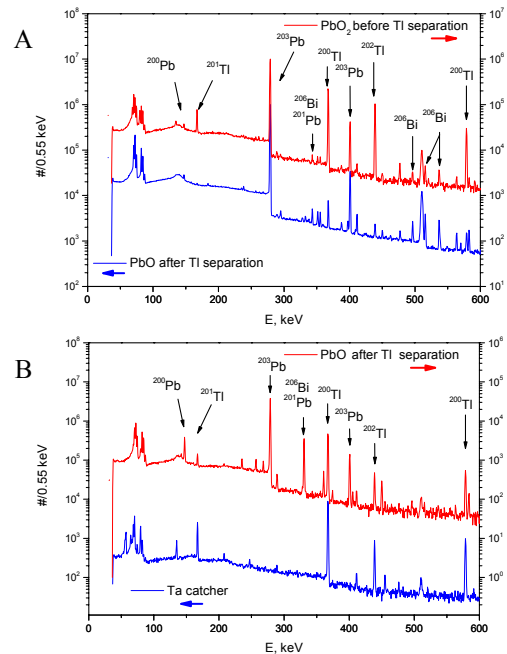
Fig. 2: γ-spectra
A) PbO_2 before (right hand axis) and PbO after separation (left hand axis) normalized to ^{203}Pb. B) PbO and the Ta catcher after separation

The pre-cleaned PbO sample was irradiated again in the PSI-SINQ-NAA. 2 days later carrier-free samples of $^{200\text{-}202}$Tl were obtained using the separation procedure described with 2h separation time reaching about 50% yield (see Fig.2, panel B). The final samples did not contain macroscopic amounts of lead or bismuth. The prepared carrier free $^{200\text{-}202}$Tl samples were used for thermochromatographic investigations [3].

REFERENCES

[1]   B. Bayar et al. *Radiochem. Radioanal. Lett.* **34**, 89 (1978).
[2]   S. König, *Diploma thesis University Bern* (2005).
[3]   B. Muther et al. this report, p.9.

THERMOCHROMATOGRAPHY OF ^{212}Pb AND $^{200-202}$Tl ON QUARTZ AND GOLD

B. Muther, R. Eichler, H. W. Gäggeler (Univ. Bern & PSI)

Adsorption experiments were carried out for carrier-free ^{212}Pb and ^{202}Tl isotopes on quartz and gold surfaces as model studies for the investigations of elements 114 and 113, respectively.

1 INTRODUCTION

The adsorption enthalpies at zero surface coverage for thallium and lead on quartz and gold surfaces show a large data spread. The reason might be that it is not easy to reach carrier free conditions with lead and thallium isotopes (see for review [1,2]). To get clarity on this problem is of general interest. Moreover, the results will help to create an appropriate setup for upcoming experiments on the superheavy elements 113 and 114, which are homologues in the same groups in the periodic table with Tl and Pb, respectively.

2 EXPERIMENTAL

^{212}Pb ($T_{1/2}$ = 10.64 h) is a decay product of ^{220}Rn $T_{1/2}$ = 55 s). To collect ^{212}Pb, the emanating ^{220}Rn was flushed out of a ^{232}Th source with a He gas jet (100 ml/min) and deposited on a Ta foil which was placed in a liquid nitrogen tank. The collection time was 10 hours, about one half-life of ^{212}Pb. Subsequently, the Ta foil was placed in a quartz tube with an inner diameter of 3 mm. The tube was then put into an array of ovens: 1) the starting oven which can be heated rapidly up to 1000°C; 2) the gradient oven, in which a linear negative temperature gradient (1000°C to 50°C) is established. At the beginning and at the end of the chromatographic column a getter oven was placed, where a clean Ta foil is heated up to 1000°C prior to the experiment to prevent oxygen and water from entering the column. The entire column is surrounded by a steel tube. The experiments were conducted at various gas flow rates of He. After stable conditions were established in the gradient oven, the starting oven was heated up and the evaporating ^{212}Pb was transported along the temperature gradient. After one hour of experimental time, the column was removed and scanned using a 1 cm collimator window with a HPGe γ-detector for the 238 keV γ-line of ^{212}Pb. The preparation of carrier free thallium isotopes is described in [3]. The $^{200-202}$Tl samples were prepared on Ta foils too and were used same way as described above. For the investigations of the adsorption properties of Tl and Pb on gold surfaces the inner surface of the chromatographic quartz column was covered by a gold foil.

3 RESULTS

From the obtained thermochromatograms (see Fig. 1 and 2) the corresponding adsorption temperatures were determined. Using a Monte-Carlo (MCS) model of thermochromatography [4] for Pb on quartz, an adsorption enthalpy of -205±5 kJ/mol was determined. This value is in good agreement with measurements performed earlier [2]. ^{212}Pb behaved in the chromatography with the stationary gold surface differently from the expectations. In the current setup it was not possible to observe a chromatographic deposition of Pb on gold. The melting point of gold (1064°C) did not allow increasing the highest

temperature in the gradient. Hence, only a limit of the adsorption enthalpy could be determined as -ΔH$_{ads}$ > 295 ± 5 kJ/mol. This limit is about 50 kJ/mol higher than the adsorption enthalpies form in earlier studies (for review see [2]).

The Thallium experiments conducted on quartz revealed a -ΔH$_{ads}$ of 119±6 kJ/mol using the MCS method. This is in good agreement with earlier works [1]. The chromatography on gold resulted in a -ΔH$_{ads}$ of 285±5 kJ/mol. This value is about 40 kJ/mol higher compared to previous studies (for review see [1]). Possibly, it was the first time that the adsorption of carrier free amounts of Tl and Pb was investigated. To approve this, these measurements will be repeated with adding some Pb and Tl carrier.
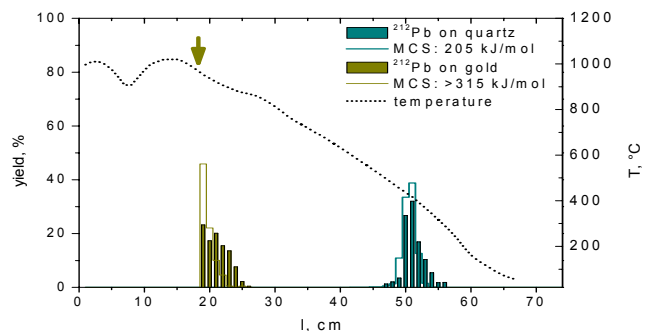
Fig. 1: Merged thermochromatograms of ^{212}Pb on quartz and on gold. Gas flow: 500 ml/min; duration of experiment: 1 h. The dark yellow arrow indicates the start of the gold coverage in the experiments with stationary gold surface.
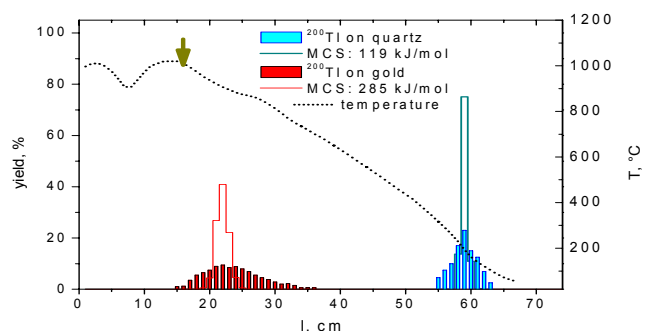
Fig. 2: Merged thermochromatograms of ^{202}Tl on quartz and on gold. Gas flow: 70 ml/min; duration of experiment: 1 h. The dark yellow arrow indicates the start of the gold coverage in the experiments with stationary gold surface. Broad peaks are due to the inefficient collimation.

REFERENCES

[1] S. König, Diploma thesis University Bern (2005).
[2] F. Haenssler, PhD thesis University Bern (2007).
[3] D. Wittwer et al. this report, p. 8.
[4] I. Zvara, Radiochim. Acta **38,** 95 (1985).

ON THE PRODUCTION OF ISOTOPES FOR RADIOCHEMISTRY USING 71 MeV PROTON BEAMS

R. Eichler, A. Serov (Univ. Bern & PSI), R. Dressler, D. Piguet (PSI),
D. Wittwer, B. Muther (Univ. Bern), S. Shishkin, O. Petrushkin (FLNR)

The future availability of proton beams for on-line isotope production will considerably expand the radioactive tracer portfolio of the radiochemistry groups at PSI. For testing purposes targets of ^{238}U, ^{232}Th, ^{209}Bi and a sample of LBE were irradiated by 71 MeV protons and the produced radioactive tracers were identified.

Radiochemical investigation methods depend on the availability of radioactive tracers. Prior to the installation of the ECR Ion source in 1992 proton beams were already used, e.g to produce Pa isotopes for gas phase chemical investigations [1]. The future availability of 72 MeV proton beams delivered in the low energy areas of PSI offers important possibilities for isotope production for radiochemical investigations in the Laboratory for Radiochemistry and Environmental Chemistry. Here we report on test irradiations performed at the PSI Philips cyclotron.

A 71 MeV proton beam was delivered to the Low Energy Area C (NeC). Targets of ThF_4 (300 µg/cm^2, on 15 µm Al backing) and Bi_2O_3 (300 µg/cm^2, on 15 µm Be backing) were irradiated at typical intensities between 20-50 nA. The recoiling products were stopped in a small (about 30 cm^3) gas volume. This volume was either flushed by 1 l/min pure argon or by a gas mixture of He and N_2 (10:1 vol-%). The products were transported using the well known carbon aerosol gas-jet technique through a 10 m long PE capillary to the sampling position. The 1 h aerosol particle sampling was performed using a filtering unit equipped with quartz wool filters for measuring long-lived activities. The filters were measured by standard γ-spectroscopy about 5 minutes after stopping the irradiation for 1h. For the determination of α-decaying products the aerosol particles were sampled using the PSI Tape system and measured at various sampling/stepping times. In the second part of the experiment a target of $^{238}U_3O_8$ (300 µg/cm^2, on 12 µm Be backing) was irradiated. The IVO-COLD system [2] was connected to the irradiation position. The setup of a 4 m long PFA transport capillary between the 20 cm^3 recoil chamber and the COLD detector and the 2.7 l/min Ar gas loop flow rate allowed for a 0.7 s transport time and aimed at the determination of volatile very short-lived as well as long-lived α-decaying nuclides. In the last part of the experiment, a sample of 1 g lead-bismuth eutectic (LBE) was irradiated for about 20 h. This sample was measured 4 days later on a HPGE γ-detector for 4 days to determine long-lived tracers.

Sample spectra measured during this experiment series are presented in Fig. 1 together with the identified tracer isotopes. The main products identified on the filter samples are typical proton activation products of the used carrier gases. Excellent production possibilities for light tracer isotopes for on-line chemical studies are available by choosing the right carrier gas mixture. The production of $^{34,35,38}Cl$, ^{38}S, and ^{132}I using the Th target and argon as carrier gas offers an interesting tracer mixture for investigations with environmental relevance. Otherwise, neutron and proton evaporation reactions (p,xn/yp) with x ≤ 8 and y = 0 or 1 and proton induced fission are the main

production paths for the tracers. Fission products are suppressed using the He/N_2 mixture due to the low stopping power of the gas. In the experiments with the ^{238}U and Bi_2O_3 targets no significant production of volatile α-decaying tracers was observed. An ^{233}U target would serve for the production of more neutron deficient isotopes (e.g. ^{211}At). A more appropriate setup using stacks of thin targets as described in [1] would considerably improve the transport yields of the proton activation products (low momentum). In the LBE sample expected products were observed (see Fig.1, lower panel), which can be used for release studies in connection with Megapie.
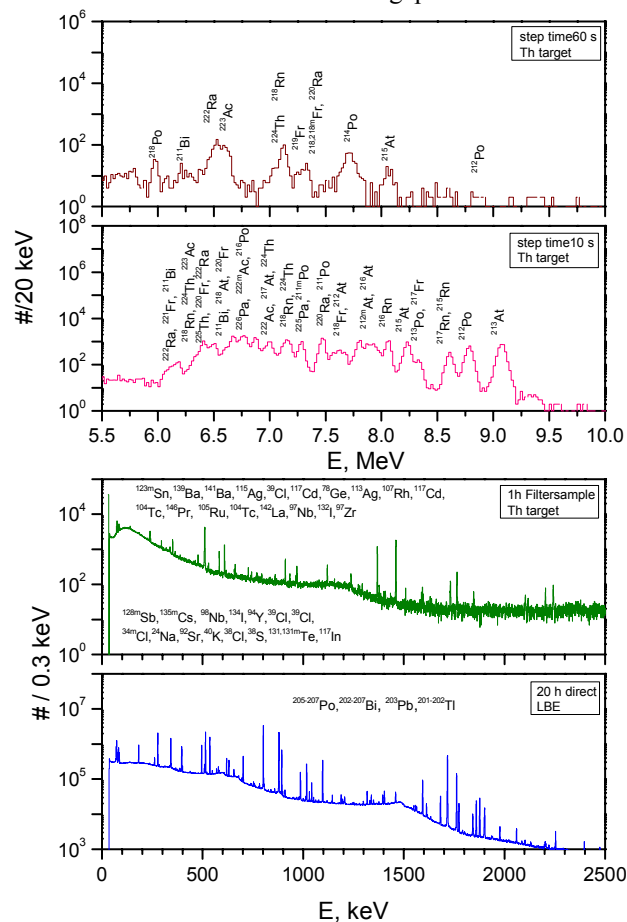
Fig. 1: − spectra accumulated during the PSI-Tape measurements using varied stepping times (upper panels) and γ-spectra from the filter measurements and from the LBE (Pb-Bi-eutectic) sample (lower panels).

REFERENCES

[1] A. Kovacs et al., Ann. Rep. Labor für Chemie PSI (1992).

[2] R. Eichler et al. this report., p. 7.

THE TRANSPORT OF Hg AND Pb USING A METAL AEROSOL GASJET

R. Eichler, A. Serov, L. Josic (PSI &Univ. Bern), R. Dressler, A. Laube, D. Piguet (PSI)

Model experiments with short-lived isotopes $^{185-186}$Pb and $^{180-182}$Hg revealed promising transport efficiencies using metal aerosol particle gas-jets.

Currently, developments are ongoing of a setup for the vacuum chromatographic investigation of transactinides. Vacuum chromatographic adsorption investigations may provide information on adsorption properties of elements on materials sensitive to surface contaminations and oxidation. Fast separation and high resolution α- and SF-spectroscopy are further advantages of vacuum techniques. However, several crucial problems have to be solved [1]. One problem is that transactinides produced in nuclear fusion reactions are recoiling from the target at the high momentum of the beam particles. Therefore, to transfer them into vacuum chromatography an effective technique is needed, either: A) thermalization at vacuum conditions, by implanting them into solid state catcher materials; or B) thermalization in a gas prior to the transfer into the vacuum. Here we show results of experiments following path B aiming at the search for the most efficient approach. Therefore, a 305 MeV ^{40}Ar beam was delivered from the PSI Philips cyclotron with an intensity of typically 10-20 pnA. Targets of ^{nat}SmO$_3$ (400 μg/cm^2) and ^{152}Gd$_2$O$_3$ (500 μg/cm^2) prepared on 15 μm Be backings by molecular plating were irradiated to produce short-lived isotopes of Hg and Pb. The beam energy in the targets was calculated as 221-217 MeV leading to the production of $^{179-188}$Hg and ^{186}Pb in the nuclear reactions: ^{nat}Sm(^{40}Ar, 6n) and ^{152}Gd(^{40}Ar, 6n) (see Fig.1). The recoiling reaction products were thermalized in a gas volume of about 40 cm^3. This volume was flushed by an aerosol gas-jet at a flow rate of 1.5 l/min. Thus the nuclear reaction products were transported through an 8 m long PE capillary to the PSI Tape system, where they were impacted in vacuum on the tape and measured sequentially by 8 PIPS detectors for α-decay at a sampling/stepping time of 10 s. The aerosol gas-jet mixture was prepared by flushing a gas mixture of He and N$_2$ (10:1 vol-%) through a spark discharge (12.5 KV, 2.5 mA) between two electrodes made from rolled metal foils (see Fig. 2). The resulting aerosol was tested for long-term stability and high efficiency transport properties of non-volatile as well as volatile elements interacting with metal surfaces. These are typical properties of the s- and p-elements of the group 12-18 of the periodic table. Thus, Hg and Pb represent good model elements. The experiments with each metal were carried out between 8 and 12 h. The transport efficiencies were compared to the standard carbon aerosol gas-jet used previously for transactinide experiments typically operated for 4 h. Unfortunately, the production rates calculated with HIVAP yield not very reliable absolute values. Therefore, the determination of absolute transport yields was impossible. Apparently, metals with lower (Cu, Ag, Au) and with very high (Ta, W) melting points are not suited. However, similar transport efficiencies were observed using metal aerosols of Rh, Ni, Fe, Pd, Pt, and Zr (see Fig.3) compared to the efficiencies obtained using this well known carbon aerosol gas-jet. Since losses of aerosol particles are expected due to beam

plasma effects. Therefore, even better transport yields are achievable working behind a physical preseparator [3].
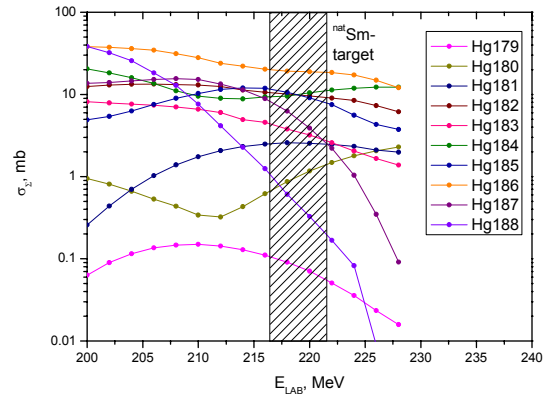
Fig. 1: Integral cross section of the formation of short-lived isotopes of Hg in the reaction according to HIVAP calculations [2]. The "thickness" of the target is indicated.
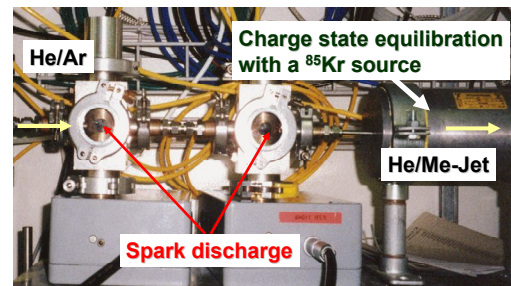
Fig 2: Aerosol production using two spark discharge units.
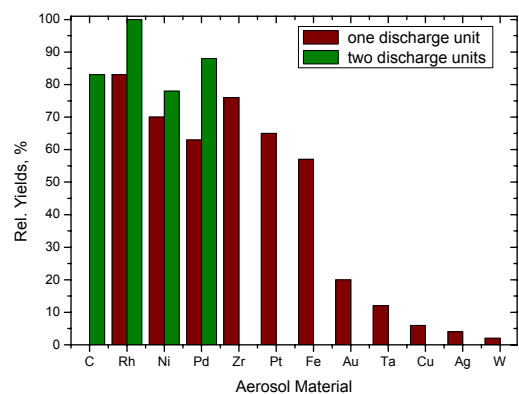
Fig. 3: Relative transport yields measured for $^{182-184}$Hg and ^{186}Pb using various materials for the aerosol particle gas-jet.

REFERENCES

[1] A. Serov et al. see this report, p. 6.

[2] W. Reisdorf et al., Z. Phys. A **343,** 47 (1992).

[3] C.E. Düllman et al., Nucl. Instr. Meth. **A551**, 528 (2005).

ENHANCED NO$_2$ UPTAKE ON AEROSOLS CONTAINING HYDROXYBENZOIC ACIDS

Yu. Sosedova, H.W. Gäggeler (Univ. Bern & PSI), M. Ammann (PSI)

The kinetics of NO$_2$ uptake on a basic aqueous aerosol containing 2,5-dihydroxybenzoic acid was observed using the short-lived radioactive tracer ^{13}N and denuder techniques. An uptake coefficient of >5×10^{-3} was measured.

1   INTRODUCTION

Aromatic compounds with one or more phenolic groups (ArOH) are ubiquitous in the environment and have been found in smoke from biomass burning as well as among the lignin degradation products in soils. It was shown that nitrogen dioxide (NO$_2$) might undergo fast electron transfer reaction with phenoxide anions in aqueous solution [1]:

$$NO_2 + ArO^- \rightarrow NO_2^- + ArO^\bullet \qquad (R1)$$

The primary reaction products of gaseous NO$_2$ with these organics are the corresponding phenoxy- type radical and nitrite anion. The latter may be subsequently protonated and released to the gas phase as HONO. In the troposphere, HONO plays an important role as OH radical source due to its photolysis [2]. Field studies indicate that HONO is mainly formed heterogeneously from NO$_2$ on the ground or airborne particles and cloud droplets. Modeling studies have mostly treated the disproportionation of NO$_2$ on humid surfaces as a source of HONO [3]. The kinetics of this reaction is however relatively slow, and it cannot contribute significantly to the budget of HONO in the atmosphere, especially not during the daytime. In environments with a high content of hydroxy-substituted aromatics, the reaction (R1) can be an additional mechanism for HONO formation. Hence, it is important to know the rate, with which NO$_2$ can be processed by aerosols containing dissolved ArOH and to give an estimate of the upper limit of the bulk accommodation coefficient. In this study, gentisic acid (2,5-dihydroxybenzoic acid) was used as a model ArOH compound.

2   EXPERIMENTAL
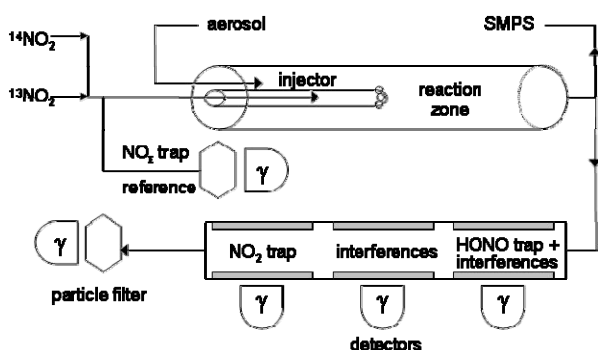
Fig. 1: The scheme of the experimental set-up.

The routine for the on-line production of ^{13}N-labeled nitrogen monoxide at PSI was reported in detail in [4], and the main experimental steps were described in the previous annual report [5] and are schematically presented on Fig. 1. The aerosol was produced from nebulizing a mixture of gentisic acid (GA) and NaOH such that GA was fully deprotonated. To vary the GA concentration, malonic acid was added as non-reactive matrix.

3   RESULTS

The kinetics of uptake of NO$_2$ on aqueous aerosols was measured at different conditions. It was found that the rate of NO$_2$ uptake was proportional to the square root of the GA concentration in the aqueous phase, as shown in the double logarithmic plot of Fig. 2, where the data plot along the line with a slope of ½. This is an indication that the uptake is limited by a bulk reaction in the liquid phase. The pretty high uptake coefficients obtained for these kinetic experiments >5×10^{-3} confirm that the bulk accommodation coefficient should be at least 0.01 or higher.
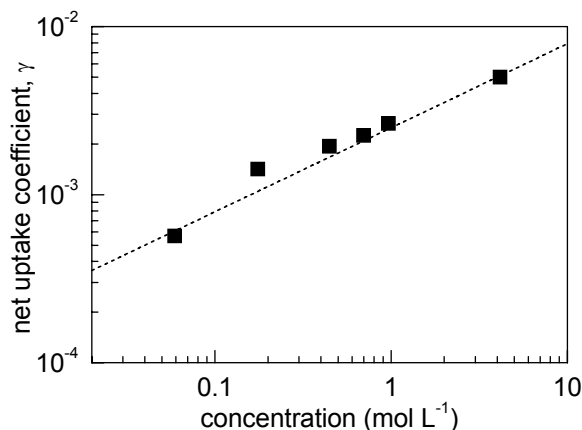
Fig. 2: Uptake coefficient γ as a function of aqueous phase concentration of GA (■) at 40 % relative humidity. The dotted line indicates the slope of the square root dependency expected for uptake limited by a bulk reaction in the liquid phase.

4   ACKNOWLEDEGMENT

REFERENCES

[1]   M. Ammann et al., Phys. Chem. Chem. Phys., **7**, 2513, 2005.
[2]   R. M. Harrison et al, J. Geophys. Res.-Atmos., **101**, 14429, 1996.
[3]   B. Vogel et al., Atmos. Environ., **37**, 2957, 2003.
[4]   M. Ammann, Radiochim. Acta, **89**, 831, 2001.
[5]   Yu. Sosedova et al., Ann. Rep. Labor Radio- & Umweltchemie, Univ. Bern & PSI, 2006, p. 11.

KINETICS OF OZONE UPTAKE TO POTASSIUM IODIDE AEROSOL

A. Rouvière, M. Birrer, M. Ammann (PSI)

The kinetics of uptake of O₃ by deliquesced KI aerosol particles at 70% relative humidity (RH) and room temperature was studied using an aerosol flow tube technique.

Aerosol particles play an important role in atmospheric chemistry and climate. In particular, they can take up gas phase species, recycle them and release them back into the atmosphere. O_3 is a very important oxidant, and several details of its transfer to the aqueous phase are not well established. In particular, organic coatings present in sea salt particles [1] may impede its phase transfer. With the aim to study such effects in detail, we first started to investigate uptake of O_3 to neat iodide particles as a model system. Iodide provides a substantial aqueous sink (reaction (R1)) [2] to drive uptake of ozone, and iodide is present in sea salt aerosol. This reaction is also important in halogen activation processes of the marine boundary layer. For this system, a previous study has already shown that organic coatings may significantly affect the iodide enhancement at the aqueous air interface [3].

$$I^- + O_3 + H^+ \rightarrow HOI + O_2 \qquad (R1)$$
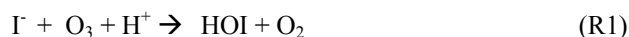
Potassium iodide particles were produced by nebulising an aqueous solution containing 1g/L KI salt and mixed with ozone in a 420 mL flow reactor, similar to our earlier studies with aqueous aerosols, e.g., by Guimbaud et al. [4]. The relative humidity was adjusted to 75%, leading to a diameter growth factor of 1.3. The residence time could be varied by changing the position of an injector delivering ozone. The particle size distribution and concentration was measured with a Scanning Mobility Particle Sizer (SMPS). The concentration of ozone (typically about 150 ppb) was measured with a photometric ozone analyzer (model ML 9810, Monitor Labs Inc, USA) after separating ozone from the particles by diffusion in an annular coflow device.
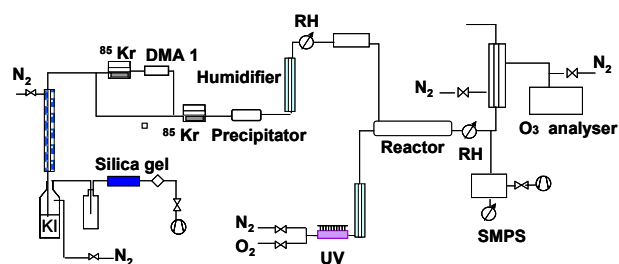
Fig. 1: Experimental set-up

Figure 2 shows the response of the ozone concentration to switching on and off the aerosol at different reaction times: the smaller the residence time, the smaller the depletion. The rate of loss of O_3 from the gas phase, described as a pseudo-first order process, where k'_g is the first order rate coefficient and t is the exposure time between the gas and aerosol surface, can be related to the uptake coefficient, γ, on the aerosol via:

$$\frac{d[O_3]}{dt} = -k'_g[O_3] \quad (1) \qquad k'_g = \frac{S\omega\gamma}{4} \quad (2)$$

where S is the aerosol surface area and ω the mean molecular velocity of O_3 in the gas phase. If the loss of O_3 is assumed to occur via the bulk phase reaction (R1), the uptake coefficient can be parameterized by:

$$\frac{1}{\gamma} = \frac{1}{\alpha_b} + \frac{1}{\gamma_{rxn}} \quad \text{with } \gamma_{rxn} = \frac{4HRT\sqrt{D_{aq}k'_{aq}}}{\omega} \qquad (3)$$

where α_b is the bulk accommodation coefficient, γ_{rxn} is the probability for reaction in the bulk liquid, T is the temperature, H is the Henry's law coefficient of O_3, D_{aq} is the diffusion coefficient of O_3 in the liquid phase, R is the universal gas constant and k'_{aq} the first order loss rate constant of O_3 in the liquid phase.

From the measured loss of O_3 in the reactor, we obtained an uptake coefficient of about 10^{-3}. On the other hand, based on equation (3) and for iodide concentrations of 10 M in the deliquesced particles, we would expect γ_{rxn} to be about 10^{-2}. Previous studies indicate that α_b for O_3 on iodide solutions is in the range of 2×10^{-3} to 1 [5,6], so that bulk accommodation could be a rate limiting step. However, it seems more likely that in our experiments, in absence of an extra source of acidity, uptake was affected by depletion of protons. Further experiments will address the effect of additional activity, and finally, the effect of organic coatings.
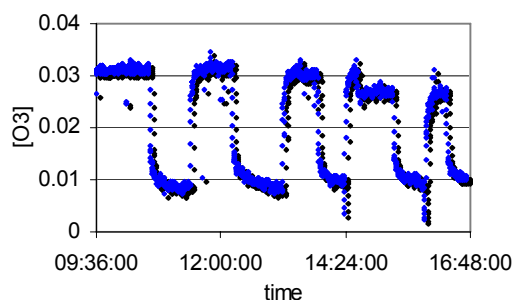
Fig. 2: Experimental profile of the O_3 concentration for different gas aerosol interaction times

ACKNOWLEDGEMENT

REFERENCES

[1] Y. Rudich, Chem. Rev., 103, 5097 (2003).
[2] S. Enami et al., J. Phys. Chem. A, 111, 13032 (2007).
[3] M. Krisch et al., J. Phys. Chem. C, 111, 13497 (2007).
[4] C. Guimbaud et al., Atmos. Chem. Phys., 2, 249 (2002).
[5] J.H. Hu et al., J. Phys. Chem., 99, 8768 (1995).
[6] R.G. Utter et al., J. Phys. Chem., 96, 4973 (1992).

FORMATION OF H_2O_2 BY OZONOLYSIS OF CONDENSED PHASE ALKENES

O. Vesna (Univ. Bern & PSI), M. Ammann (PSI)

In this study we investigated the effect of humidity and condensed phase water on the formation of H_2O_2, a likely product of the reaction of water with the Criegee Intermediate formed in the reaction between pure oleic acid or mixed oleic acid/NaCl particles and ozone.

1   INTRODUCTION

Water vapour could influence the product distribution from the degradation of unsaturated compounds by ozone, either by reaction with the Criegee Intermediates (CIs) or by influencing the structure of the aerosol. We measured hydrogen peroxide (H_2O_2) that might be formed from the decomposition of hydroxyhydroperoxides, which is an unstable product of the reaction between CI and water. We used pure oleic acid (OA) particles as well as particles also containing NaCl as a proxy for sea salt to assess the effects of water vapour alone or of the presence of condensed phase water above the deliquescence humidity of NaCl as a more realistic scenario for atmospheric particles.

2   EXPERIMENTAL

The experimental set up has been fully described in the proceeding report [1], the only difference being that the H_2O_2 production was measured online with a H_2O_2-analyzer (AL2001CL). The pure OA particles were prepared in concentrations of 5×10^6 #/cm^3 by homogeneous nucleation in a condenser behind an evaporator held at 130 ± 2 $^\circ$C. Mixed OA/NaCl was produced as follows. NaCl particles were formed by nebulising a solution containing 2 mg ml^{-1} NaCl and dried in a flow of N_2 and coated with OA in the same evaporator. The thickness of the OA film was varied by changing the temperature in the evaporator. Initial ozone concentrations were 470 ppb and 200 ppb for pure OA and for mixed OA/NaCl particles, respectively. The ozone concentration was measured online using an ozone analyzer and a co-flow separator that allows separating aerosol particles and gas flow. The relative humidity was changed from 0 to 85 % in the aerosol flow reactor.

3   RESULTS AND DISCUSSION

Fig. 1 shows a record of H_2O_2 formation and ozone uptake, when the aerosol was present in the reactor, clearly indicating a net production of H_2O_2 in presence of the OA aerosol. Some production of H_2O_2 was observed during ozonolysis of pure OA, namely 0.8 to 0.9 % (of ozone reacted) under "dry" and humid conditions, respectively, while a significant formation of H_2O_2 was measured on mixed OA/NaCl particles under humid conditions with yields between 3 and 12 % (Fig. 2).

The strong increase of the H_2O_2 yield above the deliquescence point of NaCl indicates that the yield becomes highest, when OA forms a monolayer on the aqueous substrate. For this experiment, the mass fraction of OA was such that it corresponded to the equivalent of a 40nm thick coating on the dry particles and roughly a monolayer on the deliquesced particles. The H_2O_2 yield was higher in the case of an OA monolayer on aqueous solution than in the case of pure OA particles, which suggests an important role of condensed phase water. So, this experiment indicates that unsaturated compounds internally mixed with a deliquesced aerosol may have a significant impact on the budget of H_2O_2. H_2O_2 acts as reservoir of OH radicals, and in the aqueous phase it is the most important oxidant for the conversion of SO_2 to H_2SO_4 [2].
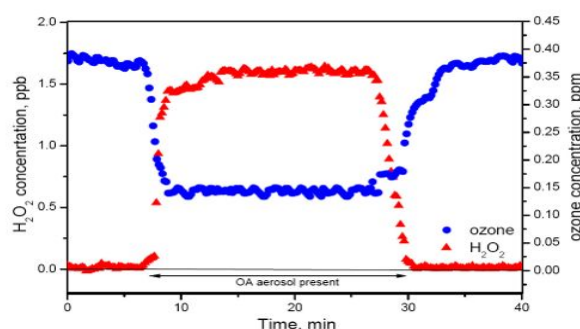
Fig. 1: H_2O_2 production and ozone uptake on pure OA aerosol at 83 % of relative humidity and 470 ppb ozone concentration.
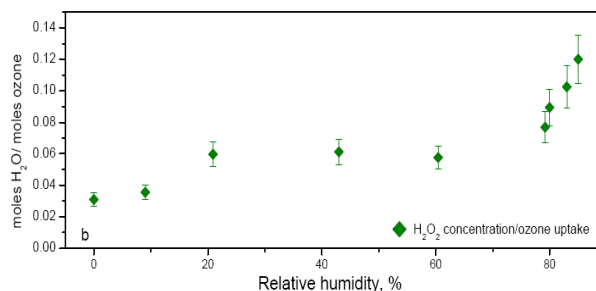
Fig. 2: The humidity dependence of the H_2O_2 yield, normalized to the amount of ozone lost in the reaction of OA on NaCl particles with ozone.

REFERENCES

[1] O. Vesna et al., Ann. Rep. Labor Radio- & Umweltchemie, Univ. Bern & PSI (2005), p. 17.
[2] J. G. Calvert et al., Nature , **317**, 27 (1985).

INVESTIGATION OF PHOTOSENSITIZED POLYMERIZATION IN ORGANIC AEROSOLS USING CHEMICAL IONIZATION MASS SPECTROMETRY (CIMS)

A. Schlierf (PSI, ETH), T. Bartels-Rausch (PSI), M. Birrer, B. D'Anna, C. George (Uni Lyon, CNRS), M. Ammann (PSI)

A new setup was developed to investigate photochemical aging of particles in aerosol experiments. Light induced aging processes on organic aerosol particles can change the aerosol's chemical composition and therefore its physico chemical properties. To display changes in composition we apply chemical ionization mass spectrometry (CIMS) in proton transfer mode.

1 PHOTOCHEMICAL AGING OF PARTICLES

Light is an efficient source of excited molecular states known to initiate chemical reactions. Also polymerization is known to be initiated photochemically, for example with benzophenone type sensitizers.

In the atmosphere polymerization can be an important pathway of chemical aging; especially primary organic compounds typically present in biomass burning aerosol can be strongly affected by photochemical processes. The investigation of the effects photosensitized processes may have on the polymerization of organic particles in the atmosphere requires a powerful analytical method. For aerosol experiments, a new setup using chemical ionization mass spectrometry (CIMS) in proton transfer mode was developed allowing the observation of parent compounds and small oligomers.

2 THE NEW EXPERIMENTAL SETUP

The setup uses a [210]Polonium based source of primary ions. Thereby, traces of water vapor are ionized to generate protonated water clusters. Based on the scheme shown in Fig. 1 we can produce water clusters with a main peak at m/z=37amu (13 kcps) from $(H_2O)_2H^+$ as suggested in [4].
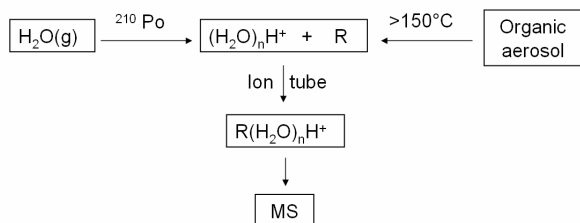
Fig. 1: Reaction scheme of proton transfer chemical ionization applied for organic aerosol samples.

The predominant cluster can be selected in tuning the applied voltages and fluxes in the CI region. The aerosol experiments are performed online with the aerosol source coupled to the CI region with a new thermal particle evaporator inlet. The sample gas was protonated in the drift tube at pressures in the 20 Torr range.

3 AEROSOL EXPERIMENTS

The sample aerosol was produced from aqueous solutions of functionalized organics using a spray aerosol source. Before injecting to the CIMS, the sample was dried using a silica gel diffusion dryer. The aerosol was evaporated at

>150°C and injected into the CI region. Here, the gaseous sample molecules can react with water clusters via a proton transfer reaction. First experiments with adipic acid show characteristic fragmentation and an efficient ionization of the analyte (spectrum in Fig. 2).
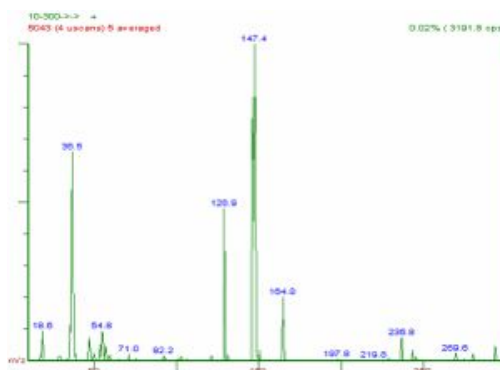
Fig. 2: A mass spectrum generated by an adipic acid aerosol using proton transfer.

Adipic acid is showing up mostly at m/z=147 and m/z=129. As kinetics and probability of the proton transfer reaction are influenced by the proton affinity and the primary ion distribution, the main peak is expected at m/z=147, which is reported to be characteristic for the molecular acid with one attached proton. The peak at m/z=129 indicates the loss of water [5], m/z=165 likely results from an additional attached water molecule.

4 CONCLUSION AND OUTLOOK

We have demonstrated the capabilities of our new setup. As a next step we are optimizing the system for online investigations of the photochemical altering of secondary organic aerosols. The next experiments will focus on the photosensitized oligomerization of aromatics typically present in biomass burning aerosol. In bulk aqueous solutions of a photosensitizer mixed with resorcinol, a representative of such aromatics, we could observe significant shift of absorption from the UV into the visible, indicating polymerization.

REFERENCES

[1] Canonica et al., J. Phys. Chem. A, **104**, 1226, 2000.
[2] George et al. Faraday Discussions, **130**, 195-210, 2005.
[3] Stemmler, Atmos. Chem. Phys., **7**, 4237, 2007.
[4] Maleknia et al., Int.J.of Mass Spectr. **262**, 203, 2007.
[5] Cappa et al, J.Phys Chem A. **111**, 3099, 2007.

LIGHT INDUCED AGING OF ORGANIC AEROSOL COMPONENTS

A. Schlierf (PSI), B. D'Anna, A. Jammoul, M. Brigante (Uni Lyon, CNRS),
C. George (Uni Lyon, CNRS), M. Ammann (PSI)

We studied light induced altering of organics typically present in atmospheric aerosols. Light induced reactions can change the chemical composition and so an aerosol's physical properties. Our results show that the absorption of mono aromatic molecules can be shifted from UV to visible light due to photosensitizers transferring triplet energy and thereby inducing oligomerisation.

1   INTRODUCTION

Ultraviolet or visible light absorbing organic constituents of atmospheric aerosols may act as photosensitizers for a number of processes. In a photosensitized process, absorption of a photon leads to an excited molecule that may transfer charge or energy to different acceptors available in its vicinity [1]. Photosensitizers may be primary organics from combustion sources or be formed in situ during oxidation in the atmosphere [2]. The significance of photosensitized processes has been demonstrated by showing enhanced uptake of atmospheric oxidants to organic films or aerosol particles [3]. In this contribution, we investigate the effects photosensitized processes may have on the fate of other organic aerosol constituents.

2   EXPERIMENTAL

Organic substrates and benzophenone-type photosensitizers were dissolved and irradiated using 6 sunlight lamps (Phillips Effect, 70W, diffuse). Benzophenone is known to photosensitize saturated or aromatic substrates via transfer of triplet energy. In case of radiative energy transfer the triplet emission spectrum of the sensitizer molecules has to be blue shifted compared to acceptor molecule. Emission of the donor and absorption spectrum of the acceptor molecule need to show spectral overlap [5]. Solutions of resorcinol (1,2- Dihydroxybenzene) and benzophenone derivatives were chosen as a laboratory test system.
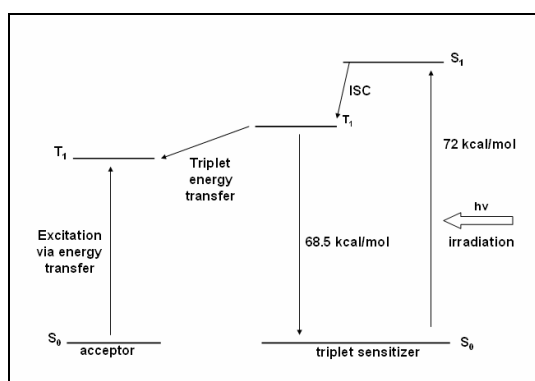
Fig. 1: Scheme of benzophenone energy transfer; the acceptor is excited to a higher energy state

3   RESULTS AND DISCUSSION

The irradiation leads to changes in the UV/VIS spectra likely caused by a photochemically enhanced reaction. Resorcinol as a mono aromatic compound shows maximum absorption in the UV range while the spectra of dimeric and oligomeric species are red shifted. This change of absorption energy results in an increase of absorption at VIS wavelengths (Fig.2), which is correlated to the irradiation time.

The red shifted absorption likely results from a chemical change of the aromatics' π system. Small aromatic molecules can undergo photosensitized polymerization accompanied by an enlarging of the π system. By enlarging the π systems, resorcinol derivatives absorb lower energy resonance frequencies compared to the parent compound.
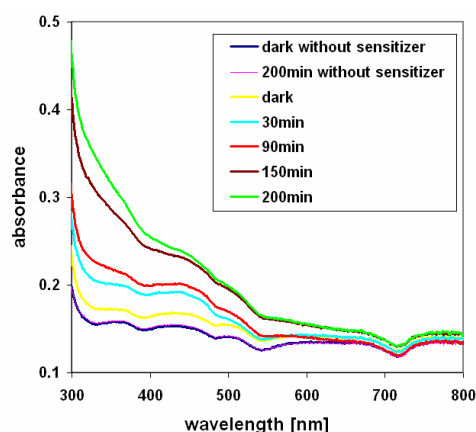
Fig. 2: UV/VIS spectra for saturated aqueous resorcinol/Benzophenone solutions at different; times of exposure to light.

4   CONCLUSION AND OUTLOOK

We have demonstrated photosensitized oligomerisation of aromatics in bulk solutions. Our results are of direct relevance to the aging of primary organic compounds typically present in biomass burning aerosol. Thus, photosensitized polymerization can change organic aerosols with respect to composition and physico-chemical properties. The knowledge derived from solution tests systems will be applied to follow photochemical reaction of these and other relevant compounds in the aerosol phase.

REFERENCES

[1]   Canonica, S. et al., J. Phys. Chem. A, **104**, 1226, 2000.
[2]   Gelencser, A. et al., J. Atmos. Chem., **45**, 25, 2003.
[3]   George, C. et al., Faraday Discussions, **130**, 195, 2005.
[4]   Stemmler, K. et al., Atmos. Chem. Phys., **7**, 4237, 2007.
[5]   Yousoke, M. et al.,Tedrahedron Letters, **48**, 639, 2006.

OBSERVATION OF PHASE CHANGES IN AEROSOL PARTICLES WITH X-RAY MICROSPECTROSCOPY

V. Zelenay (PSI), T. Huthwelker (PSI/SLS), A. Křepelová, M. Birrer (PSI),
G. Tzvetkov (PSI/SLS & Univ. Erlangen-Nürnberg), J. Raabe (PSI/SLS) M. Ammann (PSI)

We use X-ray transmission microscopy and spectroscopy at the PolLux beamline at SLS for aerosol particles in the size range of 0.3 – 1 μm to observe their structural and spectroscopical behavior during water uptake and release. With an improved environmental cell, we followed in situ the phase changes of ammonium sulfate and sodium chloride particles.

1 INTRODUCTION

X-ray spectroscopy is a powerful tool for the characterization of chemical compounds. We are using soft X-rays to perform spectroscopy at the carbon and oxygen K-edges on samples of atmospherically relevant aerosol particles. In general, the PolLux microscope is operated under vacuum or helium due to strong absorption of soft X-rays in air. To study aerosol particles under a controlled atmosphere, we introduced a gas cell that allows to control gas composition and temperature of the sample. In the previous annual report [1], we introduced a prototype of a cell, which has now been improved to a reliable cell with an easier handling (Fig. 1). First results with $(NH_4)_2SO_4$ are reported.

2 EXPERIMENTAL

Considering the strict constraints given by the PolLux microscope [1] and with a concept similar to that used by Drake at al. [2] we constructed a new cell. This novel cell consists of two parts: one comprises the gas flow inlet and exhibits one Si wafer (back wafer) with a SiN window size of 1 mm; the second part is a "clip" on which the front wafer (window size of 0.5 mm) can be fixed with a wax. Afterwards, the samples may be collected on this wafer. The clip can then be screwed onto the cell. The two windows are 50 nm SiN membranes to transmit the x-ray beam to the detector.
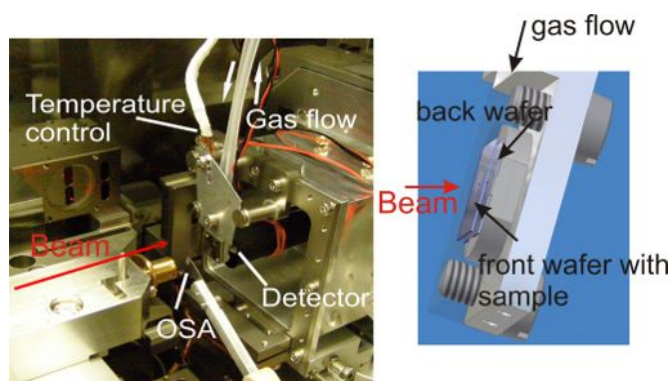
Fig. 1: *Left:* Photograph of the new environmental cell in the PolLux microscope. The most important features are indicated. OSA denotes the order sorting aperture. *Right:* Detailed view of the cell with the interior part made visible with the two Si wafers. The particles are collected on the window, through which the X-ray beam enters.

3 RESULTS

The improved setup with the environmental cell and the new flow system allowed us to measure at very well defined conditions, including control of the local temperature. We could proof the reliability of the cell by measuring water uptake and release in aerosol particles with different substances, e.g. ammonium sulfate. Fig. 2 shows four oxygen K-edge spectra as an example at different relative humidity during water release. Note that the shoulder at about 541 eV of the spectrum with the highest humidity (yellow) decreases during water release. The relative humidity was plotted against the (normalized) absorption at 541.3 eV resulting in a plot, which compares well to typical hydration/dehydration data of ammonium sulfate obtained by other techniques.
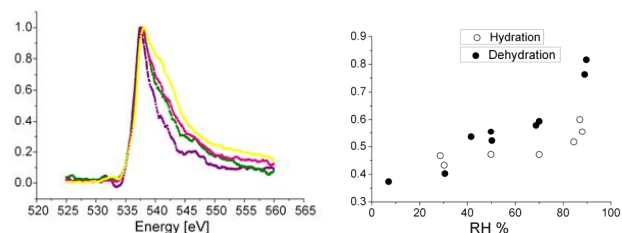
Fig. 2: *Left:* Oxygen K-edge spectra of ammonium sulphate aerosol particles showing the release (dehydration) of water. The spectra were measured at 89 % (yellow), 70 % (pink), 49.8 % (green) and 30.6 % relative humidity (RH) at 25.3 °C. *Right:* Preliminary plot of the relative humidity in the cell versus the (normalized) absorption at 541.3 eV.

REFERENCES

[1] T. Huthwelker et al., Ann. Rep. Labor Radio- & Umweltchemie, Univ. Bern & PSI, 2006, p. 15.
[2] I.J. Drake et al., Rev. Sci. Instr., **75**, 10, 3234, 2004.

SYNCHROTRON BASED 3D MICROTOMOGRAPHY OF IMPURITIES IN ICE

T. Huthwelker (PSI/SLS), M. Hutterli (BAS), M. Miedaner, F. Enzmann, M. Kersten (Uni Mainz) M. Stampanoni,
F. Marone (PSI/SLS), S. Maus (U Bergen) (PSI/SLS) M. Ammann (PSI)

Synchrotron based X-ray microtomography is used to study salt inclusions in artificial ice samples. It is demonstrated that bromine salts can be identified in a 3-D tomogram by acquiring tomograms taken at energies above and below the bromine absorption edge. We also show that the new setup allows in situ growth of ice crystals, and we demonstrate that the technique is viable to visualize impurities in natural sea ice.

1 INTRODUCTION

Ice is an abundant substance in nature. It occurs as ice particles in the atmosphere, such as hailstones or snow flakes, as snow cover on the Earth surface or as Sea ice on the ocean surface. Impurities, fractionated and released during freezing of natural water, can have substantial impact on atmospheric and oceanic chemistry. Examples include chemical processes leading to catalytic ozone destruction both in the stratosphere and in the polar troposphere. Most impurities are poorly dissolved in the ice matrix, but rather accumulate in grain boundaries and triple junctions. Such structures may form a three dimensional network, which may serve as reactor for chemical reactions. Hence, it is of interest to study the three-dimensional location and morphology of salt inclusions in ice *in situ* using a non-destructive technique. For this purpose, we use synchrotron based microtomography at the material science beamline and the new TOMCAT beamline at the Swiss Light source (SLS), using a setup as described previously [1].

2 EXPERIMENTAL

Ice samples are fit into a small closed polyamide (Plexiglas) sample holder of a few mm size (Figure 1). This sample holder is cooled by a flow of cold nitrogen. We also use a sample holder, which allows heating its lower part (See figure 1). By the heating, water can be evaporated from the bottom to the top of the sample holder, to grow ice crystals in situ.
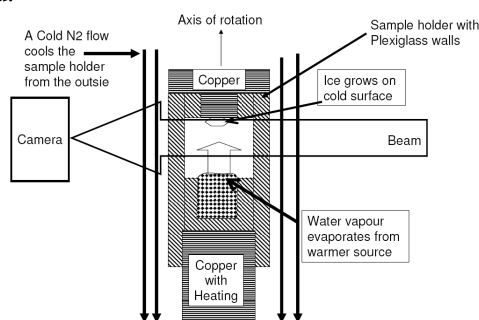
Fig. 1: Conceptual drawing of the experimental setup.

3 RESULTS

We demonstrate the possibilities of the technique using several examples. First we consider a tomogram taken from a sample consisting of an ice/NaCl/NaBr mixture. Two tomograms were taken. One (Figure 2 left) was taken at 13.4 keV, below the Br absorption edge, the other one at 13.6 keV, above the Br edge (Figure 2 middle). In the tomograms, dark structures represent strong X-ray absorption (i.e. the salt). The lightest structures represent air. In the right panel of Figure 2, we show the ratio of both reconstructed slices. In this picture, the brightest structures show a higher absorption at 13.6 keV compared to the picture at 13.4 keV, thus showing the existence of bromine in the sample.
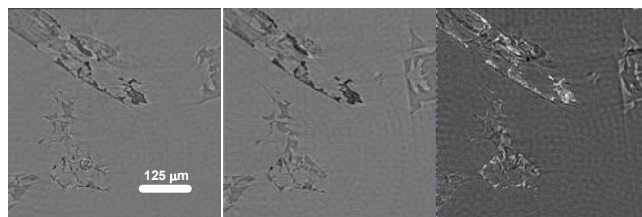
Fig. 2: Comparison of tomograms of taken at different energies, above and below the bromine edge (~13.5 keV). *Left*: 13.4 keV; *Middle*: 13.6 keV; *Right*: Ratio of both figures. The light region shows regions of enhanced bromine concentration (for description see text). The scale given is approximate.

In Figure 3 we show two further examples. The left panel shows a slice of a tomogram of small vapor grown ice crystals (A few 10 μm in size). One can see the hexagonal shape of some crystals and get an idea of the surface smoothness within experimental resolution of 1.4 μm. The right panel demonstrates that we can observe salt inclusions in ice, which was frozen from natural sea water. Here, dark structures represent the salt inclusions, the light structures air inclusions in the ice.
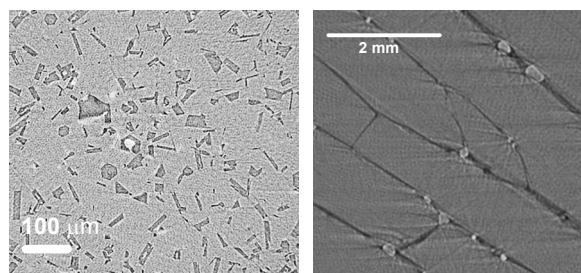
Fig. 3: Reconstructed slices from tomograms for various ice samples. *Left:* vapour grown ice crystals, as grown in the in situ growth chamber. *Right:* Mesh of salt inclusions (dark) and air bubbles (bright) in sea ice.

REFERENCE

[1] T. Huthwelker et al., Ann. Rep. Labor Radio- & Umweltchemie, Univ. Bern & PSI (2006), p. 15.

UPTAKE OF NITROUS ACID ON ICE

M. Kerbrat (PSI & Univ. Bern), T. Huthwelker, M. Birrer, M. Ammann (PSI)

The uptake of radioactively labelled nitrous acid into a packed ice bed was investigated. A method developed to retrieve and deconvolute the thermodynamic quantities governing the adsorption and the diffusion of nitrous acid onto and into the ice, respectively, is presented.

1 INTRODUCTION

It is now well established that ice-air interactions play a role in the composition of the atmosphere overlaying snowpacks [1]. However, those interactions are complex as they result from the interplay of several processes and are still not well understood. The aim of this study is to work out the thermodynamic quantities which govern adsorption and diffusion onto and into ice for nitrous acid (HONO).

2 EXPERIMENTAL

At the Paul Scherer Institute, the PROTRAC facility provides radioactive nitrogen (^{13}N) [2]. The short lived isotopes ($t_{1/2} \sim 10$ min) are continuously delivered to the laboratory in the form of nitrogen monoxide (^{13}NO), where it is chemically processed to produce radioactively labelled nitrous acid. HO^{13}NO is then continuously fed into a packed ice column.

The output of a tracer experiment is shown in figures 1 and 2. In Fig. 1, the x-axis represents the length of the ice column which continuously scanned by two gamma detectors in coincidence counting configuration. The z-axis represents the activity at a given position at a given time (y-axis).
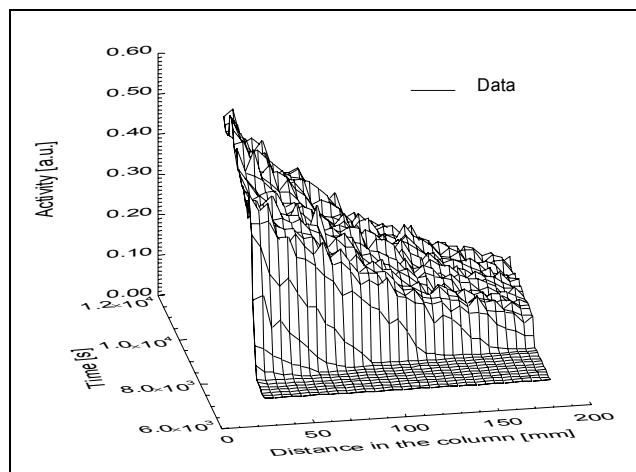
Fig. 1: Migration of HO^{13}NO in the ice column.

3 RESULTS

In Fig. 2, the migration front of HO^{13}NO in the column can be nicely seen (from yellow to red). Using a 2D numerical model [3], we could show that this front is mainly governed by adsorption. This is an important result as in most of the uptake experiments, the studied compound diffuses into grain boundaries and triple junctions present in the ice. With traditional methods it is often difficult to deconvolute the two processes, namely adsorption and diffusion.
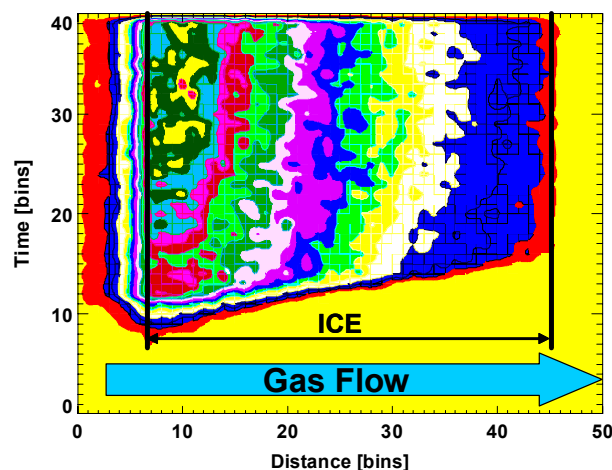
Fig. 2: Top view of the plot shown in Fig. 1, where the different colours represent different levels of the activity.

It can also be seen on Fig. 1 and 2 that after some time, the system is reaching a steady state. At that point, the activity distribution along the column will feature an exponential decay which can be also used to calculate the net velocity of migration of HO^{13}NO through the column [4]. In this approach, the migration depends on adsorption onto the surface of ice and diffusion into its bulk. By subtracting the adsorption contribution obtained using the first approach, the thermodynamic quantities governing diffusion into the bulk can be retrieved from this second approach.

Using these two approaches, we will soon be able to provide thermodynamic quantities governing adsorption of HONO onto the ice surface and diffusion of HONO into its bulk.

REFERENCES

[1] A. M. Grannas et al., Atmos. Chem. Phys., **7**, 4329, 2007.

[2] M. Ammann, Radiochim. Acta, **89**, 831, 2001.

[3] T. Huthwelker et al., Ann. Rep. Labor Radio- & Umweltchemie, Univ. Bern & PSI, p.12, 2005.

[4] M. Kerbrat et al., Ann. Rep. Labor Radio- & Umweltchemie, Univ. Bern & PSI, p.17, 2006.

THE ADSORPTION OF NO₂ ON ICE STUDIED BY X-RAY PHOTOELECTRON SPECTROSCOPY

A. Křepelová (PSI), J.T. Newberg, H. Bluhm (LBNL), T. Huthwelker, M. Ammann (PSI),

X-ray photoelectron spectroscopy (XPS) and electron yield near edge X-ray absorption spectroscopy (NEXAFS) performed at beamline 11.0.2 at the Advanced Light Source (ALS) were used to determine the impact of NO₂ adsorption on the surface melting of ice. First results are reported.

1 INTRODUCTION

Chemical processes on ice in snow and cirrus clouds are important for atmospheric chemistry, biogeochemical cycling of trace constituents and archiving of trace species in ice. Indications for the existence of surface melting on clean ice surfaces have been reported for temperatures above about -20 °C [1]. It has been suggested that the thickness of the disordered layer increases in the presence of adsorbates. We want to show that the presence of HNO_3 (formed by the reaction of NO_2 with H_2O) induces surface melting at temperatures too low for the occurrence of surface melting of clean ice, and under conditions, where a solution is not thermodynamically stable. XPS is a well established tool for surface chemical analysis under UHV conditions. NEXAFS can provide additional information on near surface disorder in ice. The beamline 11.0.2 at the Advanced Light Source (ALS) at Lawrence Berkeley National Laboratory has a capability to carry out XPS and NEXAFS experiments on ice samples in equilibrium with water vapor pressures up to several Torr. In addition, by varying the incident photon energy XPS experiments can be performed at different photoelectron kinetic energies to vary the probing depth.

2 EXPERIMENTAL

The principle of the ambient pressure photoemission spectrometer is described elsewhere [2,3]. The incident X-ray beam is admitted to the ambient pressure cell through a 100 nm thick silicon nitride window. An about 1 mm thick ice film was grown on a Peltier cooled gold substrate from water vapor and then equilibrated at -43.2°C. NO_2 was then added to the chamber to reach NO_2 partial pressures up to 0.1 Torr. The gas phase composition was monitored by a differentially-pumped mass spectrometer. O1s and N1s XPS spectra as well as O and N K-edge NEXAFS spectra were recorded at constant temperature.

3 RESULTS

Fig. 1 shows N1s and O1s XPS spectra obtained at -43.2 °C. The incident photon energies were 600 eV for the N and 735 eV for the O spectrum, *i.e.* at photoelectron kinetic energies of 200 eV. The binding energy of N1s is consistent with XPS spectra reported for nitrates. Surface nitrate is formed through direct hydrolysis of NO_2 on the ice surface, but also from adsorption of HNO_3 formed through the same process on the vacuum chamber walls.

Auger electron yield O K-edge NEXAFS spectra were measured using a kinetic energy window of 440-460 eV. Fig. 2 shows NEXAFS spectra of clean (black) and contaminated ice (green and red). The spectrum of clean ice

is consistent with literature data [4]. The peak at 535 eV is due to broken hydrogen bonds (single donor configuration), while the broad band around 543 eV is due to 4-fold coordinated water molecules. With increasing NO_2 partial pressure (green curve), a peak at around 533 eV appears that is assigned to nitrate, while the ice like features of the rest of the spectrum are retained. Under conditions where the nitrate signal is much stronger (red curve) the peak at 543 eV decreases significantly, indicating the formation of a solution.
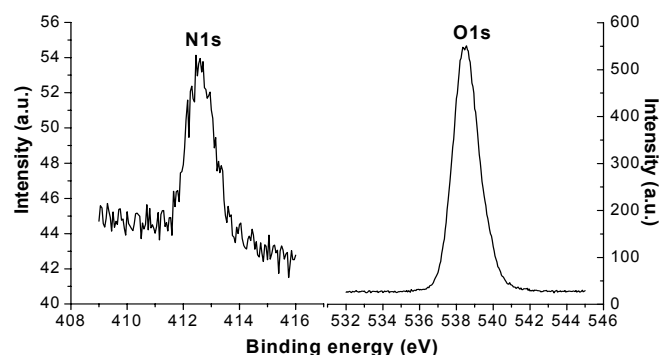
Fig. 1: Typical photoelectron spectra of N1s and O1s regions as a function of apparent binding energy. The incident photon energies were 600 and 735 eV for N and O spectrum, respectively.
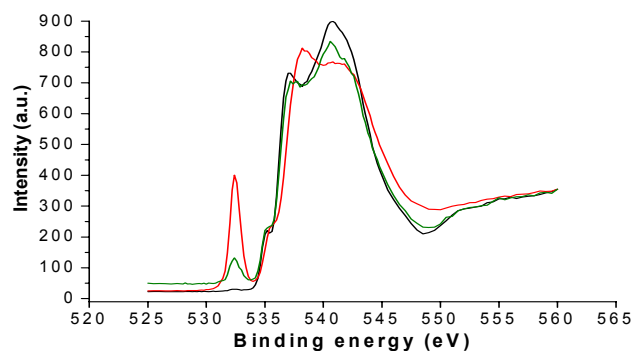
Fig. 2: Oxygen K-edge NEXAFS spectra of clean (black) and contaminated (green and red) ice.

REFERENCES

[1] J.G. Dash et al., Rep. Prog. Phys. **58**, 115 (1995).

[2] H. Bluhm et al., J. Electron Spectrosc. Relat. Phenom., **150**, 86 (2005).

[3] D.F. Ogletree et al., Rev. Sci. Instrum., **73**, 3872, 2002.

[4] H. Bluhm et al., J. Phys.: Condens. Matter, **14**, L227, 2002.

ADSORPTION OF ACETIC ACID ON ICE

M. Kerbrat (PSI & Univ. Bern), T. Huthwelker, M. Birrer, T. Bartels-Rausch (PSI), H.W. Gäggeler (PSI & Univ. Bern), B. Pinzer, M. Schneebeli (SLF), M. Ammann (PSI)

The thermodynamic quantities governing the adsorption of acetic acid on ice were determined using a chemical ionization mass spectrometer. The enthalpy and entropy of adsorption were found to be -61(±1) kJ mol^{-1} and - 84(±3) J mol^{-1}K^{-1}, respectively.

1   INTRODUCTION

Acetic acid (CH_3COOH) is a volatile organic acid, which can be found in concentrations up to 8ppbv in the firn air of snowpacks originating from the decomposition of organic compounds [1]. Our co-adsorption studies indicate that acetic acid could enhance the release of nitrous acid to the atmosphere [2]. In this study, the thermodynamic quantities governing the adsorption of CH_3COOH on ice were measured.

2   EXPERIMENTAL

A flow of gaseous nitrogen (N_2) was blown slowly over frozen acetic acid to allow saturation. The gaseous mixture of CH_3COOH and N_2 was subsequently diluted with a humid flow of N_2 to reach the desired acetic acid concentration and the desired humidity. The resulting gas mixture was continuously fed to a packed ice bed flow tube kept at temperatures between 253 and 213 K. The amount of water in the injected gas mixture was equal to the vapour pressure of ice at the temperature of the experiment.
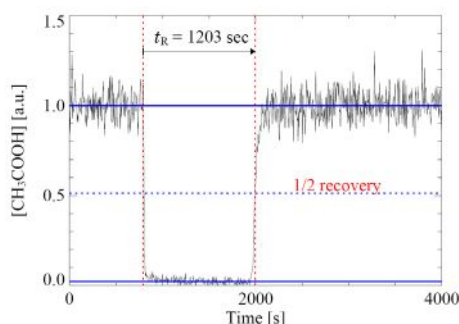
Fig. 1:   Example of a breakthrough curve showing the drop of the CH_3COOH signal once the ice is exposed and its recovery once the surface is saturated.

The ice spheres, used for the ice columns, were produced by spraying ultra pure water (MilliQ) into liquid nitrogen. After 2-3 days of annealing at -20°C, the ice balls were sieved and the fraction 400-500μm was used to fill 6 mm i.d. PFA tubes. After another 2-3 days of sintering at -20°C, the column could be used in an experiment. The specific surface area of the ice columns was measured by X-Ray tomography to be around 112 cm^2 g^{-1}.

During an experiment, the gas phase concentration of acetic acid was measured using a chemical ionization mass spectrometer (CI-MS) [3]. Water clusters were produced by passing a humid flow of nitrogen through a corona discharge and were used to transfer protons to CH_3COOH. The concentration of acetic acid as a function of time was followed during an experiment as $CH_3COOH_2^+$ i.e. m/z = 61. An example of an uptake experiment is given on Fig. 1.

3   RESULTS

The time (t_R) needed for acetic acid to break through the ice bed (see Fig. 1) can be used to calculate the equilibrium constant K_p^0 for adsorption at a given temperature [3]. From the temperature dependence of K_p^0, the enthalpy (ΔH_{ads}) and entropy (ΔS^0_{ads}) of adsorption can be calculated as shown in figure 2. The enthalpy and standard entropy of adsorption in this study were found to be -61(±1) kJ mol^{-1} and -84(±3) J mol^{-1}K^{-1}, respectively, using a molar area of $A_0 = 3.74 \times 10^7$ m^{2}mol^{-1} as standard state for the adsorbed phase [4]. Values reported in the literature are $\Delta H_{ads} = -33.5$ kJ mol^{-1}[5] and $\Delta H_{ads} = -73.1$ kJ mol^{-1}[6]. The difference between the values seems to arise from the calculated amount of acetic acid molecules present as dimers. We have so far assumed monomer adsorption only in the low coverage regime, but will make a more detailed analysis of this point.
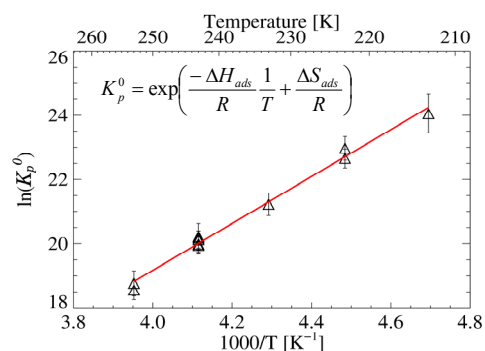
Fig. 2:   Temperature dependence of the equilibrium constant K_p^0 used to calculate ΔH_{ads} and ΔS^0_{ads}.

REFERENCES

[1]   J. E. Dibb et al., Atmos. Environ., **36**, 2513, (2002).
[2]   M. Kerbrat et al., Ann. Rep. Labor Radio- & Umweltchemie, Univ. Bern & PSI, (2006), p. 17.
[3]   C. Guimbaud et al., Int. J. Mass Spectrom., **226**, 279, (2003).
[4]   C. Kemball et al., Proc. Royal Soc. London, **187**, 53, (1946).
[5]   S. Picaud et al., J. Chem. Phys., **122**, (2005).
[6]   O. Sokolov et al., J. Phys. Chem. A, **106**, 775, (2002).

PHOTOCHEMICAL PRODUCTION OF HONO BY HUMIC ACID IN ICE

T. Bartels-Rausch (PSI), J. Kleffmann, Y. Elshorbany (Univ. Wuppertal),
M. Brigante, B. D'Anna, C. George (CNRS / Univ. Lyon), M. Ammann (PSI)

The heterogeneous conversion of NO$_2$ to HONO by soil constituents in the presence of visible light has been suggested to be of importance in the polar environment. In this joint project this hypothesis was tested with well-controlled laboratory measurements on ice doped with humic acids, an important soil constituent.

1   INTRODUCTION

The photosensitized reduction of NO$_2$ to HONO by constituents of soils such as humic acids has recently been proposed to explain the observed high concentrations of HONO in the lowermost part of the atmosphere in some regions, e.g. over forest [1]. Although experimental proof is still missing, this pathway has been suggested to also affect the atmospheric HONO budget in Polar Regions, as the snow cover is known to contain some traces of soil components [2]. Atmospheric HONO is an important precursor of hydroxy radicals and its concentration thus influences the oxidative capacity of the atmosphere.

The aim of this joint laboratory research project was to determine the importance of the photosensitized reduction of NO$_2$ on ice surfaces at low concentration of doped humic acid.

2   TYPICAL EXPERIMENTS
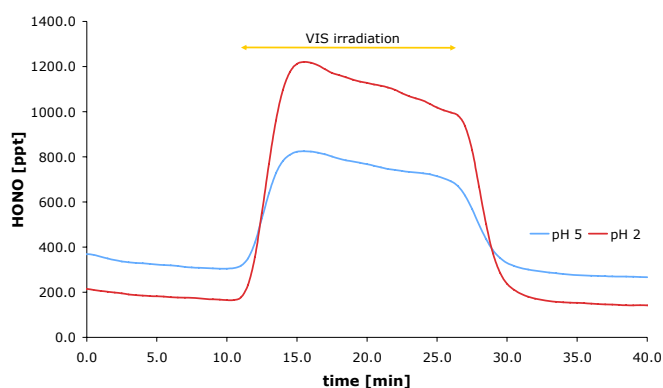
Fig. 1: Evolution of the HONO mixing ratio in the gas flow exiting the coated wall flow tube, for ice films generated from humic acid solutions adjusted to different pH values. Zero minutes denotes the beginning of an experiment**.**

For each experiment an aqueous humic acid solution, between 20 mg/l and 900 mg/l in concentration, was frozen on the walls of a quartz flow tube and irradiated with visible light for 15 minutes, while a carrier gas containing NO$_2$ was passed along the ice film. The mixing ratio of NO$_2$ was varied between 5 and 555 ppb and the temperature of the ice film was typically set to 258 K. The resulting HONO emissions from the irradiated ice surface was measured in the gas flow exiting the coated wall flow tube. As HONO is also very effectively formed heterogeneously without the presence of light, the background HONO

concentration was measured for each experiment prior and after the illumination.

The two experimental runs in Fig. 1 differ in the pH of the aqueous humic acid solution used to freeze the ice film. It can be seen that significantly more HONO is released from the ice, when the more acidic solution was frozen. In both experiments the ice contained approximately 30 µg humic acid and was exposed to 100 ppb NO$_2$. The HONO profile during the irradiation also shows a strong decrease with time, which can be attributed to a yet unidentified passivation process.

2   NO$_2$ DEPENDANCY

The dependency of HONO productions on the gas-phase mixing ratio of NO$_2$ shows a saturation behavior (Fig. 2), which is in agreement with a photochemical, heterogeneous reaction mechanism [1].
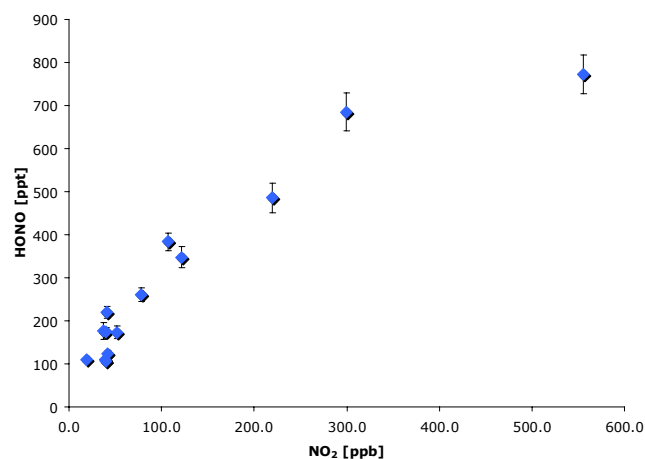
Fig. 2: Evolution of the HONO mixing ratio in the gas flow exiting the coated wall flow tube.

The results presented here - as well as the dependency of HONO production on the concentration of humic acid and on the light intensity – clearly show that HONO formation on ice and snow is enhanced in the presence of light and humic acid. Changes in the temperature of the ice film between 213 K and 258 K did now reveal any effect of temperature on the intensity of HONO production. Extrapolation of the observed HONO production rates to environmental relevant NO$_2$ and humic acid concentrations is work in progress.

REFERENCES

[1]   K. Stemmler et. al., Nature, **440**, 7081 (2006).
[2]   A. Grannas et. al., Atmos Chem Phys, **7**, 4329 (2007).

INTERACTION OF PEROXY NITRIC ACID WITH ICE SURFACES

T. Bartels-Rausch, T. Huthwelker, J. Grael, M. Ammann (PSI)

An approach to determine the partitioning of HO_2NO_2 between ice films and air was successfully tested. From such experiments, the impact of the environmental snow cover on the atmospheric HO_2NO_2 budget can be derived.

1   INTRODUCTION

Peroxynitric acid (HO_2NO_2) is present in the colder parts of the Earth's atmosphere [1], where it might be deposited to snow or ice surfaces. This decrease in the atmospheric nitrogen oxide concentration might in turn impact the oxidative capacity of the atmosphere. Here we report a strategy and first results to quantify the partitioning of HO_2NO_2 between ice and air.

The experimental set-up basically consists of the gas-phase HO_2NO_2 synthesis, the adsorption experiments in a coated wall flow tube and the detection of HNO_4 along with the synthesis by-products using a mass spectrometer.

2   OPTIMIZATION OF SYNTHESIS

Peroxynitric acid was synthesized by the reaction of HO_2 with NO_2. NO_2 was obtained from gas-phase oxidation of NO with O_3, so that this synthesis route can later be used for experiments at the PSI PROTRAC facility. HO_2 radicals were produced by the photolysis of water in a $N_2/O_2/CO/H_2O/NO_2$ mixture at 172 nm. After the synthesis, the gas flow was passed through a cooling trap at 243 K to 233 K to remove excess water vapor, HNO_3 and a large fraction of H_2O_2.
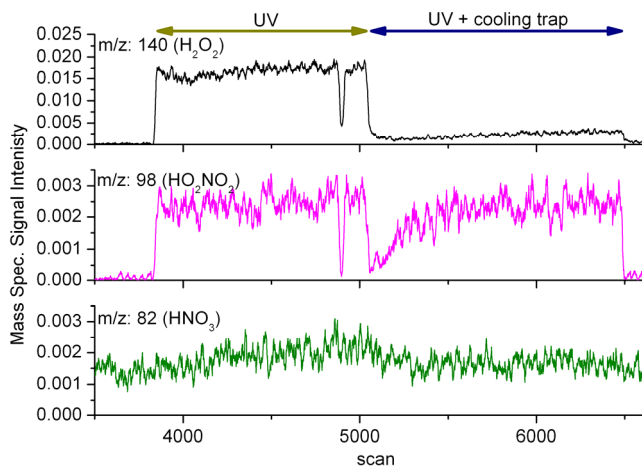
Fig. 1: An example of traces detected by the mass spectrometer. A scan denotes ~2s.

The synthesis was monitored using a mass spectrometer. Using SF_6^- as chemical ionization reagent, it was possible to monitor HO_2NO_2 and important by-products simultaneously [2]. Figure 1 clearly shows that only very little amounts of HNO_3 were formed during the photolysis. HNO_3 and H_2O_2 were furthermore very efficiently removed in the cooling trap at 243 K. H_2O_2 was detected as m/z of 140. This signal has previously been assigned to $SF_4O_2^-$

derived from HO_2 [3]. Our data now indicate that also the reaction of H_2O_2 with SF_6^- leads to this ion fragment. This conclusion is based on the observation that the intensity of the SF_4O_2-signal is independent of changes in the residence time of NO_2 in the flow system. A longer residence time should lead to a higher reaction yield of HO_2 with NO_2, and thus a decrease in the HO_2 trace in the mass spectrometer. Calibration of the mass spectrometer signals for the different species is work in progress. The experiments presented here were performed with an initial NO_2 mixing ratio of ~40 pbb in the UV-lamp, which was converted to HO_2NO_2 with a yield of about 30 to 50 %.

3   INTERACTION WITH ICE

Figure 2 shows the retention of HNO_4 in the ice coated wall flow tube at different temperatures. In agreement with the expected adsorption process, the retention increases with decreasing temperature. After 20 to 40 minutes the HNO_4 signal rises to its initial value. The equilibrium concentration does furthermore not show any temperature dependence. This indicates that only a small fraction of HNO_4 is irreversibly taken up by the ice surface. Thus, the main interaction of HNO_4 with ice seems to be reversible in nature and consequently this coated wall flow tube approach is well suited to investigate the adsorption behavior of HO_2NO_2 on ice surfaces.
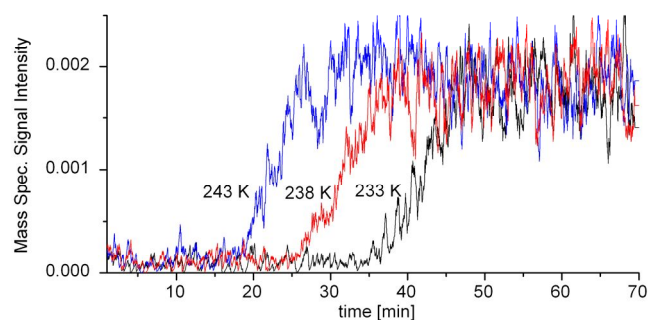
Fig. 2: The evolution of HO_2NO_2 concentration exiting the coated wall flow tube is shown with time at different temperatures. Zero min. denotes the time when the carrier gas started to flow through the coated wall flow tube.

REFERENCES

[1]   Talbot et al., Geophys. Res. Let., **26**, 3057 (1999).
[2]   Slusher et al., Geophys. Res. Let., **28**, 3875 (2001).
[3]   Bardwell et al., Phys. Chem. Chem. Phys., **5,** 2381 (2003).

RECONSTRUCTION OF CENTRAL ASIAN TEMPERATURES DURING THE LAST 750 YEARS USING ICE CORE δ^{18}O DATA

A. Eichler, A. Laube, S. Olivier, K. Henderson (PSI), T. Papina (IWEP), M. Schwikowski (PSI)

We established a highly-resolved temperature reconstruction for the last 750 years using an ice core δ^{18}O record from a Siberian Altai ice core. The temperature record shows minima during the solar minima and an increasing trend since the mid 18th century with 3.2±1.7 °C between the Maunder minimum and the end of the 20th century.

In order to place recent climate change in a longer term context highly resolved, millennial scale temperature reconstructions are required. We established a temperature record using ice core δ^{18}O data from Belukha glacier in the Siberian Altai (49°48'N, 86°34'E), that is of particular interest, since it is from a strong continental region with very few palaeo data available. Using annual layer counting and volcanic reference horizons we determined that the upper 138 m of the ice core cover the period 1250-2001.

For the calibration of the δ^{18}O ice core record instrumental temperature data from Barnaul, Russia (52°26'N, 83°31'E) were used, which is the closest station with data spanning more than 100 years. Snow accumulation at Belukha glacier is assumed to occur in spring, summer, and autumn, since winter months December-February account only for 4% of the annual precipitation in the period 1950-1990 at the 10 km distant Ak-kem station [1]. Thus, for the calibration of the δ^{18}O record only March-November averages of the Barnaul temperature data were considered.
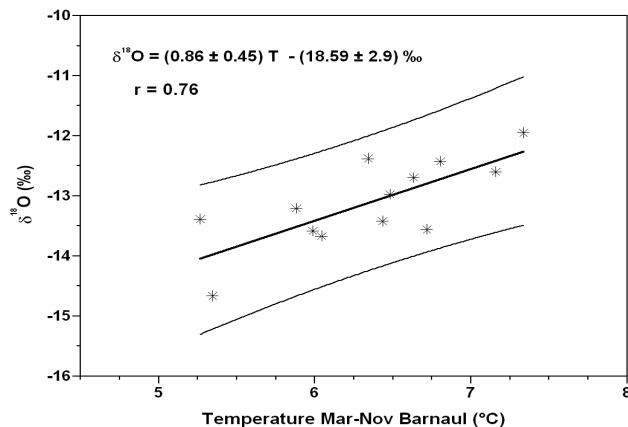
Fig. 1: Correlation between 10-year δ^{18}O means and Mar-Nov temperature means from the station Barnaul in the period 1850-1980. Given are the 95% confidence bands and 2σ uncertainties of the slope and intercept values.

Because of the dating uncertainty in the δ^{18}O record and potentially varying seasonality of snow preservation we used 10-year averages, which show a strong correlation with the Barnaul temperature data (Fig. 1, r = 0.76, p<0.001) for the period 1850-1980. Thus, δ^{18}O in precipitation at Belukha glacier is suitable as proxy of atmospheric temperature. This result is consistent with the spatial variation of δ^{18}O responses in Central and Southeast Asia obtained from instrumental data set covering the period 1961-1993 [2]. North of the Tibetan Plateau with predominant local recycling of water vapor, δ^{18}O in precipitation is primarily controlled by temperature, whereas in the monsoon influenced southern parts precipitation amount is the crucial factor. The derived slope

of the linear regression line of (0.86±0.46) ‰/°C for the calibration period 1850-1980 (Fig. 1) is in agreement with the slope estimated for the year 1990 using Global Network of Isotopes in Precipitation (GNIP) data from 9 stations in Central Asia (0.55±0.26) ‰/°C [1]. The respective slopes for the Central Asian area vary between about 0.3 and 1.1 ([2], [3]), reflecting different moisture sources, air mass trajectories, calibration periods, and seasonal inputs, for instance.

Using the derived slope of (0.86±0.46) ‰/°C we reconstructed the temperature record for the last 750 years (Fig. 2), revealing centennial fluctuations and a positive trend starting from the mid of the 18th century. The relative temperature increase of 3.2±1.7 °C exceeds that of Northern Hemisphere reconstructions with typical ΔT of 0.8-1°C between the Maunder minimum and the end of the 20th century [4]. This is consistent with instrumental data and model simulations [5] suggesting that warming is strongest at the highly continental sites in North America and North Central Asia. Periods of low temperatures occur around 1300, 1450-1550, 1700, 1840, and 1930, which coincide with periods of low solar activity (Wolf, Spörer, Maunder, Dalton, Gleissberg minimum).
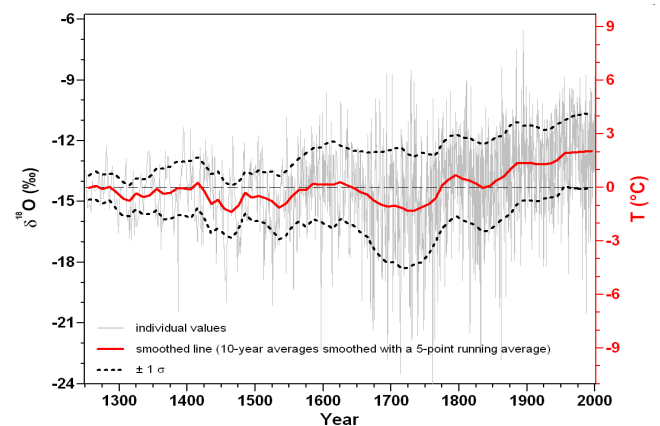
Fig. 2: δ^{18}O-derived temperature reconstruction.

ACKNOWLEDGEMENT

REFERENCES

[1] K. Henderson et al., J. Geophys. Res., **111**, D03104, doi: 10.1029/2005JD005819 (2006).

[2] L. Araguás-Araguás and K. Fröhlich, J. Geophys. Res., **103**, 28721 (1998).

[3] T. Yao et al., Ann. Glaciol., **43**, 1 (2006).

[4] G.C. Hegerl et al., Nature, **440**, 1029 (2006).

[5] R.S. Bradley et al. In: K. Alverson et al. (eds.) Paleoclimate, Global Change and the Future. Springer Verlag, Berlin, 105 (2003)..

SOLAR INDUCED TEMPERATURE CHANGE DURING THE PAST 750 YEARS IN THE HIGHLY CONTINENTAL SIBERIAN ALTAI

A. Eichler, A. Laube, S. Olivier, K. Henderson (PSI), J. Beer (EAWAG), T. Papina (IWEP), M. Schwikowski (PSI)

A temperature record from the Siberian Altai is highly correlated with a reconstruction of total solar irradiance suggesting that solar activity changes are the main driver for the temperature variation in this continental region during the last 750 years. A mean lag of 30 years between the solar forcing and the temperature response hints to an indirect mechanism involving ocean-induced changes in atmospheric circulation.

Sun's role in Earth's temperature variations is still debated. Comparisons of temperature reconstructions for the last millennium with solar variability on regional to global scales reach from no relationship (e.g. [1]) to good correspondence (e.g. [2], [3]). Spatial variation of the sun-temperature relationship is poorly known.

We directly compared a temperature record from a Siberian Altai ice core (period 1250-2001, [4]) with a reconstruction of the total solar irradiance (TSI) based on sunspot observations [5] extended using ^{14}C tree ring data [6]. Our temperature record correlates very well ($r^2 = 0.7$) with the obtained TSI reconstruction (Fig. 1a), suggesting that the sun was the main driving force for the temperature variation during the last 750 years. Due to the strong continentality of the site large seasonal temperature gradients of typically 30°C between mean January and July values are observed. This might be the reason for the sensitivity of the temperature response to small changes in sun activity. However, the processes by which solar variability can affect tropospheric temperatures are still uncertain. Discussed are three mechanisms: 1) direct changes in the energy input into Earth's atmosphere through variations in TSI; 2) changes in stratospheric chemistry through variations of solar UV irradiance that are much stronger than variations in TSI itself; and 3) changes in cloud cover induced by modulations in the cosmic ray flux.
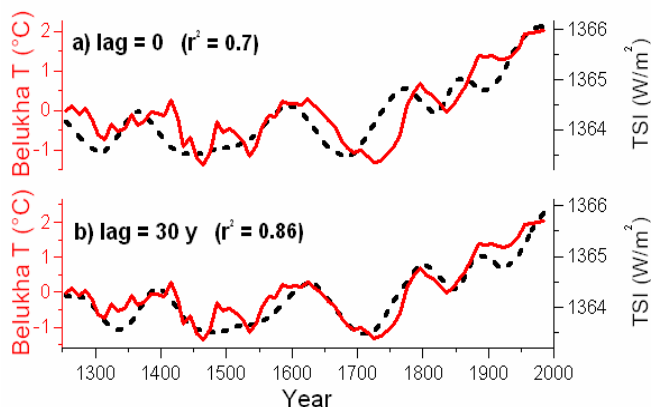
Fig. 1: a) Reconstructed temperature (red) and TSI (black, dashed). b) Same as a), but the TSI curve was shifted by 30 years to produce the best match with the temperature curve.

Interestingly, the highest correlation between our temperature record and the TSI ($r^2 = 0.86$) was obtained when introducing a lag of 30 years (Fig. 1b). Cross correlation analysis revealed that the observed lag is not constant, but varies between 10 and 40 years. Nevertheless, the always positive lag suggests a certain response time between the initial solar signal and the regional temperature. Mechanisms 1)-3) mentioned above only operate on much shorter time-scales and are therefore not sufficient to explain the observed lag. Possible justifications for decadal lags are changes in ocean and atmospheric circulations triggered by variations in TSI. Waple et al. [7] showed that there is a significant response in northern hemisphere surface temperature patterns (period 1650-1850) to the long-term solar variability when lagged by 10-30 years. This lag was explained by an ocean thermal response to the forcing. Using a climate model and empirical temperature reconstructions for the period 1650-1850 Shindell et al. [8] proposed a mechanism, how solar forcing can excite the North Atlantic Oscillation/Arctic Oscillation (NAO/AO). An increase (decrease) in solar radiation leads to a warming (cooling) of the tropical and subtropical sea surface temperature (via increased (decreased) lower stratospheric ozone) causing temperature and pressure changes corresponding to a high (low) NAO/AO index. During periods dominated by one particular phase of the NAO (+/-), summer temperatures in Central Siberia tend to be warmer/cooler, respectively (e.g. [9]). The influence of both, NAO and solar activity on the Belukha temperature record is corroborated by a spectrum analysis revealing typical NAO periodicities at 2.3 and 8.3 years as well as typical solar periodicities at 10.9, 79, and 205 years.

Although direct measurements indicate a decrease in TSI since 1985, the obtained lag of 10 to 40 years might result in a continuing increase of the regional temperatures in the Siberian Altai considering only solar forcing. Thus, our study suggests that in continental areas TSI changes might still be an important forcing factor. Such regional response to individual forcings is not visible when using global mean temperatures.

ACKNOWLEDGEMENT

REFERENCES

[1] M. Stuiver, Nature, **286**, 868 (1980).
[2] A. Mangini et al. Earth Plan. Scien. Lett., **235**, 741 (2005).
[3] N. Scafetta and B.J. West, Geophys. Res. Let., **33**, doi: 10.1029/2006GL027142 (2006).
[4] A. Eichler et al., this report p. 24.
[5] L. Lean, Geophys. Res. Lett., **27**, 2425 (2000).
[6] S.K. Solanki et al., Nature, **431**, 1084 (2004).
[7] A.M. Waple et al., Clim. Dyn., **18**, 563 (2002).
[8] D.T. Shindell et al., Science, **294**, 2149 (2001).
[9] M. Ogi et al., Geophys. Res. Lett., **30**, 1704, doi: 10.1029/2003GL017280 (2003).

TRACE ELEMENT ANALYSES IN SNOW FROM URDOK GLACIER, EASTERN KARAKORAM TO DETERMINE THE PROVENANCE OF MINERAL DUST

Ch. Stenger, H.W. Gäggeler (Univ. Bern & PSI), Ch. Mayer (CG BAdW), M. Schwikowski (PSI)

The aim of this study was to determine the origin of three visible mineral dust layers in a snow pit from Urdok glacier. By comparing the rare earth element (REE) pattern of the Urdok samples with that of well known possible source areas of mineral dust, deserts in China were identified as main provenance.

Mineral dust in ice and snow has aeolian origin and is therefore an excellent tracer for the investigation of atmospheric circulation. In order to gain knowledge about the past atmospheric behavior, the origin and composition of the mineral dust has to be known. Concentrations of trace elements, like the REE, can be used as proxy for the different geological processes in different regions all over the world. The chemical composition, especially for the REE, makes it possible to determine such a geological region and consequently the provenance of the dust itself. In order to estimate the origin of mineral dust, in a study by Svensson et al. (2000) samples from different possible source areas (PSA) were collected [1]. The PSA samples were acid digested and the concentrations of the REE were analyzed and normalized to the Ce concentration. Finally a principal component analysis (PCA) was applied, transforming the multidimensional dataset into a new reference frame. The first component explains the greatest variance of the dataset, the second component the next lower variance and so on [2]. By plotting the new two-dimensional dataset, samples with the same behavior are located in the same area of the plot (e.g. China/Mongolia and Alaska/Canada/US in Fig. 1). The PCA was performed with the free statistical software PAST version 1.74 [3].

Samples from a snow pit were collected at 5400 m a.s.l. at the Urdok glacier in the Karakoram region, Pakistan (Fig. 2). For the digestion 20 g melted snow was evaporated until less than 1 ml remained in the Teflon vessel. Afterwards, 4.5 ml conc. HNO_3 s.p, 1.5 ml conc. HCl s.p. and 1.5 ml conc. HF s.p. was added. The digestion was performed in closed Teflon vessels for 12 min at 180°C in a microwave oven. The solution was evaporated to less than 1 ml, filled up to 10 g with ultrapure water, and analyzed for REE with collision-reaction interface inductively coupled plasma mass spectrometry (CRI-ICP-MS, Varian 820) [4]. Detection limits for the REE elements were less than 3 ppt, except for La (5.7 ppt), Ce (3.3 ppt) and Sm (3.7 ppt). Urdok snow pit samples were treated similarly to PSA samples. The normalization was done to eliminate differences in the concentrations and make the comparison of the REE pattern possible. The ratios La, Pr, Nd, Eu, Gd, Tb, Dy, Ho, Er, Tm and Lu to Ce were used for the PCA.

Fig. 1 shows results of the PCA of the Urdok samples and the PSA from [1]. The PSA from China, Mongolia and Tibet span a pentagon with the Tibet sample in the centre. All Urdok snow samples with high mineral dust load appear close to the Tibet and the China PSA. Urdok samples with low mineral dust content are spread over a wide range, far away from most PSA samples. This suggests that with such low concentrations the main variance in the REE pattern is due to analytical uncertainty, limiting source attribution to samples with high mineral dust content.
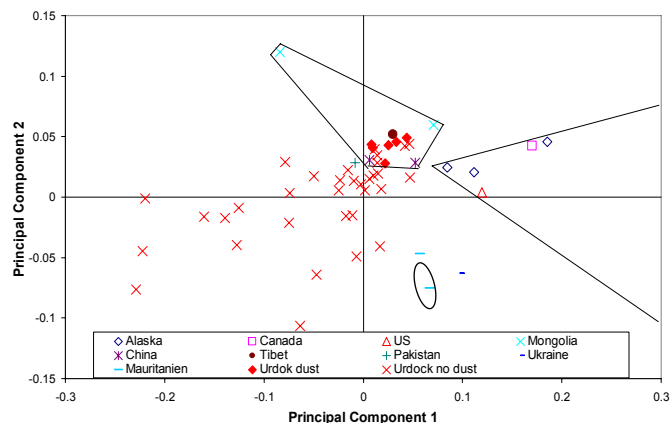
Fig. 1: PCA of PSA samples from [1] and of Udork snow samples with high (red diamonds) and low (red x) mineral dust content.
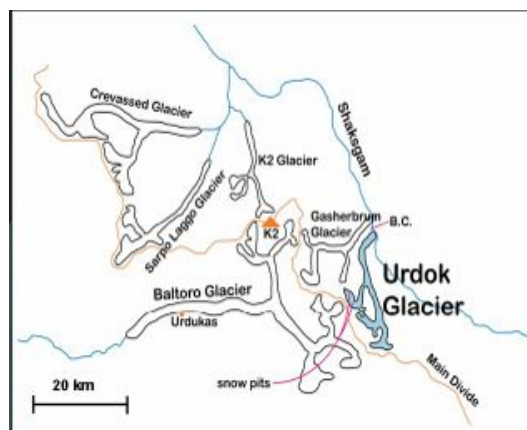
Fig. 2: Map of Urdok glacier in the central Karakoram with snow pit location (approx. Pos. 35° 45.5' N, 76° 42.7' E).

ACKNOWLEDGEMENT

REFERENCES

[1] A. Svensson et al., *J. Geophys. Res.*, **105**, 4637-4656 (2000).

[2] L. Tobler et al., Annual Report Labor Radio- & Umweltchemie 2006, p. 32.

[3] ∅. Hammer, D.A.T. Harper and P.D. Ryan, PAST: Palaeontological Statistics software package for education and data analysis, *Palaeontologia Electronica*, **4(1)**, 9 (2001).

[4] Ch. Stenger et al., Annual Report Labor Radio- & Umweltchemie 2006, p. 31.

MERCURY BEHAVIOUR IN SEASONAL SNOW COVER AT THE JUNGFRAUJOCH

S. M. Biner, A. Ćirić, H. W. Gäggeler (Univ. Bern & PSI), M. Schläppi, L. Tobler, M. Schwikowski (PSI)

Mercury (Hg) was analyzed in snow pit, firn core and surface snow samples in order to identify possible loss mechanisms. Comparison of Hg fluxes indicates that no significant loss occurred. However, elevated concentrations were observed in the topmost cm of the surface snow layer, a finding which cannot be explained yet.

1   INTRODUCTION

Mercury (Hg) exists in different forms in our environment and has a very complex geochemistry, summarized in the Hg cycle. Emission sources can be natural (e.g. soils, forests, volcanoes, lakes and open oceans) and anthropogenic (emissions from fossil fuel combustion, waste incineration and mining). Hg is highly toxic and can easily enter the food chain. Elemental Hg has a long residence time in the atmosphere and is globally distributed. The deposition back to the ground is just a matter of time. In order to estimate anthropogenic and natural emission sources in the past, natural archives such as glacier ice cores can be used. However, in the case of Hg, it is not clear if it is fully preserved in snow and ice. Schuster et al. 2002 reported a Hg profile from the Upper Fremont Glacier (UFG) [1]. The continuity of the Hg profile and the presence of various concentration peaks attributed to volcanic eruptions and anthropogenic activities were interpreted as an indication that Hg is preserved in ice. Another study from Lalonde et al. (2002) presented results that Hg is highly labile in snowpacks and could be rapidly reduced and re-emitted [2]. The aim of this study was therefore to investigate Hg preservation in the seasonal snow cover at the high-alpine research station Jungfraujoch (3450 m a.s.l.).

2   EXPERIMENTAL

Snow pit samples and firn cores were collected at the Jungfraujoch in March, April, and June 2007. In addition, surface snow was sampled in August 2007. Hg concentrations were determined with cold vapour-atomic fluorescence spectrometry (CV-AFS, MERCUR, Analytik Jena). After melting, all Hg species in the liquid samples were oxidized to Hg^{2+} by adding BrCl-solution. Afterwards the excess of free halogens had to be neutralized with $NH_2OH*HCl$. The dissolved Hg^{2+} in the liquid sample is reduced to Hg^0 with $SnCl_2$. Gaseous elemental Hg is purged by Ar from the solution and collected onto a gold trap for preconcentration. After thermal desorption Hg is transported to the fluorescence cell and detected [3].

3   RESULTS AND DISCUSSION

Hg concentrations were in the lower ng/L (ppt) range where the analytical limit is reached (limit of determination: 1.2 ng/L). We could show that Hg is preserved in the seasonal snow cover, since the concentration profile observed in March could be recovered in April and June (Fig.1). Hg fluxes during the overlapping time period showed no significant difference.
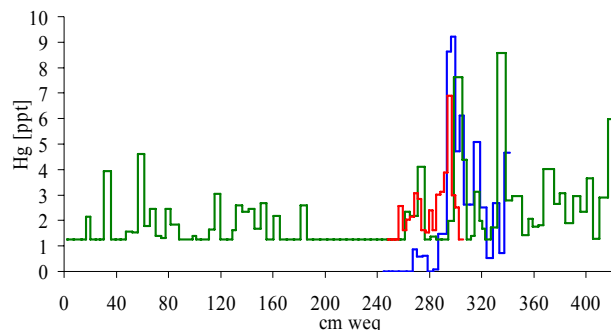
Fig. 1: Hg concentrations in the firn core samples from March (red), April (blue) and June 2007 (green). Concentrations below the limit of determination were replaced by the determination limit. The data set for core April is blank corrected.

A particular loss of Hg was observed in the topmost snow layers during the exceptional conditions in August 2007 with rainfall during the first three days and strong solar irradiation on the last day (Fig. 2). We assume that the Hg is partly percolated with rain and melt water and the other part was re-emitted to the atmosphere due to photoreduction processes. The topmost cm of the surface snow layer showed elevated concentrations of Hg. This was also observed in March, April, and June, but cannot be explained yet.
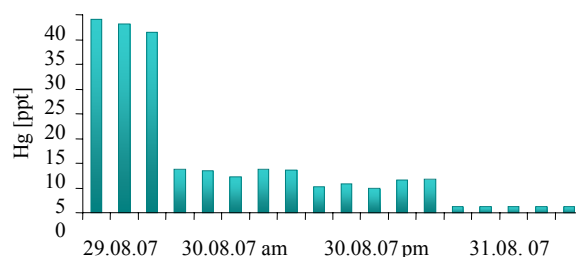
Fig. 2: Hg concentrations of surface snow samples from the Jungfraujoch. Concentrations below the limit of determination (all values for 31.08.07) were replaced by the determination limit.

REFERENCES

[1] Schuster et al., Environ. Sci. Tech., **36**, 2303–2310, (2002).

[2] Lalonde et al., Environ. Sci. Technol., **36**, 174-178 (2002).

[3] United States Evironmental Protection Agency (US EPA), Method 1631 (2001).

^{14}C-DATING OF GLACIER ICE – EXAMPLES FROM THREE CONTINENTS

*M. Sigl, T. Kellerhals, M. Ruff (Univ. Bern & PSI), T. M. Jenk (Niels Bohr Inst.), S. Szidat (Univ. Bern),
A. Eichler (PSI), H.-A. Synal (ETHZ & PSI), L. Wacker, M. Suter (ETHZ), M. Schwikowski (PSI)*

*Carbonaceous aerosols extracted from glacier ice have been dated on the Mini Radiocarbon Dating System
(MICADAS). The potential of this newly developed method is highlighted on examples from three mid-latitude ice
cores. With this unique tool the challenging dating of basal ice can now be achieved.*

INTRODUCTION

Appropriate and precise age-depth models are essential for palaeo-environmental studies [1]. However, often there is a lack of sufficient dating options in ice core archives especially close to bedrock. To overcome this problem a method has been developed using the insoluble organic carbon (OC) fraction of aerosols incorporated in past precipitation to determine ^{14}C concentrations in samples at a microgram level [2].

METHODS

Detailed procedures on sample decontamination and preparation, separation of the OC fraction and AMS ^{14}C determination using the MICADAS system can be found in [2].

Overall blank values for the decontamination, filtration and combustion steps are 1.55±0.74 μg for the carbon mass (m_c) and 0.62±0.10 for the fraction of modern carbon (f_M). Measurements of different reference materials assure the high quality of the AMS based dating [3].

Ice with known age is rare. For validation purpose independently dated ice from Antarctica [4], Greenland [5] and the Alps [6] has been collected but analyses is ongoing, except for one sample from a horizontal ice core at Scharffenbergbotnen (Antarctica) which has been dated to 4580-4150 cal yrs BP. This age is in good agreement with the supposed age of Mid-Holocene [5].

Until now samples from the following ice cores have been analyzed:

Colle Gnifetti, 4450 m, Swiss Alps, 82 m, drilled 2003;

Illimani, 6300 m, Andes, 125 m, drilled 1999;

Belukha, 4062 m, Altai, 140 m, drilled 2001.

Sample sizes reach from 0.3 m up to 1.3 m in length, with an according mass range of 263 g up to 1055 g after decontamination processes. OC concentrations vary between 17 μg/kg (Colle Gnifetti) and 242 μg/kg (Illimani) giving concentrations of 8-90 μg C in the finally measured CO_2 samples. Hence a broad range in precision can be expected from the dating results.

All conventional ^{14}C ages were calibrated using OxCal v3.10 software with the IntCal04 calibration curve and presented here as years before drilling. Additionally the ages of other reference horizons (e.g. volcanoes, dust events) and age model outputs (Fig. 1) are given.

RESULTS

At **Colle Gnifetti** the ages of 9 samples continuously increase with depth, indicating the presence of more than

10,000 year old ice near bedrock. Fitting a simple two parameter flow model [7] through well known reference horizons in the upper part and the ^{14}C dating points in the lower part gives the depth-age model in Fig. 1 [8].
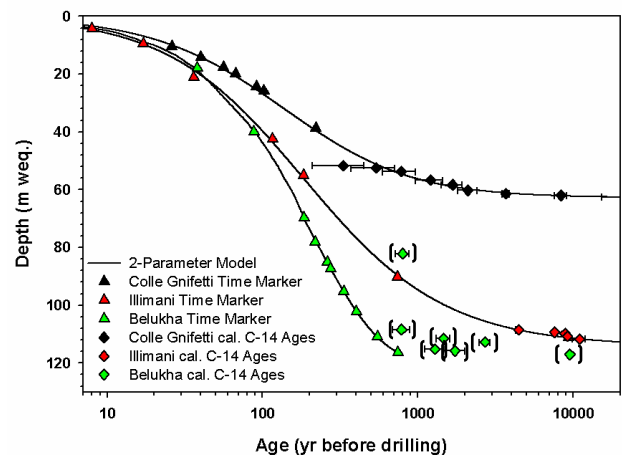
Fig. 1: Age-depth model for Colle Gnifetti, Illimani and Belukha ice cores with ^{14}C dating points and independently dated reference horizons.

In the **Illimani** samples an increase in age with depth was also observed (Fig.1). The ages of the lowermost 3 samples are however equal within their uncertainty, indicating the possibility that ice may be frozen to bedrock 11,000 years ago. Wiggle matching with independently dated ice from a parallel core corroborates the accuracy of our ^{14}C-based dating [9].

So far our efforts on ^{14}C dating of samples from the **Belukha** ice core failed. We think this is due to the utilization of silicon oil, that contains fossil carbon ($f_M = 0$) during ice core drilling process on Belukha. This probably led to a contamination of the samples, which is unfortunately variable in its amount and thus not allows for correction. As expected from the low f_M of the contaminant, this obviously results in an overestimation of the ages (Fig. 1).

REFERENCES

[1]   M.E. Davis et al., Ann. of Glaciol. **43** (2006).
[2]   T.M. Jenk et al., Nucl. Instrum. Meth. B, **259** (2007).
[3]   M. Ruff et al., Radiocarbon **49**(2) (2007).
[4]   A. Grinsted et al., Geophys. Res. Lett. **30**, (2003).
[5]   N. Reeh et al., Ann. of Glaciol. **35**, 136-144 (2002).
[6]   M. Grosjean et al., J. Quat. Sci. **22**, 206 (2006).
[7]   L.G. Thompson et al., Ann. of Glaciol. **14**, 288 (1990).
[8]   T.M. Jenk et al., J.Geophys. Res., submitted.
[9]   S. Knüsel, PhD Thesis, Univ. of Bern (2003).

TEMPERATURE – STABLE ISOTOPE RELATIONSHIP FROM COLLE GNIFETTI - ICE CORE, SWITZERLAND

M. Sigl (Univ. Bern & PSI), T.M. Jenk (Niels Bohr Inst.), C. Barbante (Univ. Venice),
C. Boutron (LGGE) M. Schwikowski (PSI)

Time series relationships and trends from an Alpine ice core and station data are shown over the last 240 years and reveal unexpected connections between climate and proxy parameter that challenge a straightforward interpretation of the proxy data in terms of temperature reconstruction.

Stable isotope records from ice cores are widely used to reconstruct past climate conditions especially in polar regions [1], but increasingly also in mid-latitude high-alpine environments [2]. Temperature during condensation of water vapour leaves a fingerprint in the isotopic composition of precipitation, which can be used to decipher site temperature, applying methods of linear regression [3].

Details on the study site of the ice core location as well as applied methods of $\delta^{18}O$ determination are given elsewhere [4]. The ice core is well dated [5] and long-term trends of $\delta^{18}O$ have already been discussed in a previous report [6].

Often spatial variability of (multi-) annual mean $\delta^{18}O$ in precipitation is used to investigate the sensitivity of ice core $\delta^{18}O$ to mean annual temperature. Following that approach the sensitivity can be estimated by regressing monthly values of $\delta^{18}O_{precipitation}$ of nearby GNIP stations against monthly temperature values. For the months June-July-August the slope of the regression line is 0.80±0.09 ‰/°C taking data from Meiringen, Gutannen and Grimsel from 1970-2004 located north of the ice core site [4].

However, as the Alps are situated in a region where the climate evolution is rather well known from long-term homogenized station data [7] as well as from various climate proxies down to monthly resolution [8] we can study also the temporal behaviour of the proxy-climate relation by directly comparing their time series.

For correlation studies we smoothed predictor and predictant with a 5-year moving average to deal with the dating uncertainty within the proxy data. The time period covered by our temporal calibration studies is 1765 to 2003. As suspected correlations where in general highest between climate variables and proxy between 1930 and 2003 indicating a better reliability in dating compared to time periods prior (Fig. 1). Surprisingly correlations between $\delta^{18}O$ and mean temperature of months when accumulation takes place (e.g. Apr-Sep, Jun-Aug) are with r = 0.28 resp. 0.29 (Sion 482 m; 1866-2001) quite low. The highest correlations are observed with February temperature at this climate station in the Valais valley (r=0.64; p< 1%).

In Fig. 1 temperature time series inferred from gridded homogenized station data [7] are compared with the $\delta^{18}O$ record. They show that the observed high correlation between T_{Feb} and $\delta^{18}O$ are however not stable through time but seem to change in an anticorrelation in the mid 19th century. Assuming correct dating, it is not clear how T_{Feb} should modulate a yearly $\delta^{18}O$ value, which, due to preferred erosion of winter snow, presents mostly summer conditions. It can be in a way that cold winter conditions either lead to less erosion or to more deposition of the

isotopically depleted winter snow and therefore a higher relative fraction within the annual mean value. It might be that the NAO as most important driver of climate variability in European winter is somehow linked to these processes. Regarding long-term trends highlighted by a 31-year smoothing it becomes obvious that the $\delta^{18}O$ curve shows a systematic offset before 1900 and does not indicate colder winter temperatures as seen in the station data for a cold Little Ice Age period.
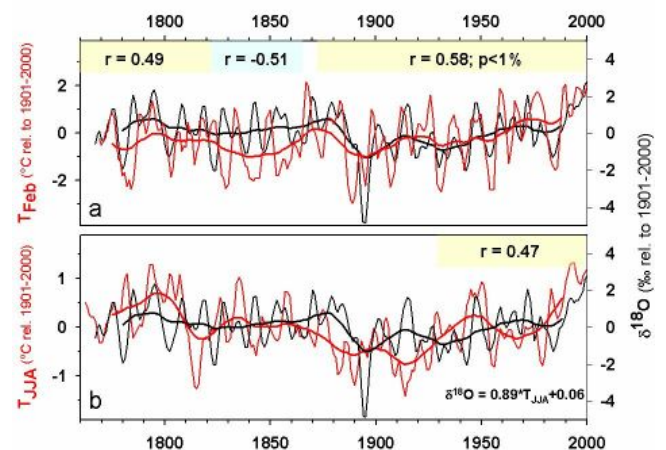
Fig. 1: Comparison between the $\delta^{18}O$ ice core record (black line, weighted 5-yr. running means, smoothed line is a 31-yr. running average) and temperatures anomalies relative to 1901-2000 of **a)** February (T_{Feb}) and **b)** June-July-August (T_{JJA}) from gridded station data (46°N,7°E) of the same time resolution. Highlighted are periods with rather high correlation (yellow) or anticorrelation (blue). Significances of the correlations have been calculated by correcting for autocorrelation [9]. For T_{JJA} the slope of the regression is shown for the period 1930-2000.

REFERENCES

[1] S.J. Johnsen et al., J. Quat. Sci., **16** (2001).
[2] K. Henderson et al., J. Geophys. Res., **111** (2006).
[3] W. Dansgaard, Tellus, **16** (1964).
[4] D. Bolius, PhD thesis, Univ. of Bern (2006).
[5] T.M. Jenk et al., J. Geophys. Res., submitted.
[6] D. Bolius et al., Ann. Rep. Labor Radio- & Umweltchemie, Univ. Bern & PSI (2005), p. 26.
[7] I. Auer et al., Int. J. Climatol. **27** (2007).
[8] C. Casty et al., Int. J. Climatol. **25** (2005).
[9] Dawdy & Matalas, In V.T. Chow (Ed.) Handbook of Applied Hydrology (1964).

FIFTEEN CENTURIES' RECORD OF ATMOSPHERIC LEAD CONTAMINATION FROM THE COLLE GNIFETTI ICE CORE, SWISS-ITALIAN ALPS

J. Gabrieli, C. Barbante (Univ. Venice), M. Sigl (Univ. Bern & PSI),
M. Schwikowski (PSI), C. Boutron (LGGE Grenoble)

Concentrations of lead and 23 other elements were determined at high resolution in the deepest 40 m of an ice core from Colle Gnifetti glacier (Monte Rosa). The palaeorecord reflects the history of atmospheric Pb contamination over the last 15 centuries.

INTRODUCTION

Few ice core records from the Alps are currently available and normally cover a rather short period of at best few centuries. A noteworthy exception is the Colle Gnifetti saddle in the Monte Rosa area (4450m a.s.l., Swiss-Italian Alps). Here the net accumulation rate is only 0.3 m weq because of wind erosion during winter seasons. For this reason at this site it is possible to recover well preserved environmental and climatic records older than 1000 years. In 2003 two parallel cores were drilled in the saddle with length of about 81 m. The first core, characterized by an excellent firn/ice quality except for a small section between 76 and 78 m, has just been analyzed for major ions, stable isotopes at PSI. The dating carried out both by traditional and new methods [1] confirmed that several thousand years old ice is present.

Here we present a preliminary highly resolved record of lead for the deepest 39 m core section.

METHOD

To achieve high resolution records and to simplify the decontamination process a continuous ice core melting (CIM) device coupled to a quadrupole inductively coupled plasma mass spectrometer (ICP-Q-MS) was constructed [2,3]. The uncontaminated meltwater flux is split, allowing continuous conductivity measurements and the collection of discrete samples. The meltwater from the outer section is introduced into a solid phase C18 (SPE) cartridge, previously washed and conditioned for on-line organic compounds extraction (Fig. 1).
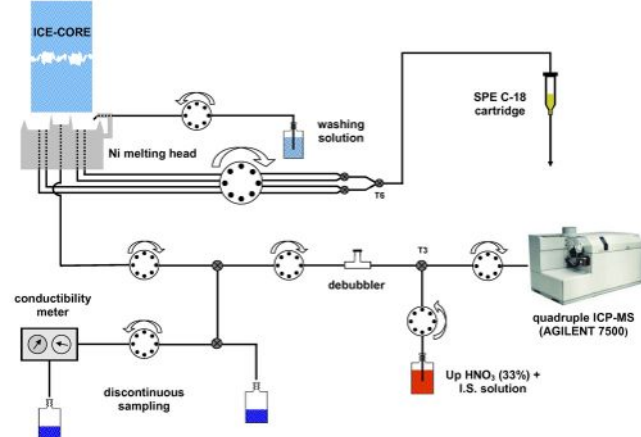
Fig. 1: Coupling of CIM device to analytical system.

RESULTS

The chronological record of lead is shown in Fig. 3. As expected a concentration increase is observed from the first

part of 19th century corresponding to the beginning of the industrial period [4]. The maximum concentration measured was 2.8 ng/g with a mean value of 0.24 ng/g. The record also shows an interesting feature with increased concentrations between 800 and 1000 (Fig. 3). The calculated enrichment factor is greater than 100 from 800 to 1200 suggesting a substantial anthropogenic contribution, not well explainable at this time. Comparison with others elements, organic compound such as PAHs and levoglucosan and data from different palaeorecords (peat moss and lake sediments) could help us to answer this question.
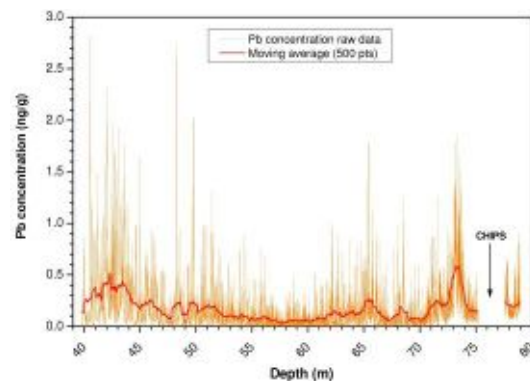
Fig. 2: Pb concentration record for the deepest 39 m of the Colle Gnifetti core analysed by CIM ICP-Q-MS.
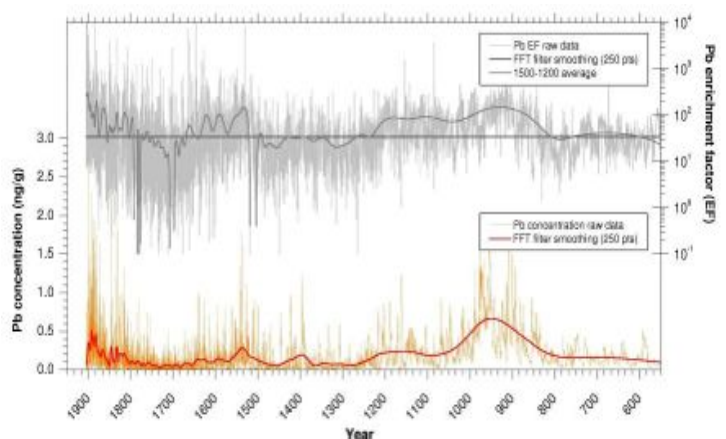
Fig. 3: Pb concentration and enrichment factor over the last 15 centuries.

REFERENCES

[1] Jenk et al., *J. Geophys. Res.*, submitted.
[2] Osterberg et al., *Environ. Sci. Techn.*, 40, 3355 (2006).
[3] Knüsel et al., *Environ. Sci. Techn.*, 37, 2267 (2003).
[4] Schwikowski et al., Environ. *Sci. Techn.*, 38, 957 (2004).

ANTHROPOGENIC AEROSOL RECORD FROM A HIGH-ALPINE ICE CORE (COLLE GNIFETTI)

F. Thevenon (Univ. Bern), M. Sigl (Univ. Bern & PSI), M. Schwikowski (PSI)

The insoluble carbonaceous aerosols entrapped in the Glacier Colle Gnifetti (45°N, 7°E; 4450 m asl) have been analyzed for reconstructing pre-industrial biomass burning activity and fossil fuel combustion aerosol emissions.

1   INTRODUCTION

Aerosols provide the dominant negative (cooling) climate forcings, masking some of the greenhouse gas-induced warming and limiting the ability to use the modern temperature record for accurate predictions of future climate [1]. In particular, open questions are related to the nature of the combustion-originating aerosols as well as to its contribution to the climate system, and its spatiotemporal variability with regards to past human activities and land management. In order to reconstruct the anthropogenic disturbances (caused by biomass burning and fossil fuel combustion) on past climate, we analyzed combustion aerosols transported to the Alps and deposited on Colle Gnifetti glacier during the last centuries.

2   STUDY SITE AND METHOD

In 2003 a 80-m long ice core was drilled down to the bedrock on the high-alpine glacier saddle Colle Gnifetti, located in the Monte Rosa massif (45°N, 7°E) at an altitude of 4450 m asl.. Due to the preferential wind erosion of light winter snow at this site, the glacier saddle accumulates snow mainly during summer, implying preservation of the last 400 years at reasonable time resolution (Fig. 1). In order to extract the combustion-originating aerosols, we analyzed the insoluble carbonaceous particles with an elemental analyzer coupled to a mass spectrometer, after removing mineral (by HCl acidification) and organic (by thermal oxidation at 320°C) carbon components. To make our results comparable to a similar study on the Glacier Fiescherhorn [2], the measured elemental carbon (EC or black carbon) values were multiplied by a factor of 2.

3   RESULTS

The Colle Gnifetti EC record (Fig. 1) and the carbon isotopic composition of EC (δ^{13}C) which provided indication about the type of vegetation being burnt [3] indicate relatively low biomass burning activity (13±5 μg EC kg^{-1}) before the beginning of the fossil fuel era around 1850 AD, whereas the δ^{13}C values suggest that the combustion of wood (-24 to -25 ‰) was the main source of pre-industrial atmospheric EC emissions, especially during the cold period of the Little Ice Age (Fig. 1). Average EC values during industrial (1850-1975) and modern times (1950-1975) increased from 26 to 39 μg EC kg^{-1}, respectively. These results demonstrate the human impact on the emissions of carbonaceous aerosols throughout the last centuries, and point out the increasing contribution from the fossil fuel combustion after 1850. EC concentrations are in general agreement with results from the Fiescherhorn glacier [2], but slightly lower than published in a previous study on a different core from Colle Gnifetti [4].
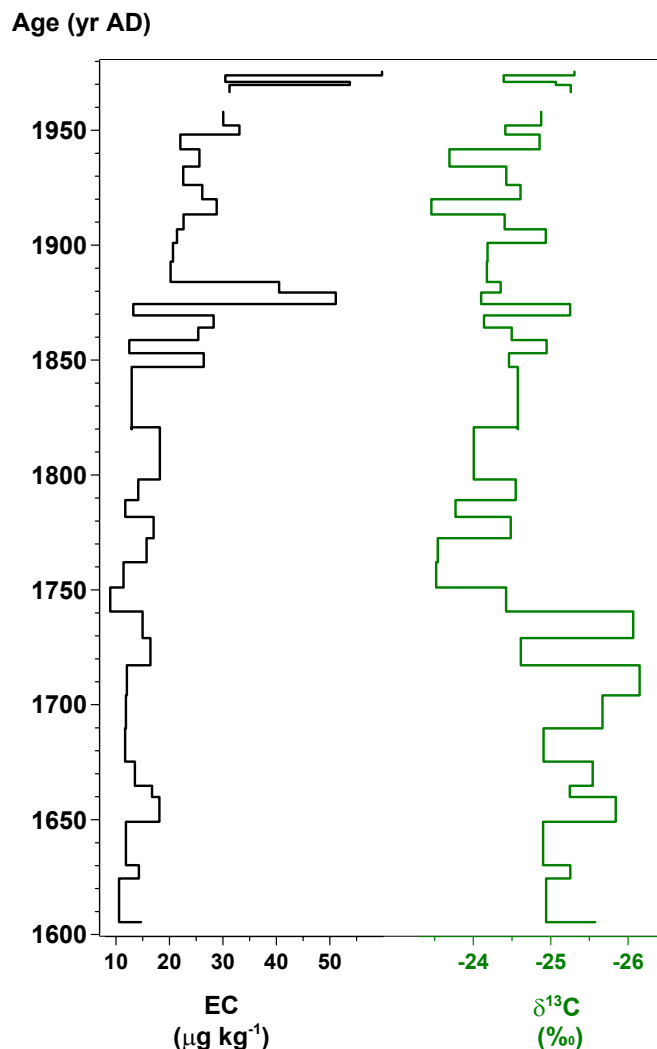
Fig. 1: Elemental Carbon (EC) and δ^{13}C records of Colle Gnifetti ice core.

REFERENCES

[1]   IPCC, 2007. The Physical Basis of Climate Change. Intergovernmental Panel on Climate Change.

[2]   T.M. Jenk, S. Szidat, M. Schwikowski, H.W. Gäggeler, S. Brütsch, L. Wacker, H.-A. Synal, M. Saurer, *Atmos. Chem. Phys*. **6**, 5381-5390 (2006).

[3]   J.S. Clark, E.C. Grimm, J. Lynch, P.J. Mueller, *Ecology* **82**, 620-636 (2001).

[4]   V.M.H. Lavanchy, H.W. Gäggeler, U. Schotterer, M. Schwikowski, U. Baltensperger, *J. Geophys. Res*. **104**, 21227-21236 (1999).

CRYSTALLOGRAPHIC AND CHEMICAL ANALYSIS OF FOLIATION: GRENZGLETSCHER, VALAIS, SWITZERLAND

R. Rüegg, M. Lüthi (VAW ETHZ), M. Sigl (Univ. Bern & PSI), M. Schwikowski (PSI)

We found strongly anisotropic glacier ice with c-axes aligned perpendicular to foliation in three horizontal ice cores from the surface of Grenzgletscher, Valais, Switzerland. The ice cores recovered from the surface are about 0.7 m long and cross-cut a well developed foliation. Grain size is compatible with an estimated age of the cores of 30 to 150 years. Complementary analysis of chemical species and isotope ratio show seasonally looking variations which are, however, not correlated. Also no correlation with air bubble density or grain size could be found. We conclude that the foliation visible at the glacier surface is not identical to the initial stratigraphy, but formed by processes related to ice deformation.

INTRODUCTION

Ice in the ablation area of temperate glaciers is anisotropic not only close to the bedrock, but throughout the ice mass. Indication for this anisotropy is the compact banded structure of foliation visible on the glacier surface and in moulins and boreholes. Foliation is defined by alternating lenses or discontinuous layers of bubble-rich and clear ice, or of fine and coarse grained ice. Foliation layers are often folded and are typically between 0.5 and 20 cm thick. Foliation often crosscuts primary stratification which indicates that it is formed as a new structure by ice deformation.

METHODS

Three horizontal ice "cores" were recovered from the surface of Grenzgletscher (Valais, Switzerland) for structural and chemical analysis [1]. The sampling locations are in the confluence zone of Grenzgletscher and Gornergletscher, at an elevation of about 2500m a.s.l.

All ice cores were analyzed for their visible features. The only structural feature visible in the back-lighted ice cores is a layering of different appearance due to the varying density of air bubbles. These layers were classified into four different classes of air bubble density (none, low, medium, high).

Thin sections for c-axis fabric analysis were prepared with a microtome. Ice crystal orientation was measured on the thin sections using polarized light. The process was greatly facilitated by using the Automatic Ice-Texture Analyser (AITA) and the Investigator software to analyze the fabric.

About 30 ice samples (typical volume $60 \times 15 \times 15$ mm^3) were cut from each ice core to analyse chemical species of the different layers. Ion concentrations of the melted ice samples were analyzed with standard ion exchange chromatography. The oxygen isotope ratio $\delta^{18}O$ was determined with an isotope ratio mass spectrometer on the same ice samples prepared for the chemical analysis.

RESULTS AND DISCUSSION

Glacier ice from the surface of the ablation area of Grenzgletscher is highly anisotropic. In ice core thin sections we found a fabric with three or five maxima in areas with coarse grained ice, and a double maximum at a site with fine-grained ice. The fabric maxima were aligned perpendicular to the visible foliation, defined by layers of bubble rich ice.

The foliation on the glacier surface is not identical to the primary stratification. No correlation between ion concentration, stable isotope composition, grain size or density of air bubbles could be found in the ice cores (Fig. 1). A further piece of evidence is a band of yellow ice that approximately follows a flow line throughout the ablation area, and which is in concordance with the surrounding folded foliation.

Ice anisotropy seems to be an important aspect of mountain glaciers that has been neglected in modeling efforts. It has been shown in laboratory experiments that a pre-existing fabric is rapidly overgrown by recrystallization, and has little influence on the final fabric, i.e. the memory of the material is very limited. This gives rise to the possibility to include the effects of anisotropy in a flow model as a local quantity, determined by the instantaneous strain rate field.
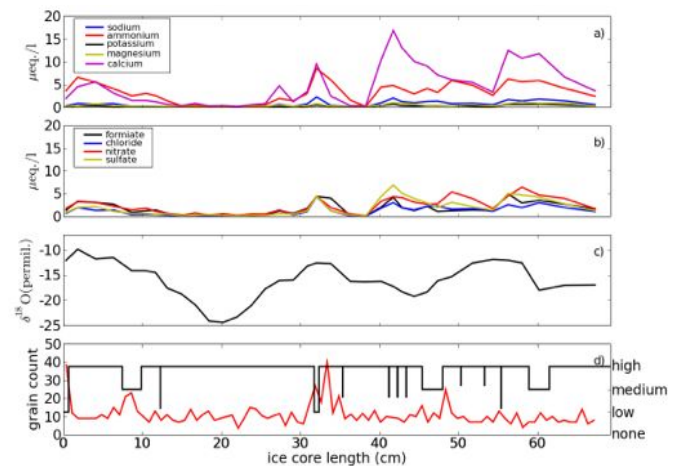
Fig. 1: Parameters analysed in the Center core. a) Cation and b) anion concentrations in μeq./l. c) Stable isotope ratio is given by $\delta^{18}O$ in ‰. d) Number of grains in thin sections perpendicular to foliation, counted in regular intervals. The histogram shows density of air bubbles classified as none, low, medium and high. Length along the ice core is given from north to south.

REFERENCE

[1]   R. Rüegg, M. Lüthi, M. Schwikowski, M. Funk, A. Svensson, G. Durand, *J. Glac.,* submitted.

AMMONIUM AS NEW PROXY FOR TROPICAL TEMPERATURES IN AN ICE CORE FROM NEVADO ILLIMANI, BOLIVIA

Th. Kellerhals, H.W. Gäggeler (PSI & Univ. Bern), S. Brütsch, M. Schwikowski (PSI)

The ammonium record of an ice core from Nevado Illimani, Bolivia, was used to reconstruct past temperature in this region for the last ~1600 years. Considerably colder temperatures are inferred for the 14th to 17th century, while relatively warm temperatures prevailed over much of the 11th to 13th century.

1   INTRODUCTION

The temporal and spatial extent of climate fluctuations during past millennia is vividly debated. While the terms "Little Ice Age" and "Medieval Warm Period" can be used beyond controversy to describe the most recent advances of mountain glaciers in Europe during the 16th – mid 19th century and the relatively warm conditions in Europe during the 10th – 12th century, there notion for globally synchronous cold and warm periods has been dismissed. There is evidence for colder and warmer periods in numerous locations also outside the influence of the North Atlantic [1], but their timing, magnitude and spatial extent are unclear. This is especially true for the tropics, where proxy data are scarce. Furthermore, temperature reconstructions using oxygen isotopes in tropical ice cores are hindered by the oxygen isotopes' sensitivity to precipitation in tropical regions [2].

Here we present the ammonium record of an ice core from Nevado Illimani (16°39'S, 67°47'W; ~6300m asl), Bolivia, as a new proxy for tropical temperature.

2   CALIBRATION

The timescale for the Illimani core was derived from a multiproxy approach including annual layer counting, tritium and volcanic reference horizons for the upper part of the core (including the "1258 AD" volcanic eruption) and ^{14}C dating [3] for the lower part. A two parameter model was fitted to these time markers to get a continuous depth – age relationship.

Ammonium in the Illimani ice core is believed to originate mainly from the tropical vegetation in the Amazon Basin and to be transported by easterly winds to the Illimani. Warmer (colder) tropical temperatures are thought to influence the source strength and to result in higher (lower) amounts that are deposited on the glacier.

Because there are no long time series of instrumental station data available for this region, the gridded HadCruT3 30°S – 30°N tropical temperature anomalies [4] from 1850 to 1998 were used for this analysis. The NH_4^+ data were averaged to yearly values and split into different series for calibration(1998-1924) and verification (1924-1850) (Fig. 1). The calibration series was significantly correlated (p<0.001) with the annual tropical temperature anomalies.

3   RECONSTRUCTION

The reconstructed temperature anomalies for the last 1600 years (Fig. 2) show a period with lower temperatures during the 7th to 10th century followed by relatively warm conditions during the mid 11th to the 13th century. A considerably cooler period is observed from the 14th to the 17th century. In the following centuries, a rise in temperature can be noticed that exceeds in the late 20th century the range of past variation.

Fig. 1: Top panel: Yearly averaged NH_4^+ values (black) and smoothed with a binomial filter (brown). Bottom panel: 30°S – 30°N temperature anomalies [4] (red), reconstructed temperature anomalies from NH_4^+ for the calibration period (blue) and the verification period (purple).
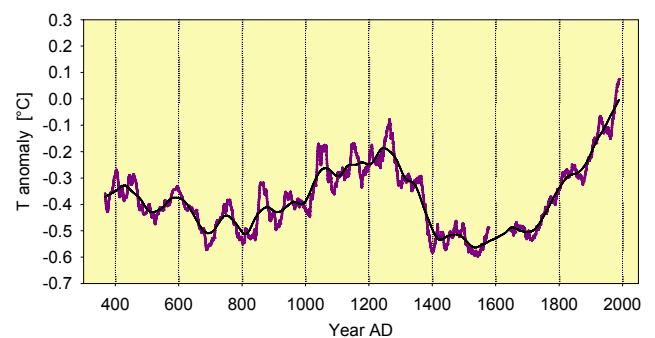
Fig. 2: Reconstruction of the tropical temperature from the NH_4^+ record; 31 years moving average (purple) and smoothed (black).

REFERENCES

[1] P. D. Jones and M. E. Mann, Rev. Geophys., **42,** RG2002 (2004).
[2] G. Hoffmann et al, Geophys. Res. Lett., **30**, 4, 1179 (2003).
[3] M. Sigl et al, this report, p. 28.
[4] P. Brohan et al, J. Geophys. Res., **111**, D12106 (2006)

A PRONOUNCED DRY SPELL IN SOUTH AMERICA ~5000 YEARS AGO AS RECORDED IN AN ICE CORE FROM NEVADO ILLIMANI, BOLIVIA

Th. Kellerhals, H.W. Gäggeler (PSI & Univ. Bern), A. Laube, M. Schwikowski (PSI)

A remarkable mid-holocene dry event has been detected in an ice core form the eastern Bolivian Andes. It occurred ~5000 years ago, lasted for several hundred years and was synchronous with other reconstructions of extraordinary dry climatic conditions in South America, Africa and Asia.

1   INTRODUCTION

In contrast to the last glacial stadial, for which numerous events of abrupt climate change (e.g. Heinrich events, Dansgaard-Oeschger events) are known, the Holocene was perceived until recently as a period of relatively stable climatic conditions. However there is also evidence for major climatic disruptions in various regions of the world. There were, for example, periods with very low lake levels in tropical east Africa [1] and effects of these droughts were noticed in Africa, the Middle East and western Asia [2].

Here we present results from the chemical and isotopic investigation of the lowermost 6 meters of an ice core that was drilled on Nevado Illimani (16°39'S, 67°47'W, ~6300 m a.s.l.), located in the eastern Bolivian Andes, which indicate that a pronounced dry spell occurred also on the Bolivian Altiplano.

2   METHODS

Dating of this section of the core was possible through microgram level ^{14}C analysis by accelerated mass spectrometry. Five calibrated ages from 4400 ± 160 years BP to 10900 ± 1050 years BP have been determined. These ages, along with reference horizons from known volcanic eruptions in the upper part of the core were used to establish a continuous age-depth relationship by fitting a two parameter model to these time markers.

The analyses of $\delta^{18}O$ were performed by isotope ratio mass spectrometry (Delta Plus XP, Finnigan MAT) with a precision of $\pm 0.1‰$. The concentrations of major ionic species (cations: Na^+, NH_4^+, K^+, Mg^{2+}, Ca^{2+}; anions: F^-, $HCOO^-$, $CH_3SO_3^-$, Cl^- $NO3^-$, SO_4^{2-}, $C_2O_4^{2-}$) were determined using standard chromatographic techniques.

3   RESULTS AND DISCUSSION

During the end of the last glacial stage, $\delta^{18}O$ values were low (-22‰), indicating a cold and wet climate (Fig. 1). After ~10 kyr BP, they start to rise and stabilize at -16‰ a few thousand years later. This 6‰ rise is thought to reflect the transition to a warmer and drier climate as $\delta^{18}O$ in the tropics both depends on temperature and precipitation.

Around 5 kyr BP, a second sharp rise of ~2‰ is observed. This rise is paralleled by a very pronounced increase in the concentrations of the ionic species, as exemplified for calcium and sodium (Fig. 1). These concentrations are the highest throughout the whole core and extend over a section of approximately 1m, covering a time span of several hundred years. After this excursion, both $\delta^{18}O$ values and ion concentrations sharply return to lower values. Previous

studies have found that on a seasonal and interannual timescale, high dust values on the Illimani occur in the dry season and during prolonged El niño phases [3]. We therefore interpret the enriched $\delta^{18}O$ values and the greatly enhanced ion concentrations as a signal of an extraordinary dry period.
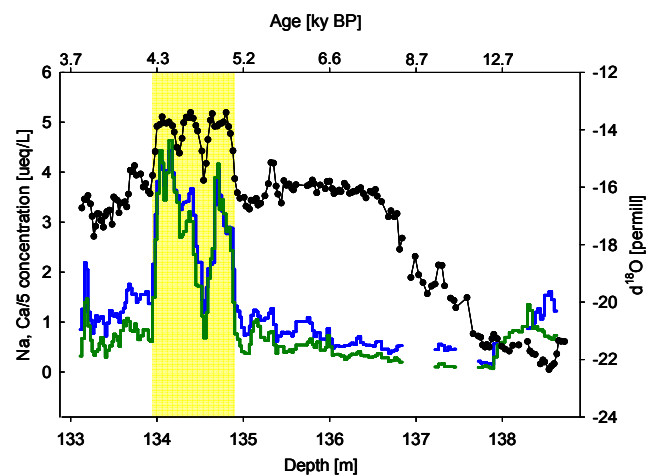
Fig. 1: $\delta^{18}O$ record (black), right scale, together with sodium (blue) and calcium (green) concentrations, left scale, for the last ~6m of the Illimani core, covering a time span from the late glacial stage to the mid-holocene.

An extremely dry period is also reported from nearby lake Titicaca between 6 an 5 kyr BP, when it fell to it's lowest level of the past 25 kyr [4]. Additional evidence for a widespread period of aridity comes from the Gulf of Oman [5], where a similar double peak structure is observed and from Western Tibet [6].

REFERENCES

[1]   F. Gasse, Quat. Sci. Rev., **19**(1-5), 189-211 (2000)
[2]   F. Street-Perrot and R. Perrot, Nature., **343**, 607 (1990).
[3]   S. Knüsel et al, J. Geophys. Res., **110**, D01102 (2005).
[4]   P. Baker et al, Science, **291**, 640 (2001).
[5]   Cullen et al, Geology, **28**(4), 379-382 (2000).
[6]   F. Gasse and E. Van Campo, EPSL, 126, 435-456.

RESPONSE OF REGIONAL CLIMATE AND GLACIER ICE PROXIES TO EL NIÑO-SOUTHERN OSCILLATION (ENSO) IN THE SUBTROPICAL ANDES

E. Dietze (TU Dresden & PSI), A. Kleber (TU Dresden), M. Schwikowski (PSI)

We studied the relationship and teleconnection patterns between regional climate in the subtropical Andes and glacier ice proxies as derived from the Tapado ice core. Only major ion concentrations seem to capture ENSO variability in the Cerro Tapado region.

1   AIM OF STUDY

El Niño-Southern Oscillation (ENSO) is an important element of earth's ocean-climate system. To further understand its past variability, proxy records from climate archives need to be studied. Ice cores from high alpine glaciers may contain high resolution ENSO proxy information given the glacier site is climatologically sensitive to ENSO. We investigated the signals of ENSO in the climate of the subtropical Andes in the proximity of Cerro Tapado glacier (30°08'S, 69°55'W, 5550m a.s.l.), where a 36 m long ice core was drilled in 1999 [1]. Several proxy records derived from this ice core were studied with regard to their relation to local and regional climate as well as to ENSO.

2   RESULTS

We used annual and semi-annual precipitation and temperature time series from meteorological stations in the region and interpolated grids for correlation analyses with some ENSO indices (SOI, Niño 3.4 index, CEI) and ice core-derived proxies net accumulation, stable isotope ratio $\delta^{18}O$, major ion concentrations, see Fig. 1.
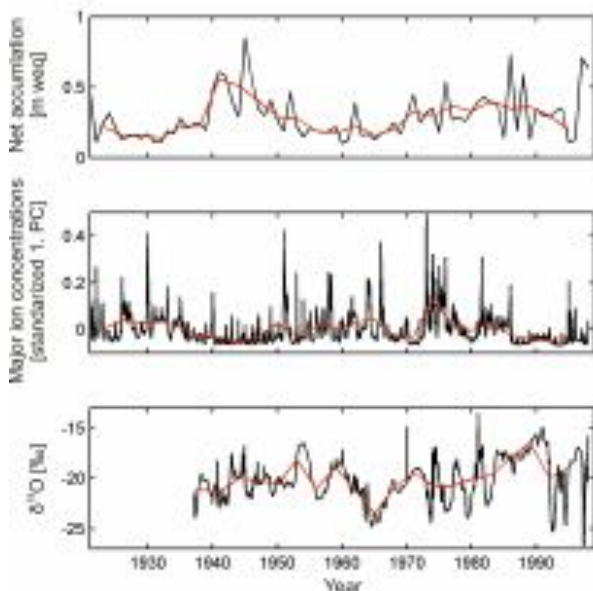
Fig. 1: Records of Cerro Tapado ice core proxies net accumulation, first PC of major ion concentrations and $\delta^{18}O$. Original data sets in black and three-year non-moving averages ending 1995 in red.

This resulted in a spatial distribution of regional ENSO-teleconnection patterns of different intensities. Only in the western, i.e., Mediterranean Andes precipitation is higher (lower) during El Niño (La Niña) events, especially at higher altitudes depending on the latitudinal shift of the subtropical jet stream and frontal activity during austral winters. However, temperature anomalies respond to ENSO more stably in space and time, being higher (lower) during El Niño (La Niña) events in most of the subtropical Andes all year long. Glacier ice proxies are found to be predominantly connected to eastern Andean summer rain climate, which contradicts previous studies and the modern mean spatial boundary between subtropical summer and winter rain climate derived from the grid data (Fig. 2).
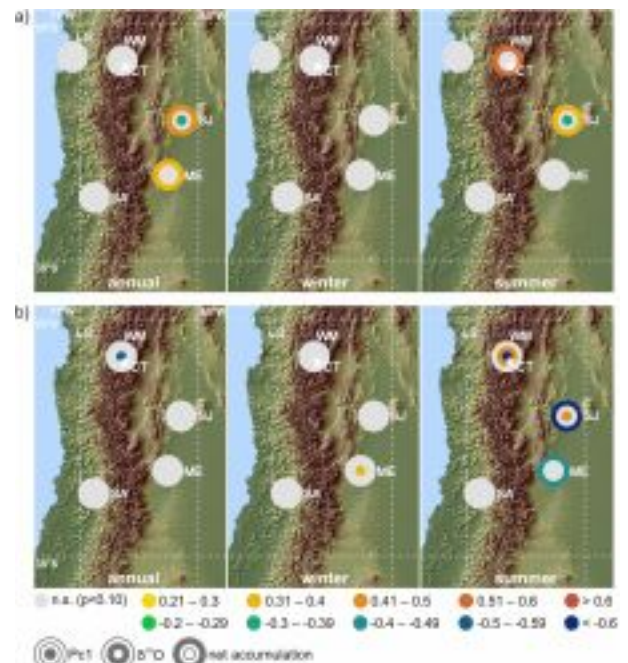
Fig. 2: Coefficients of correlation between Cerro Tapado ice core proxies (inner to outer ring: PC1 of the major ion concentrations, $\delta^{18}O$ and net accumulation) and meteorological data of a) precipitation and b) temperature. WM: grids [2] close to Cerro Tapado (CT); LS: La Serena, SA: Santiago, SJ: San Juan, ME: Mendoza meteorological station.

This is supported by a low connection of the glacier records to ENSO, as summer precipitation in north western Argentina does not respond to ENSO. Only major ion concentrations seem to be altered by ENSO via local temperature, indicating a reduction of sublimation and mineral dust input during El Niño years due to a lower water vapour gradient between snow and air. Thus, major ion concentrations are suitable ENSO proxies in the Cerro Tapado region.

REFERENCES

[1] P. Ginot, PhD Thesis, Univ. Bern (2001).

[2] C.J. Willmott and K. Matsuura, Center for Climatic Research, Univ. Delaware (2001).

DATING OF THE ICE CORE FROM CERRO MERCEDARIO, ARGENTINA

A. Ciric, H. W. Gäggeler (Univ. Bern & PSI), E. Vogel (Univ. Bern), J. Eikenberg, L. Tobler, M. Schwikowski (PSI)

Nuclear dating with ^{210}Pb and annual layer counting using ammonium and δ^{18}O peaks result in slightly different ages at 35 m water equivalent depth of 105± 10 (1 σ) years and 75±10, respectively. The tritium maximum in 1964/1965 from the nuclear weapon tests has not yet been found. Thus, dating of the Mercedario ice core has still a high uncertainty.

In 2005 a 104 m ice core from the La Ollada glacier on Cerro Mercedario (31°58'S, 70°07'W, 6100 m a.s.l.) was recovered [1]. A set of different parameters has been analyzed in this core such as major ions (e.g. Na^+, NH_4^+, Ca^{2+}, Cl^-, NO_3^-, SO_4^{2-}) using ion chromatography, δ^{18}O and δD with isotope ratio mass spectrometry, Hg with atomic fluorescence spectroscopy, ^{210}Pb with α - spectroscopy, ^{3}H with liquid scintillation counting and several trace elements with inductively coupled plasma mass spectrometry [2].

Dating the ice core was performed by annual layer counting (ALC) using the ammonium and δ^{18}O profile, showing pronounced seasonal patterns throughout the whole core. Annual δ^{18}O averages of the last 45 years are comparable with annual temperature averages of Santiago (33°S) which supports the dating. However, the annual layer counting uncertainty is rather high, (75±10 years at 35 m water equivalent (weq.) depth), because of the occurrence of double peaks and shoulders in the δ^{18}O.

As additional method, nuclear dating with ^{210}Pb is applied. ^{210}Pb has a half-life of 22.3 years and is a member of the natural decay chain of ^{238}U via gaseous ^{222}Rn that constantly emanates from the earth's crust. It is attached to aerosols and then removed from the atmosphere by wet or dry deposition. This method can be used to date firn and ice up to 150 years [3]. Fig. 1 shows the background corrected ^{210}Pb activity for the upper 35 m weq. This correction is due to the background of the detectors and not equal for each data point. The resulting age is 105±10 years at the depth of 35 m weq. with an annual accumulation of 0.33 m weq. It is unclear if the ^{210}Pb signal is disturbed due to the high abundance of mineral dust [4] or if the background is overestimated. Both could explain the discrepancy compared to dating with ALC. The latter could be effected as well by years without snow accumulation.

An important reference horizon is the maximum in the tritium activity resulting from the nuclear weapon tests (1964/1965, northern hemisphere: two years earlier). Tritium (^{3}H) is a radioactive β-emitter and has a half-life of 12.3 years. ^{3}H was analyzed with liquid scintillation counting (LSC) in samples between 9.2 and 14.4 m weq. depth, where the horizon was assumed. However, no ^{3}H peak could be detected. Except for one sample at 10.1 m weq., all values were below detection limit (DL) and even negative ones resulted due to background correction. Assuming that this one sample represents the ^{3}H horizon, an annual accumulation of around 0.26 m weq. would result, which is slightly lower than expected from ^{210}Pb dating and annual layer counting. In addition, the ^{3}H activity would be lower than in other ice cores from the Southern Hemisphere, e.g. Cerro Tapado (maximum 32 T.U. [5]).
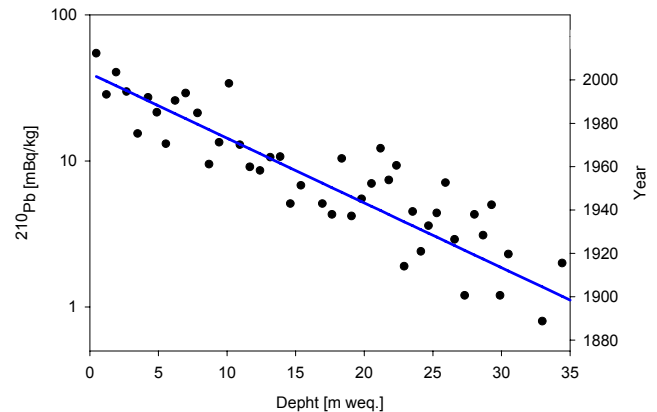
Fig. 1: Background corrected ^{210}Pb activity (mBq/kg, black dots) against depth. The resulting age is indicated by the blue line.

There are two possible explanations: The ^{3}H horizon is not located at this depth or the LSC method is not sufficiently sensitive. The next steps are finding the correct background correction for ^{210}Pb by analyzing deeper parts and using a more sensitive method for ^{3}H determination, which is mass spectrometry of its daughter ^{3}He [6]. Radiocarbon dating of the last two cores is also ongoing [7] as is glacier flow modeling.

REFERENCES

[1] M. Schwikowski et al., Annual Report Labor Radio- & Umweltchemie 2006, p. 36.
[2] L. Tobler et al., this report, p. 38.
[3] H. W. Gäggeler et al., J. of Glaciol. **29**(101), 165-177 (1983).
[4] A. Ciric et al., this report, p. 37.
[5] P. Ginot, PhD thesis, University of Bern, 2001.
[6] B. M. Oliver et al., Appl. Radiat. Isot., **38** (11), 959-965 (1987).
[7] T. Jenk et al., Nucl. Instrum. Meth. B, **259** (2007).

MAJOR IONS IN THE MERCEDARIO ICE CORE

A. Ciric, H. W. Gäggeler (Univ. Bern & PSI), S. Kälin, M. Schwikowski (PSI)

Mineral dust is a main component in the Mercedario ice core. This is seen in the high abundance of calcium and sulfate, in the chloride to sodium ratio lower than the typical sea salt ratio and in the excess of cations in the ion balance.

Ice core records of trace species like sulfate, calcium and ammonium can be used to reconstruct past atmospheric composition and changes in atmospheric circulation [1]. Understanding the past atmospheric composition and its natural variability may help to determine the anthropogenic influence on earth climate. During the last year the ion record of the Mercedario ice core (104 m) was completed. The analysis of 3512 samples (resolution 2-2.5 cm water equivalent (weq.)) was performed with ion chromatography, a sensitive method for quantifying anions and cations down to the lower ppb (μg/l) range. We analyzed the following ions: Na^+, NH_4^+, K^+, Mg^{2+}, Ca^{2+}, F^-, Cl^-, NO_3^-, SO_4^{2-}, $CH_3SO_3^-$, $CH_3CO_2^-$, HCO_2^-, and $C_2O_4^{2-}$.

Sulfate and calcium are the most abundant species in the Mercedario ice core (Fig. 1) and account for 54% of the analyzed ions. Mineral dust is possibly their main origin, but there are also anthropogenic sources, especially for sulfate (e.g. fossil fuel combustion) [2]. A high correlation between these two species is observed, but the sulfate to calcium ratio differs when looking at samples with visible dust (slope: 0.68, R^2=0.78) or samples without visible dust (slope 0.84, R^2=0.65). In both cases sulfate is less abundant than calcium.

The origin of nitrate (abundance 15%) is not yet clear. Possible sources are marine and soil emissions, biogenic emissions, biomass burning, fossil fuel combustion and lightning. Slightly higher concentrations are observed in the upper 10 m weq., possibly indicating increased anthropogenic emissions.

Chloride and sodium (abundance 17%) are assumed to originate mainly from sea salt, but they have also other sources as seen in the chloride to sodium ratio. In sea water this ratio is 1.16 [3], whereas it is 1.01 in the Mercedario core. The higher amount of sodium might be due to input of mineral dust or halites. The assumption that both ions have more than one source is supported by a bimodal frequency distribution of the logarithmic values of the concentrations (Fig. 2).

The high abundance of mineral dust is also seen in the ion balance by an excess of cations (Fig. 3). A component that we cannot analyze is carbonate, the corresponding anion of calcium and magnesium in carbonates. The excess in anions is used to identify volcanic layers as dating horizons. Mainly sulfate, chloride and fluoride are then increased [4]. Five layers with strong anion excess were detected, but only one consists of more than one sample. Additionally, a slight anion increase was observed in the upper 10 m weq., possibly due to anthropogenic influences. Higher sulfate to calcium ratios appear in this part. The increase can be due to anthropogenic sulfur dioxide emissions from fossil fuel combustion [5] or copper mining.
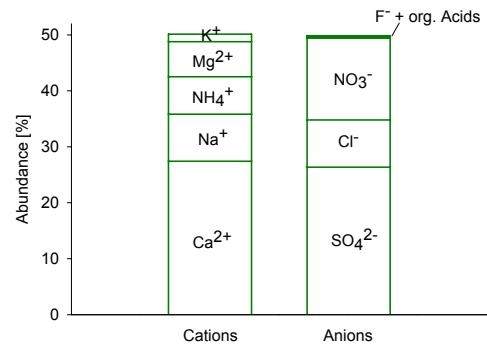
Fig. 1: Relative abundance [%] of anions and cations in the Mercedario ice core.
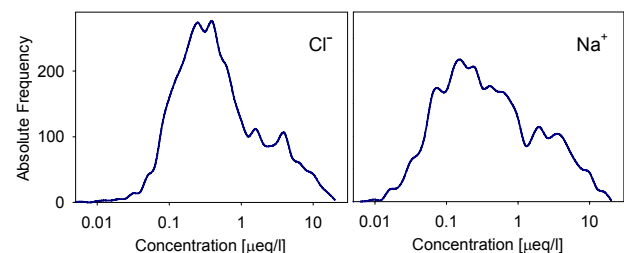
Fig. 2: Frequency distribution of chloride (left) and sodium (right) in the Mercedario ice core.
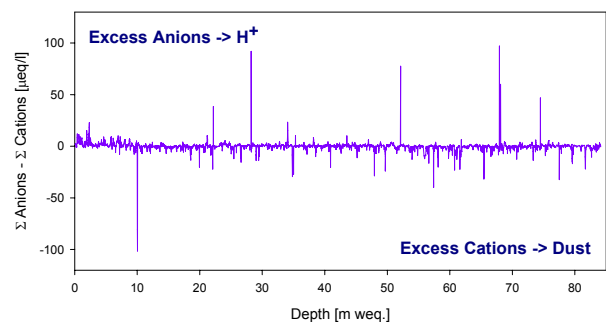
Fig. 3: Ion balance of the Mercedario ice core showing sporadic excesses in anions (e.g. volcanic events) and cations (e.g. mineral dust).

REFERENCES

[1] S. Kaspari et al. Geophys. Res. Lett. **34**, L16701, doi:10.1029/2007GL030440 (2007).

[2] S. Olivier et al., J. Geophys. Res. Atmospheres **111**, D05309, doi:10.1029/2005JD005830 (2006).

[3] W.C. Keene et al., J. Geophys. Res., **91** (D6), 6647-6658 (1986).

[4] G. A. Zielinski et al., J. Geophys. Res., **100**, 20937–20955 (1995).

[5] M. Schwikowski et al., Tellus, **51B**, 938-951 (1999).

TRACE ELEMENT ANALYSIS OF THE MERCEDARIO ICE CORE WITH CIM-ICP-SF-MS

L. Tobler (PSI), A. Ciric (PSI & Uni Bern), Y. Bächtiger, M. Schwikowski (PSI)

*Concentrations of trace elements are determined with **C**ontinuous **I**ce **M**elting (CIM) **I**nductively **C**oupled **P**lasma **S**ector **F**ield **M**ass **S**pectrometry (ICP-SF-MS) in an ice core from the La Ollada glacier on Cerro Mercedario, Argentina. Method comparison with Ion Chromatography (IC) for Ca, Mg, and Na showed good agreement. Records of soil derived elements are highly correlated and suggest pronounced seasonality.*

INTRODUCTION

The knowledge of trace element concentrations in ice cores from high-mountain glaciers helps to reconstruct past atmospheric conditions and air pollution. This is a prerequisite for the prediction and interpretation of future climate variations. Trace elements are of interest because they provide the possibility to identify various sources and to understand biogeochemical cycles. The intent of this work is to analyze an ice core drilled at the La Ollada glacier on Cerro Mercedario (31°58.S, 70°07.W, 6100 m a.s.l.) [1] in the Central Argentinean Andes for trace elements, in order to get insight into the past of South America's climate and air pollution, e.g. from mining and smelting of heavy metals. Results of the trace element analysis of the first few meters between 55 and 66 m depth are presented.

EXPERIMENTAL

Ice bars of about 70 cm length and 2.3 x 2.3 cm^2 area are cut out of the inner part of the ice core with a band saw in a cold room. Each ice bar is then placed on a melting head at 55°C inside a freezer for analysis. The melt water of the inner part of the ice bar is acidified to ~ 0.25 mol HNO$_3$, shortly behind the melting head. Sample uptake is done by a self-aspirating nebulizer of the APEX introduction system (Elemental Scientific Inc., Omaha, USA) and the generated dry aerosol is transported to the ICP-SF-MS (Element1, Finnigan MAT, Bremen, Germany). Accuracy and reproducibility of the method were shown in previous works [2, 3]. Parallel ice bars of the same ice core were already analyzed by ion chromatography [4].

RESULTS

The comparison of the ICP-SF-MS results to the IC results for the elements Mg and Na is given in Fig.1. The records for Na show in general a good agreement. However, the results for Mg give larger deviations, which can be explained by the fact that with IC only soluble Mg is analyzed, whereas with ICP-SF-MS, Mg containing dust particles in the samples are at least partly dissolved by the acidification and /or destroyed by the hot plasma. At all, the appearance of small stones and visible dust particles in this ice core is exceptional. Therefore, many elements, having their source mostly from soil derived particles, show highly significant correlation coefficients (r > 0.945), which are found for the elements Al, Cs, Fe, Mg, Rb, Sc Th, U, V, and Zr. As an example the records of four of these elements are presented in Fig. 2. They were chosen according to their concentration levels, covering the range from ng/L up to mg/L. The fluctuation of these concentration signals might be attributed to strong seasonal variations with high dust deposition during austral summer. The analysis of the upper part of this ice core is still ongoing.
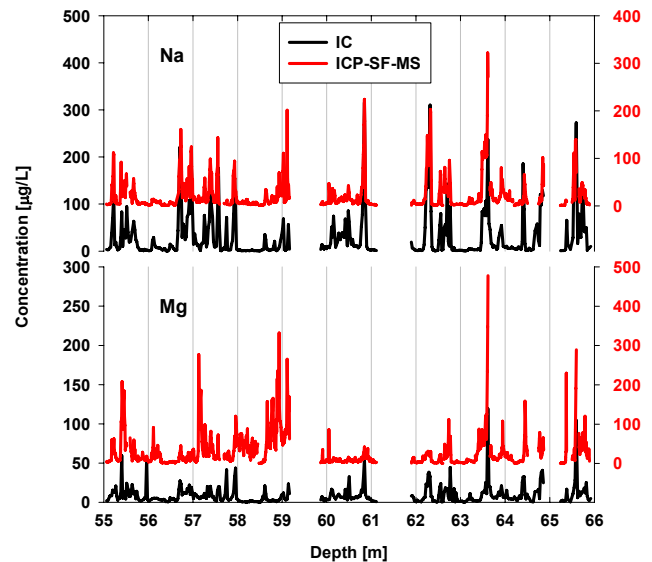
Fig. 1: Comparison of the IC and ICP-SF-MS analyses for an ice core section from Cerro Mercedario.
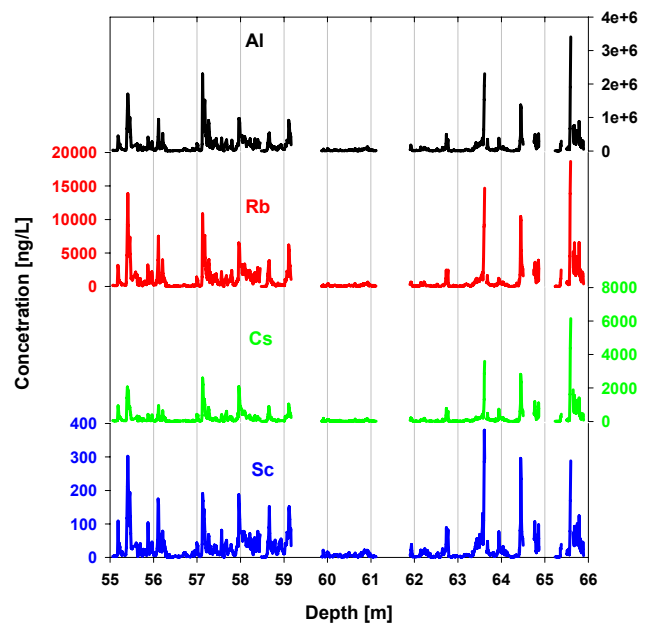
Fig. 2: Records of soil derived elements in an ice core section from Cerro Mercedario.

REFERENCES

[1] M. Schwikowski et al., Annual Rep. Lab. for Radio- and Environ. Chemistry, Uni Bern & PSI (2005), p. 36.
[2] S. Knüsel et al., Environ. Sci. Technol., 37, 2267-2273 (2003).
[3] T. Kellerhals et al., Annual Rep. Lab. for Radio- and Environ. Chemistry, Uni Bern & PSI (2006), p. 27.
[4] A. Ciric et al., Annual Rep. Lab. for Radio- and Environ. Chemistry, Uni Bern & PSI (2006), p. 28.

FIRST RESULTS OF THE ICE CORE FROM PIO XI, SOUTHERN PATAGONIAN ICE FIELDS

M. Schläppi (PSI & Univ. Bern), G. Casassa, A. Rivera (CECS), A.-L. Grauel, M. Schwikowski (PSI)

Major ion concentrations and the stable isotope ratio $\delta^{18}O$ were determined in the 50.6 m long ice core from Pio XI. First results show a well preserved signal with a strong influence of marine air masses.

An ice core from the Patagonian Ice Fields may provide basic information on precipitation at high latitudes, changes in position and strength of westerly airflow, and could close the information gap between tropical and subtropical latitudes in South America and Antarctica [1]. A 50.6 m ice core drilled in the accumulation area of Pio XI glacier in 2006 is investigated. At that site effects of melt water formation are assumed to be small because of the altitude of 2600 m asl. First results show a clear oceanic signal.

Major ion concentration were analysed with ion chromatography for the upper 34.4 m (21.8 m weq) and the stable oxygen isotope ratio $\delta^{18}O$ was determined with stable isotope mass spectrometry for the upper 36.9 m (22.5 m weq) and between 42.1 m (26.4 m weq) and 50.6 m (32.4 m weq).

Major ion concentrations show the dominance of sea spray constituents Na^+ and Cl^- (Tab.1). Other ion concentrations are rather low, especially for ions with anthropogenic origin such as NO_3^-, NH_4^+, but also for mineral dust tracers like Ca^{2+} and Mg^{2+}. Interesting is the high contribution of sea salt to the Mg^{2+} concentration (126%) which cannot be explained yet (Tab.1).

Tab. 1: Mean ion concentrations (μEqL^{-1}) and contribution by sea salt (%) in the ice core.

	Na^+	NH_4^+	Mg^{2+}	Ca^{2+}	Cl^-	NO_3^-	SO_4^{2-}
Mean ion conc. ($\mu Eq\ L^{-1}$)	1.70	0.12	0.30	0.19	1.97	0.24	0.53
Contribution by sea salt (%)	100	12	126	38	100	4	45

Previous studies [2] showed that the Cl^- to Na^+ ratio is a good indicator of melt water percolation. In the case of Pio XI core both ion concentrations are highly correlated (r=0.84; n=856) and from surface till 9 m weq depth the mean ratio is in good agreement with the sea salt ratio of 1.17, suggesting that no significant melting took place (Fig.1). Around 10 m weq, 15 m weq and 19 m weq fluctuation in sea salt ratio indicate strong melting effects.
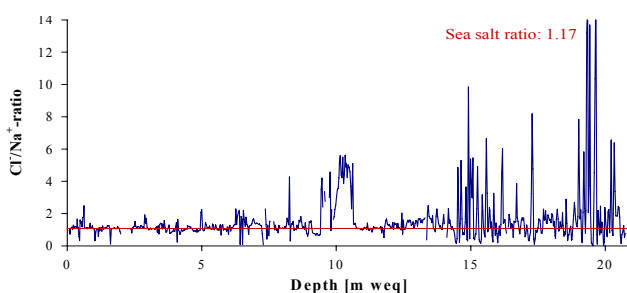
Fig. 1: Cl^-/Na^+ ratio against depth (blue).

The $\delta^{18}O$ record shows large fluctuations between -23.6‰ and -7.5‰ (Fig. 2). We assume that these fluctuations reflect seasonality. The average of -14.8‰ is higher than expected for this altitude from previous studies [1]. Interesting is also the long term oscillation of around 6.5 m weq.
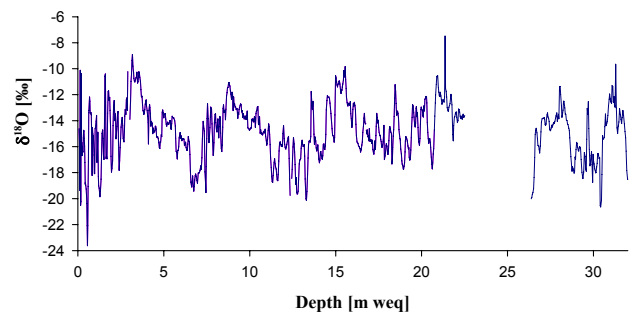
Fig. 2: $\delta^{18}O$ record of Pio XI ice core.

Previous studies demonstrated that dimethylsulfate (H_3C-S-CH_3) is oxidised to sulfate (SO_4^{2-}) and has a seasonal cycle at marine sites with maxima in summer [3]. At Pio XI sea salt sulfate (ss sulfate) concentrations show seasonal fluctuation presumably due to the stronger westerlies in summer (Fig. 3) [4]. High non sea salt sulfate (nss sulfate) concentrations suggest that marine dimethylsulfate is an additional source of sulfate [4]. Further work will focus on dating. This includes identification of annual layers and nuclear dating (^3H and ^{210}Pb).
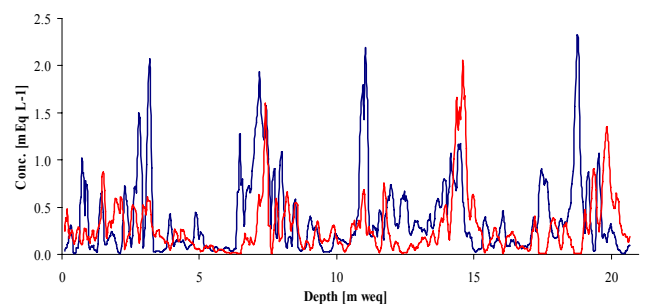
Fig. 3: ss sulfate (blue) and nss sulfate (red) concentration (five points running mean) against depth in upper 21 m weq of Pio XI ice core.

REFERENCES

[1] M. Schwikowski et al., Annals of Glaciology, **43**, 8-13 (2006).
[2] A. Eichler et al., Tellus, **53B**, 192–203 (2001).
[3] G.P. Ayers et al., Nature, **349**, 404-406 (1991).
[4] J.F Carrasco et al, In: The Patagonian Ice Fields, Kluwer Academic, 29-41 (2002).

ALGAL BIOVOLUME OF THE PIO XI ICE CORE FROM THE SOUTHERN PATAGONIAN ICEFIELDS

P. Santibáñez, G. Casassa, P. Labarca (CECS), S. Kohshima (Tokyo Institute of Technology), J. Jaramillo (Universidad Austral de Chile), M. Schläppi (PSI & Univ. Bern), M. Schwikowski (PSI)

A 50 m long ice core of Pio XI, Southern Patagonian Icefield, was retrieved during August 2006. The snow algae content of the core was analysed. The biological analyses will be a valuable tool for dating and to estimate past annual glacier mass balance.

INTRODUCTION

The Patagonian Icefields are temperate glaciers, where the analysis of ice cores is difficult since seasonal signals of isotopic contents and chemical species are strongly disturbed due to melt water and percolation [1, 2]. Consequently, other methods are necessary to characterise and date ice cores from these glaciers.

Studies of microorganisms that live on temperate glaciers can provide a novel method for ice core dating. Analyses of snow algae have been performed earlier in snow and ice cores such as in Yala glacier in the Nepal Himalayas [3], Tyndall glacier in the Southern Patagonia Icefield [2, 4], Sofiyskiy glacier in the Russian Altai [5], and Volcán Mocho-Choshuenco and Volcán Osorno glaciers in the Chilean Lake District [6]. These investigations together with other studies of algal communities of the glacier surface conclude that snow algae are a useful seasonal and annual marker for ice core dating and assessment of past annual mass balance at low-mid latitudes and low altitudes [e.g. 7, 8]. Here we show algal biovolume results for the first 23 m of the PIO XI core.

METHODS

Sample processing

The ice core samples were cut at the PSI cold room in sections of 20 cm long to 40 m, down to were cut in sections of 10 cm long, scraping off a 1 cm section of the core surface for eliminating possible contaminants. The samples were packed into sterile plastic bags (*Nasco* Whirl-Pack) and later melted at room temperature in a laboratory at PSI, each sample being bottled in a 50 mL sterile plastic container. All samples were then immediately preserved in a freezer at –20º C.

Sample analysis

The samples were mounted and fixed inside a laminar flow table in a laboratory at PSI. Filtering of 20 mL samples was performed using hydrophilic polytetrafluoroethylene (PTFE) membrane filters (JHWP013000: 0.2 μm pore size, 13 mm diameter; Millipore, USA). Each filter was mounted and fixed in glycerol, formalin and water solution (1:1:1 volume) on a glass slide under cover-slip. The glass slides were then sipped to CECS, Chile, where biological analyses were performed.

Counts of microalgae and pollen grains were made with a fluorescent microscope (OLYMPUS BX-FLA). The total cell number of microalgae was estimated on each filter by counting the cells along 5 to 7 parallel transects.

The algae cells were classified according to their morphotypes, which correspond to microalgae showing the same morphological and size characteristics. Mean cell volume was estimated by measuring the size of 20 – 80 cells for each morphotype, classifying their sizes in intervals of 1 μm. Algal biovolume was determined using the technique developed by Yoshimura and others (1997, 2000) and Hillebrand and others (1999).

RESULTS

Seventeen morphotypes of microalgae were observed in the first 23 m of the ice core (Fig. 1a). Fifteen morphotypes belong to Division Chlorophyta and two morphotypes belong to Division Cyanophyta. Algal biovolume values are less than those reported in other ice core studies. Nevertheless, important fluctuations and many peaks are observed in the algal biovolume profile (Fig. 1b), the largest peaks presumably being formed during the melt season. Therefore, together with chemical, isotopic and physical profiles, the algal biovolume in this ice core is expected to be valuable for dating and to estimate the past annual glacier mass balance.
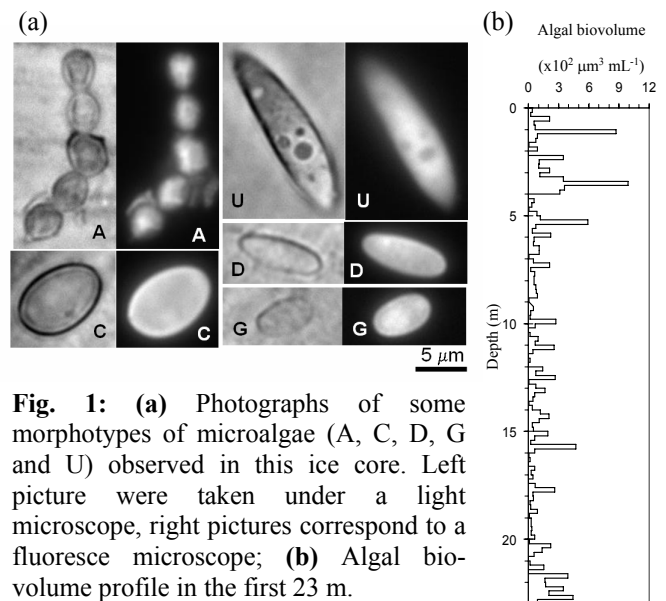
Fig. 1: **(a)** Photographs of some morphotypes of microalgae (A, C, D, G and U) observed in this ice core. Left picture were taken under a light microscope, right pictures correspond to a fluoresce microscope; **(b)** Algal biovolume profile in the first 23 m.

REFERENCES

[1] M. Schwikowski et al., Annals Glaciol. **43**, 8-13 (2006).
[2] T. Shiraiwa et al., Annals Glaciol. **35**, 84-90 (2002).
[3] Y. Yoshimura et al., J. Glaciol. **46** (153), 335-340 (2000).
[4] S. Kohshima et al., Global Planet. Change. **59**, 236-244 (2007).
[5] J. Uetake et al., Annals Glaciol. **43**, 70-78 (2006).
[6] P. Santibáñez et al., submitted to J. Glaciol.
[7] Y. Yoshimura et al., Arct. Antarct. Alp. Res. **29** (1), 126-137 (1997).
[8] N. Takeuchi and S. Kohshima, Arct. Antarct. Alp. Res. **36** (1), 92-99 (2004).

PRODUCTION OF AN ICE-STANDARD

D. Hofer, T. Stocker (KUP), T. Huthwelker, L. Tobler, M. Schwikowski (PSI), B. Wehrli (ETH Zurich)

Glacial ice cores are recorders of atmospheric composition and therefore provide information about the climate system in the past. Usually sample preparation for chemical analysis is very laborious and therefore continuous ice melting systems are applied. For these techniques an ice-standard is desired.

INTRODUCTION

Glaciochemical data from ice cores provide valuable information about past climate variability and atmospheric chemistry. However, sample preparation for chemical analysis of trace and ultratrace components in ice core is very tedious, stimulating the development of a continuous ice core melting system [1]. This development has reduced sample preparation time and increased sample resolution. Over the past decade, ice core melter systems have utilized in-line continuous flow analysis (CFA) techniques [1, 2] or have coupled a melter to various trace analysis techniques (ion chromatography, inductively coupled plasma mass spectrometry, stable isotope mass spectrometry etc.) see e.g. [3-7]. For calibrating these ice core analysis systems, an ice-standard would be highly desirable.

Two ideas of producing an ice-standard were tested.

IDEA 1:

Ice grains, made of a standard solution, are pressed until the pores become enclosed. By using the home-build ice grain apparatus at PSI [8], it was possible to check the practicality of this idea.

It was not a problem to reach densities that ensured closure of the pores between the grains. Unfortunately, chemical analysis of the ice grains with inductively coupled plasma aass spectrometry (IPC-MS) revealed high trace element concentrations (e.g. Zn, Ca, Cu, Pb, Fe, Na), suggesting that contamination of the ice grain surface occurred during the production processes. It was not possible to identify the sources, but the most likely candidate is liquid nitrogen.

Fig. 1: Photo of the produced ice grains with diameters of 700-1000 μm.

IDEA 2:

A rotated cylinder in a frigid ambiance freezes radial. Thereby the dissolved substances get displaced to the rotation axis. The result is a high concentration at a defined place.

First tests with dissolved colour pigments and different rotation velocities showed promising results. However, the analysis of the radioactive iodine-131 after the freezing, performed with single photon emission computed tomography (SPECT) showed the incompleteness of the segregation.

Other problems were small bubbles and the uncontrolled growth of ice dendrites. The situation improved upon faster rotation.
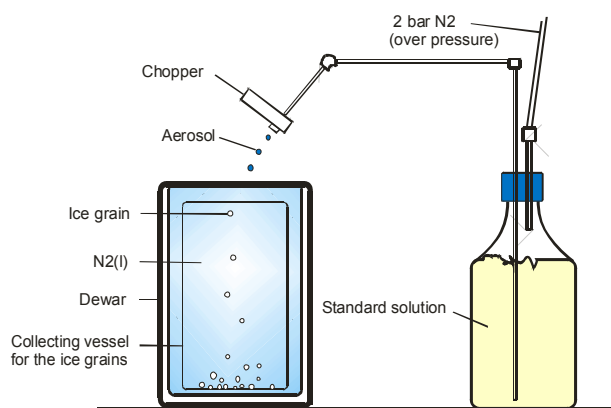
Fig. 2: Schematic of the ice-grain apparatus.

CONCLUSION

The results show that using the segregation phenomenon is not suitable for a chemical ice standard. The distribution of the substances in the ice cylinders was too inordinate and the interferences because of dendrites and bubbles were too strong.

The idea of pressed ice grains has much more potential. The problem with the contaminations should be solvable. This method allows the fabrication of multi component standards. By stacking different standard cylinder separated by clean ice cylinders the production of a very useful ice standard for calibration of CFA systems should be possible.

REFERENCES

[1] A. Sigg et al., Environ. Sci. Technol. **28**, 204 (1994).
[2] R. Röthlisberger et al., Environ. Sci. Technol. **34**, 338 (2000).
[3] R. Udisti et al., Ann. Glaciol. **30** (1), 20 (2000).
[4] M. Leuenberger et al., Anal. Chem. **74**, 4611 (2002).
[5] J.R. McConnell et al., Environ. Sci. Technol. **36**, 7 (2002).
[6] S. Knüsel et al., Environ. Sci. Technol. **37**, 2267 (2003).
[7] E. Osterberg et al., Environ. Sci. Technol. **40**, 3355 (2006).
[8] T. Bartels-Rausch et al., Atmos. Chem. Phys., **2**, 235 (2002).

COMPOSITION OF TWO ICE CHUNKS THAT FELL OUT OF THE CLEAR SKY IN HABSBURG (AG) AND ALBERSWIL (LU)

S. Schmoker, M. Schläppi (Univ. Bern & PSI), R. Rüegg (VAW ETHZ), S. Brütsch, A. Laube, L. Tobler,
M. Schwikowski (PSI)

Sources for large ice chunks falling out of the clear sky are discussed controversially, including extraterrestrial material, aircrafts, and hailstone formation. Chemical and stable isotope analysis of the two ice chunks collected in Habsburg and Alberswil indicated that they were formed by freezing of technical water on an aircraft. This contradicts the hypothesis that such ice blocks are large hailstones.

INTRODUCTION

The phenomenon that large blocks of ice, weighing up to hundreds of kilograms, fall out of the clear sky has been observed in various regions of the world [1]. It is usually believed that the chunks originate from aircraft icing processes, wastewater loss from aircraft lavatories or leakage of water tanks. Recently, on the basis of chemical and stable isotope analysis of several ice chunks collected in Spain in the year 2000 it was concluded that they were large hailstones. A novel mechanism for generating was proposed, involving nucleation on remnants of jet contrails and growing in a particularly moist lower stratosphere [2]. However, this hypothesis is discussed controversially.

Two ice chunks that were collected in Habsburg and Alberswil, Switzerland gave us the opportunity to test the hypothesis.

EXPERIMENTAL

The first ice chunk crashed through the roof of a house in Habsburg (AG) shortly after noon on 31 December 2006. The second one fell also at noon on 13 March 2007 in Alberswil (LU) on a meadow, leaving a pile of ice and a crater. In our ice room both chunks were photographed and samples were cut along a horizontal profile using our band saw (Fig. 1). Samples were analysed for pH, major ion concentrations, trace elements, and stable isotope composition $\delta^{18}O$ and δ^2H with a pH electrode, ion chromatography, ICP mass spectrometry, and stable isotope mass spectrometry, respectively. In addition, thin slices were prepared for structural analysis. For comparison, samples of technical water collected on different commercial flights and potable water from the region were analysed as well.

RESULTS

The mean stable isotope composition of the ice chunks from Habsburg and Alberswil is rather similar with $\delta^{18}O$ of 7.05 and 6.54‰ and δ^2H of 47.8 and 45.7‰, respectively. All values fall onto the meteoric water line, excluding extraterrestrial water as a possible source. The mean ion concentration and the pH are comparable to that of technical water used in aircraft lavatories (Fig. 2). The main difference to typical rainwater or cloudwater is the high degree of mineralisation and the high pH. We therefore conclude that the two ice chunks were formed by freezing of technical water on the outside of an aircraft.

Fig. 1: Photo of the cross-section of the ice chunk from Habsburg.
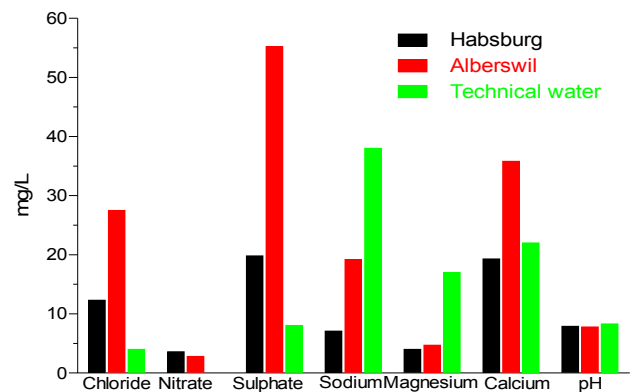
Fig. 2: Mean ion concentrations in ice chunks and technical water used in aircrafts (in mg/L except for pH which varied between 7.8 and 8.3).

REFERENCES

[1] J. Martinez-Frias & A. D. Huertas, Ambio, **35**, 314-316 (2006).
[2] X. Bosch, Science **297**, 765 (2002).

EXCITATION FUNCTIONS FOR THE PRODUCTION OF ^{129}I AND ^{36}Cl IN THE REACTION ^{209}Bi(p,xn/yp)Z

D. Schumann, J. Neuhausen (PSI), R. Michel (ZSR Hannover), H.-A. Synal, V. Alfimov (ETH Zürich), J.-Ch. David (CEA-Saclay)

^{129}I and ^{36}Cl were chemically separated from proton-irradiated bismuth targets by distillation followed by precipitation of the silver salts. From the content of the radionuclides determined by Accelerator Mass Spectrometry (AMS), the cross sections were calculated. The results are compared with theoretical predictions.

INTRODUCTION

For the development of high power spallation targets heavy metals such as Pb, Bi and Hg are of special interest, due to their high number of released neutrons. The estimation of the residue nuclide production in these elements is important for radiation safety considerations. Thin proton-irradiated Bi targets were used to determine the cross sections of long-lived residues. In [1] we reported on the separation of ^{108m}Ag from this target material. The present report is dedicated to the determination of the excitation functions for the production of ^{36}Cl and ^{129}I.

EXPERIMENTAL

A description of the proton-irradiated bismuth targets including the beam history can be found in [1].

Chlorine and iodine can be separated from the target material dissolved in half concentrated HNO_3 by distillation in a N_2 stream. At first, iodine is distilled into hydrazine solution at a temperature of 55°C. Then this valve is closed and the other one for the chlorine distillation is opened. The temperature is increased to 70°C and Cl is directly absorbed in $AgNO_3$ solution. Details of this separation equipment can be seen in the schematic view of Fig.1.
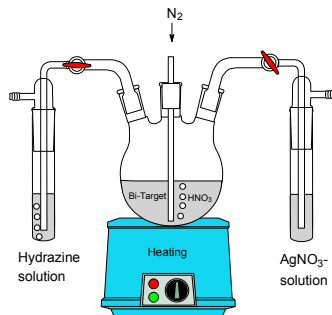
Fig.1: Schematic view of the separation apparatus

The hydrazine solution is acidified with HNO_3 and AgI is precipitated adding $AgNO_3$ solution. After washing the precipitate twice with bi-distilled water the sample is ready for AMS measurement.

The AgCl precipitate is dissolved in NH_3-solution and $Ba(NO_3)_2$ is added to remove possible traces of sulphur (^{36}S), the stable isobar of ^{36}Cl. Subsequently, AgCl is re-precipitated by acidifying the solution. After washing with bi-distilled water the sample is ready for the AMS measurements, which were carried out at the Van de Graaff EN tandem accelerator at IPP(ETHZ).

RESULTS AND DISCUSSION

In Figs. 2 and 3 the cross sections for the production of ^{36}Cl and ^{129}I, respectively, in dependence on the energy of the projectile are shown. The lines show the theoretical predictions obtained by INCL4+ABLA calculation code [2,3].
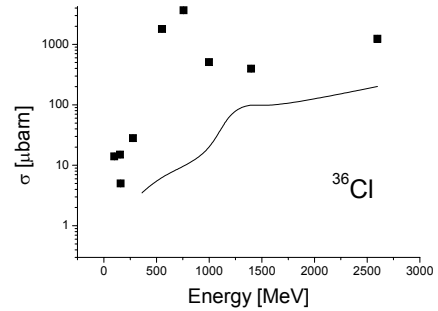
Fig.2: Measured cross sections (squares) and calculated excitation function (line) for the production of ^{36}Cl from irradiation of bismuth with protons in dependence on the projectile energy
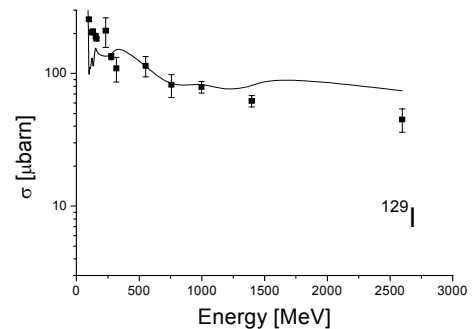
Fig.3: Measured cross sections (squares) and calculated excitation function (line) for the production of ^{129}I from irradiation of bismuth with protons in dependence on the projectile energy

As was observed earlier [4], calculations agree well for residues with intermediate (^{129}I), or masses close to the target material whereas light nuclei like ^{36}Cl or ^{26}Al are systematically underestimated. Obviously, the used reaction models (Intra-Nuclear Cascade Model combined with evaporation/fission) are not sufficient for a correct simulation. Probably, multi-fragmentation or another binary splitting as a possible reaction path has to be taken into consideration, too.

Likewise, at the moment we do not have any explanation for the strange trend of the production of ^{36}Cl in the energy range between 500-1000 MeV, which is also slightly pronounced in the calculations. A similar trend was observed for the production of ^{36}Cl in Pb-targets [4].

REFERENCES

[1] D. Schumann et al., PSI Annual Report 2006, p. 37.
[2] A. Boudard et.al., Phys. Rev. **C66**, Art. No. 044615 (2002).
[3] A.R. Junghans et al., Nucl. Phys. **A629**, 635-655 (1998).
[4] D. Schumann et al., ND2004, Santa Fe, AIP Vo.769, p. 1517.

ESTIMATION OF THE SOLUBILITY OF ELEMENTS IN LIQUID LEAD, BISMUTH AND LEAD BISMUTH ALLOY

J. Neuhausen, R. Dressler, B. Eichler, R. Eichler, D. Schumann (PSI)

The solubility of elements in liquid lead, bismuth and the eutectic alloy of these metals plays an important role for the understanding of the chemical behavior of impurities in future high power spallation targets. Experimental data for solubilities in these metals are incomplete. We use thermodynamic relations and enthalpies of solution and formation of compounds obtained using a semi-empirical model to calculate solubilities for a large number of elements. Results are compared with known experimental data.

1   INTRODUCTION

In future high power liquid metal spallation targets impurities will be produced by corrosion and various nuclear reactions. For heavy liquid metals such as eutectic lead bismuth alloy (LBE), these impurities comprise the complete periodic table ranging from H to Po. In the reactor core of accelerator driven systems (ADS) contaminations with actinides may also occur. After long-term irradiation, the impurity elements may reach concentrations in the ppm-range or even larger. A fundamental parameter for understanding the chemical behavior of nuclear reaction products in such systems is their solubility in the liquid metal. For lead and bismuth, a considerable amount of experimental data exists, while data for some of the most prominent nuclear reaction products are still missing. For LBE only few solubility data, mainly for steel alloying components, are known. One of our tasks within the FP6 project EUROTRANS [1] is the estimation of solubility data based on theoretical evaluations. In this report, we show the results of thermodynamical solubility calculations using enthalpy data calculated with the Miedema model [2]. A similar approach proved valuable for the estimation of the solubility of a few metals in liquid metals [3].

2   CALCULATION PROCEDURE

For the description of the solubility equilibrium of two elements, two cases have to be distinguished: Systems with equilibrium between a pure solid element and the saturated liquid and systems where the liquid is in equilibrium with a chemical compound of the two elements. In this report, we will focus on the former type of system. For the latter case, no satisfactory results were obtained so far.

We consider the heterogeneous equilibrium system of a pure solid element A and a liquid metal B:

$$A \text{ (s, pure)} \Leftrightarrow A \text{ (liquid in B)}$$
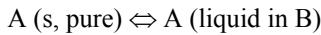
In equilibrium, the chemical potential of the dissolved component A equals the chemical potential of the pure solid element A. From the equality of the chemical potentials we derive equation (1) for the solubility of A in liquid B,

$$\ln(x) = \frac{(\Delta S_{melt}(A(s)) + \Sigma \Delta S_{trans}(A(S)) + \Delta \overline{S}_{ex}(l))}{R}$$
$$- \frac{(\Delta H_{melt}(A(s)) + \Sigma \Delta H_{trans}(A(s)) + \Delta \overline{H}_{mix}(AB(l)))}{RT} \quad (1)$$

with the mole fraction x, molar melting enthalpy and entropy of A, $\Delta H_{melt}(A(s))$ and $\Delta S_{melt}(A(s))$, molar enthalpies and entropies of phase transitions in solid A,

$\Delta H_{trans}(A(s))$ and $\Delta S_{trans}(A(s)$, partial molar excess entropy of mixing $\Delta \overline{S}_{ex}(l)$ and the partial molar enthalpy of mixing liquid A and B, $\Delta \overline{H}_{mix}(AB(l))$.

In our approach, the thermodynamic constants for phase transitions and melting are taken from literature and the enthalpy of mixing is approximated by the partial molar enthalpy of solution at infinite dilution, which is calculated using the Miedema model [2]. This approximation is only valid for small solubilities. The excess entropy is neglected.

3   RESULTS

Fig. 1. shows a comparison of calculated solubilities in Pb at 800 K with literature data [4]. Results for Bi are similar. Qualitatively, the periodicity of the solubility is represented well by the results of calculations. Metals of groups 6 to 9 (e.g. Cr, Fe, Co) show rather low solubilities in lead, whereas heavier elements of groups 11 to 15 such as Ga, Ag, Sb and Au show large solubilities. Generally, the agreement of calculated and literature values is acceptable. For a spallation target environment one can conclude that after long term irradiation some of the elements produced by spallation (Ta, W, Re, Os) and fission (Nb, Mo, Tc, Ru) will exceed their solubility limit.
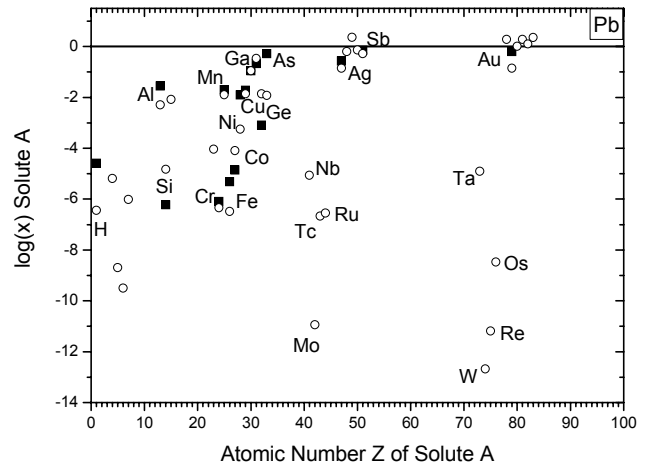
Fig. 1: Calculated solubility in lead at 800 K (circles) and literature data (squares) for elements A that are present as pure solid elements in the solubility equilibrium.

REFERENCES

[1]   http://nuklear-server.ka.fzk.de/eurotrans/Start.html

[2]   F.R. de Boer et al., Cohesion in Metals, Transition Metal Alloys, North-Holland, Amsterdam 1988.

[3]   C. Guminski, Z. Metallkunde, **81,** 105 (1990).

[4]   J. L. Courouau, CEA Technical Note NT STR LCEP 2003/001.

RADIOCHEMICAL ANALYSIS OF LEAD SAMPLES FROM SINQ TARGET 4

D. Schumann, J. Neuhausen, S. Horn, S. Lüthi, Y. Dai (PSI), P.W. Kubik, H.A. Synal, V. Alfimov (ETHZ)

Target 4 from the SINQ facility at PSI was analyzed concerning its radionuclide inventory by γ-spectrometry, Liquid Scintillation Counting (LSC) and Accelerator Mass Spectrometry (AMS) after chemical separation.

1   INTRODUCTION

Nuclear data for the radionuclide production in spallation targets are obtained both by theoretical predictions and measurements of real target systems. The described work is the beginning of an extended radiochemical characterization of Target 4 from the SINQ facility at PSI serving as benchmarks for the validation of the calculation codes developed within the HINDAS project [1]. The work is partly funded by EC (EUROTRANS/NUDATRA).

2   EXPERIMENTAL

Fig 1: Photo of the SINQ-target

SINQ targets consist of lead rods clad with SS 316L or Zircaloy tubes (Fig.1). Target 4 was in use from 20th March 2000 till 23rd December 2001. It was irradiated with 590 MeV protons and got a total beam dose of 10.03 Ah.

Special irradiation positions

Zircaloy-2 frame

Cooling water

AlMg$_3$ container

sample position rod 3
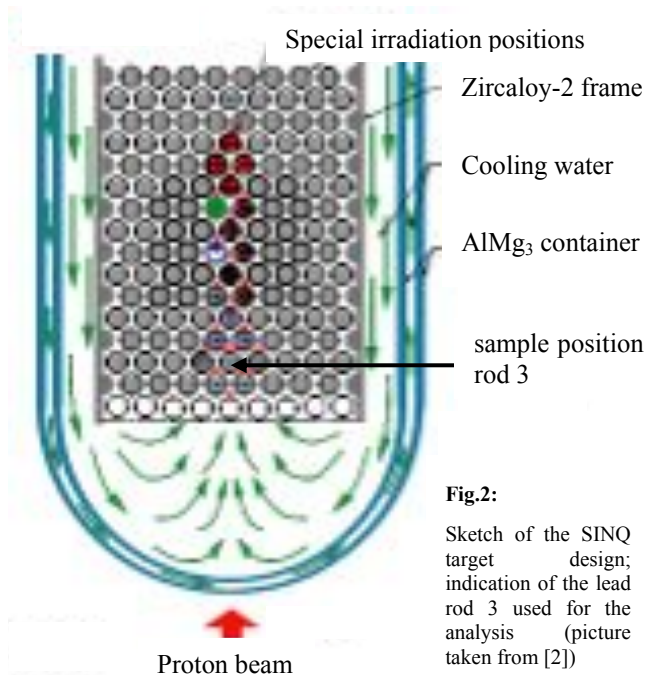
Fig.2:

Sketch of the SINQ target design; indication of the lead rod 3 used for the analysis (picture taken from [2])

Proton beam

In Fig.2, a schematic view of the position of rod 3 used for the present work can be seen. Details of the Target 4 construction and parameters can be found in [2].

This rod was cut into several disks (Fig.3). For the analysis, we used disks number 9 and 14 (D9 and D14). The respective neutron and proton fluxes are shown in Tab.1.

Table 1: Proton and neutron fluxes at sample positions

Sample	Proton flux [10^{25}/m^2]	Neutron flux [10^{25}/m^2]
D9	3	7.5
D14	0.9	5.5

First, a detailed γ-analysis was carried out using a high purity germanium detector. After chemical separation [3], ^{55}Fe and ^{63}Ni were measured by LSC as well as ^{26}Al and ^{36}Cl by AMS (ETH Zurich).
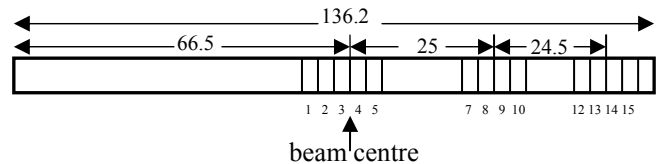
Fig.3: cutting of the lead rod 3 into sample disks with 1.5 mm thickness

3   RESULTS AND DISCUSSION

Table 2: Content of selected radionuclides in Rod 3 (measuring dates: γ: 09/2006, LSC 11/2006)

	D9 [Bq/g]	D14 [Bq/g]		D9 [Bq/g]	D14 [Bq/g]
^{207}Bi	3.00·10^7	1.01·10^7	^{106}Ru	4.83·10^6	3.91·10^6
^{172}Lu/^{172}Hf	2.00·10^7	5.41·10^7	^{110m}Ag	1.29·10^6	3.93·10^5
^{173}Lu	2.76·10^7	4.30·10^7	^{125}Sb	1.32·10^6	-
^{194}Au/^{194}Hg	1.86·10^7	3.13·10^6	^{133}Ba	2.8·10^6	7.94·10^5
^{102}Rh	5.53·10^6	1.44·10^5	^{44}Sc/^{44}Ti	8.00·10^4	2.84·10^4
^{202}Tl/^{202}Pb	4.80·10^5	1.87·10^5	^{108m}Ag	3.75·10^5	1.56·10^4
^{60}Co	3.67·10^6	1.40·10^6	^{194}Os/^{194m}Ir	2.61·10^4	-
^{54}Mn	2.29·10^5	7.01·10^4	^{26}Al	0.5	0.2
^{58}Co	1.55·10^6	9.47·10^5	^{36}Cl	9.5·10^1	4.8·10^1
^{55}Fe	8.73·10^7	5.99·10^7	^{63}Ni	6.30·10^8	4.52·10^8

Table 2 shows the analysis results for samples D9 and D14. For a full characterization of the radionuclide distribution within the SINQ target system, more samples have to be analysed, especially from the beam central line (D3, D4) as well as 3-4 more central rods from the target. Moreover, the determination of other long-lived radionuclides like ^{10}Be, ^{60}Fe ^{59}Ni, ^{53}Mn is also planned.

REFERENCES

[1]   HINDAS Final Scientific Report, FIS5-00150
[2]   Y. Dai et.al., J Nucl Mat 343 (2005) 33
[3]   D. Schumann et.al., NIM B 264 (2007) 83

PREPARATION OF A ^{60}Fe TARGET FOR NUCLEAR ASTROPHYSICS EXPERIMENTS

D. Schumann, J. Neuhausen, S. Horn, S. Köchli (PSI), F. Käppeler for the FZK collaboration

A target containing $1.2 \cdot 10^{16}$ atoms ^{60}Fe was prepared for studying the nuclear reaction ^{60}Fe$(n,\gamma)^{61}$Fe, a key reaction for the understanding of the composition of the early Solar System (ESS).

INTRODUCTION

The isotope ^{60}Fe, with a half-life of 1.5×10^6 yr, plays a key role in tracing the history of the early Solar System. Current comprehensive attempts at reconstructing the inventory of short-lived radioactivity between Fe and Pb that were found to be alive in the ESS [1,2] showed that ^{60}Fe (together with ^{107}Pd, ^{41}Ca, ^{36}Cl, ^{26}Al, and ^{10}Be) must be considered as a late addition to the protosolar nebula. Whether this material stems from a supernova or a nearby asymptotic giant branch (AGB) star is still an open question.

Neutron capture cross sections are required for calculating the s-process production of ^{60}Fe. The stellar (n, γ) rates for the unstable isotopes, ^{59}Fe and ^{60}Fe, which govern the stellar production and destruction of ^{60}Fe, are presently obtained by theoretical calculations using the Hauser-Feshbach statistical model, which exhibits typical uncertainties of 30 to 50% for the resonance dominated cross sections in the mass region around Fe [3]. The results from calculations of the ^{60}Fe cross section with the statistical model codes NON-SMOKER [4] and the MOST [5] differ by a factor of three. Because the s-process abundances are directly determined by the respective stellar (n, γ) rates, the present cross section uncertainties translate into uncertainties in the calculated ^{60}Fe yields of more than a factor of two, thus clearly obscuring the abundance predictions of the stellar models.

Experimental solutions to this problem are, therefore, urgently needed. Precondition for such an experiment is the availability of a sufficient amount of target material. As was reported earlier [6], one possibility for gaining such rare isotopes is the exploitation of accelerator waste from the PSI facilities.

EXPERIMENTAL

For the separation of the ^{60}Fe sample, 3.5 g of copper chips drilled out from a beam dump irradiated with high-energetic protons were dissolved in half-concentrated HNO$_3$. The sample contained about 150 MBq ^{60}Co and 2 MBq ^{44}Ti as the main contaminations disturbing the measurement of the ^{61}Fe production. They have to be separated carefully to nearly zero level. Additionally, ^{55}Fe is produced simultaneously during the irradiation. Eventually, the sample inclosed also traces of stable iron isotopes, stemming partly from the nuclear reaction itself, partly from the drilling equipment.

5 mg stable Co and La, each, were added to the solution and La(OH)$_3$ carrying both ^{60}Fe and ^{44}Ti was precipitated with concentrated ammonia solution. Cobalt as well as copper form soluble ammonia complexes under these conditions and remain in solution. The precipitate was dissolved in diluted HNO$_3$ and the procedure was repeated several times till a colourless solution was obtained. The lanthanum hydroxide was then dissolved in 7 M HCl and iron was separated by liquid-liquid extraction with Methylisobutyketone (MIBK). The aqueous phase containing nearly the entire amount of ^{44}Ti was stored for further experiments.

Back extraction of iron from the organic phase was carried out with 0.1 M HCl. The extraction procedure was repeated twice. A γ-measurement was performed to determine the activity of ^{60}Co and ^{44}Ti as well as Liquid Scintillation Counting (LSC) for the ^{55}Fe content. Afterwards, the solution was stored for 245 days. Three weeks before starting the experiment the γ-measurement was repeated and a terminal extraction step was performed. The chemical yield of the final purification was determined by LCS measurement of ^{55}Fe again. The content of stable iron in the final sample was determined by ICP-OES. In the end, the solution was evaporated to dryness onto a graphite target backing.

RESULTS

The content of ^{60}Fe was determined using the incrowth of the daughter nuclide ^{60}Co:

γ-measurement on 25th January 2007:   2.8 Bq ^{60}Co
γ-measurement on 2nd October 2007:   19.5 Bq ^{60}Co

For a small time difference $t \ll T_{1/2}$ (^{60}Co) the number N of ^{60}Fe atoms can be calculated by the following formula, with $\lambda_{^{60}Fe}$ and $\lambda_{^{60}Co}$ being the decay constants of ^{60}Fe and ^{60}Co, respectively:

$$N_{^{60}Fe} = \frac{\delta A_{^{60}Co}}{\lambda_{^{60}Fe} \cdot \lambda_{^{60}Co} \cdot t} \quad \text{with } \delta A_{^{60}Co} = 16.7 \text{Bq}$$

Taking into account the chemical yield of 89% for the final purification step, we obtained a total content of $1.18 \cdot 10^{16}$ atoms ^{60}Fe within the target. Additionally, the target contained 460 μg stable iron, 99.6 MBq ^{55}Fe as well as contaminations of ^{44}Ti and ^{60}Co of 0.3 and 0.4 Bq, respectively, determined on 3.10.2007. This represents a chemical decontamination factor of $\sim 3 \cdot 10^8$ for ^{60}Co and $\sim 5 \cdot 10^6$ for Ti.

A first successful neutron irradiation experiment for the determination of the neutron capture cross section for ^{60}Fe at stellar energies started on 29th October 2007 at FZ Karlsruhe, Germany. Data analysis is under way and results will be published soon.

REFERENCES

[1] M. Busso et.al., Annu. Rev. Astron. Astrophys. 37 (1999) 239.
[2] G.J. Wasserburg et.al, Nucl.Phys. A 777 (2006) 5.
[3] Z.Y. Bao et.al, 2000, Atomic Data Nucl. Data Tables, 76, 70.
[4] T. Rauscher et.al, 2000, Atomic Data Nucl. Data Tables, 75, 1.
[5] S. Goriely 1998, http://www-astro.ulb.ac.be
[6] D. Schumann et.al, J.Phys.G 2007, in press.

BEHAVIOR OF IMPURITY ELEMENTS IN MERCURY

J. Neuhausen, D. Schumann (PSI)

For the mercury spallation target designed within EURISOL-DS a separation of radionuclides from mercury is planned. It was shown that Au dissolved in Hg can be adsorbed on an amalgamated copper plate. We extended this study to other elements that show a high solubility in mercury. In this report we present some qualitative results.

1 INTRODUCTION

In the frame of the FP6 project EURISOL-DS [1] we study the removal of radioactive impurities from mercury. Earlier experiments revealed that carrier-free gold readily adsorbs to an amalgamated Cu-plate [2]. From this, it seems reasonable to assume that other elements that show a rather high solubility in mercury and that are known to chemically interact with copper will show a similar behavior. We selected those elements, for which activated samples with suitable half-life can be prepared by neutron activation. After irradiation at SINQ, small amounts of the elements were mixed with mercury. We studied the behavior of these mixtures and the adsorption of the solute on amalgamated copper.

2 PREPARATION OF ACTIVATED SAMPLES

Samples of metallic Zn, Ag, Cd, Sn, and Sb were irradiated at SINQ. The amount of metal and the irradiation time was adapted in such a way that the dose rates did not exceed the allowed limits. Typical sample masses were around 100 mg and the irradiation time was 1 h (exception Ag: 3 min). After several days of cooling, the samples were analyzed by γ-spectrometry. The following main nuclides were detected in the samples (amongst others):

Zn-sample: ^{65}Zn ($T_{1/2}$=244d), ^{69m}Zn ($T_{1/2}$=14h)

Ag-sample: ^{110m}Ag ($T_{1/2}$=250d)

Cd-sample: ^{110m}Ag ($T_{1/2}$=250d), ^{106m}Ag ($T_{1/2}$=8.3d),

^{105}Ag ($T_{1/2}$=41d), ^{115m}Cd ($T_{1/2}$=45d), ^{115}Cd ($T_{1/2}$=53d)

Sn-sample: ^{113m}Sn ($T_{1/2}$=115d)

Sb-sample: ^{124}Sb ($T_{1/2}$=60d)

3 PREPARATION OF AMALGAMS

Small amounts of the activated metals were mixed with Hg under ambient conditions in PE-vessels to give mixtures of mole fractions of 10^{-4} (Sn) and 10^{-5} (Zn, Ag, Sb). For the Cd samples we were interested in the behavior of non-carrier-added Ag. Therefore, we mixed the complete Cd-sample with Hg, resulting in a Cd mole fraction of 8×10^{-3}. After mixing, many samples showed visible solid precipitations on the liquid-gas interface and at the wall of the PE-vessel. The mixtures were filtrated. A part of the filtrated Hg was afterwards transferred to a new vessel, were it was exposed to amalgamated Cu-plates. γ-spectra of the mixtures, empty vessels, filters and Cu-plates were taken after each operation.

4 BEHAVIOR OF AMALGAMS AND SORPTION BEHAVIOR OF DISSOLVED ELEMENTS

All experiments were conducted under ambient conditions.

Ag: The diluted Ag-amalgam showed no solid precipitations on the surface. Ag is actually dissolved in Hg. Only a very small fraction of Ag is adsorbed to the Cu-plate even after long-term exposure (≈6 months). During this time, the activity decrease in the Hg was below the detection limits. On the Cu-plate, where the activity measurement is more sensitive because self-absorption of Hg is missing, a small increase of Ag-activity was observed.

Cd: The Cd-amalgam was mainly used to elucidate the behavior of non-carrier-added Ag in mercury. The activity of Cd dissolved in Hg was too low for reasonable γ-measurements: Most of the Cd remained floating on top of the liquid metal or sticking to the walls of the vessel in form of a paste-like grey mass with metallic luster, though according to literature data the solubility of Cd in Hg at room temperature should be about 10%. The non-carrier-added Ag adsorbed to the Cu-plate in measurable amounts, but compared to Au [2] the adsorption is slow and incomplete.

Sb, Sn: The amount of Sb mixed with Hg exceeded its solubility by a factor of 2. While the surface of the Sb-amalgam remained clean, a dark precipitate showed up at the Hg/PE interface. After filtration, measurable Sb-activity was still present in the liquid. From this sample, 70% of the activity was adsorbed to a Cu-plate within 1 hour. The rest of the activity could not be adsorbed even when a fresh Cu-plate was used. A sample of Sb-amalgam that was aged for 20 days, showing visible precipitation at the Hg/PE interface, was also exposed to a Cu-Plate. The activity present as dissolved Sb was substantially adsorbed to the Cu-plate, while the precipitate remained unchanged. Sn shows a similar behavior, but slower adsorption.

Zn: The diluted Zn-amalgam proved to be rather sensitive to air. Thus, solid layers show up after short time on the surface of the liquid and the walls of the vessel. The activated Zn was associated with these solids rather than the liquid phase and no substantial adsorption on Cu was detected.

5 CONCLUSION

It is shown that metal absorbers can be used as an option for extraction of radionuclides from liquid metals. However, these reactions have to be studied in much more detail. The air sensitivity of some of the sample clearly shows the necessity of an inert gas system for such experiments.

REFERENCES

[1] http://www.eurisol.org
[2] J. Neuhausen et al., Ann. Rep. Labor Radio- & Umweltchemie, Univ. Bern & PSI (2006) p. 48.

NEW PROTON IRRADIATION FACILITY IN PROSCAN AREA

W. Hajdas, R. Brun, K. Egli (PSI), R. Harboe-Sorensen, A. Mohamadzadeh, R. De Marino (ESA-ESTEC)

New Proton Irradiation Facility PIF test site was installed in the experimental area of the PROSCAN biomedical accelerator. First protons were delivered in September 2007 and since then several test and exposure runs were successfully conducted. Primary beam energies can be set between 70 and 250 MeV. Further reduction down to few MeV is possible with a local degrader. Beam profiles can be adjusted to uniformly cover targets with areas of tens cm^2. Beam intensities of up to 10 nA allow for efficient irradiations by both space and particle physics communities.

The new exposure site of the PIF facility has been installed in the experimental area of the PROSCAN biomedical accelerator – see Fig. 1. The area has been commissioned in August 2007 and first beam have been successfully delivered in September. Experimental setup for PIF irradiations is arranged in a similar manner as in the low energy site in the NEB area. This way, the former facility users can conduct their standard tests without any additional modifications. Moreover the beam line itself has been equipped with new, more advanced diagnostics like extra profile and current monitors. The experimental setup consists of a large bench with a local dosimetry block and a user frame fixed on the XY-table. A laser aligned with the beam line axis is mounted at the rear side of the bench. The beam dump is located directly in the area wall. The dosimetry block consists of two flat, air filled ionization chambers ICs and the XY wire chamber WC for monitoring of the beam intensity and profiles. A local energy degrader made of 7 Cu-plates of various thicknesses is placed between the chambers – see Fig. 2. The degrader allows for a quasi continuous setting of the energy on target down to ca. 10 MeV. Both setting of the energy with the degrader

provided for PIF by the European Space Agency ESA – the main user of the facility.

Fig. 2: Dosimetry block (ICs, WC) and energy degrader.

Fig. 3: Plastic scintillator detectors on DUT frame.

Initial energies of protons entering the area can be set between 70 and 250 MeV. Beam optics setups available to date exist for energies of 235, 200, 150, 100 and 70 MeV. They are optimized for both wide and narrow field beams at DUT with FWHM between 60 and 6 mm respectively. Maximum beam intensities allowed for the PIF site are 2 nA for energies above 200 MeV and 10 nA for energies below 100 MeV. The intensity can be remotely set from the operating console in the PIF barrack. As the day shifts are reserved for biomedical applications, the facility runs either during the late and night shifts or at weekends. Beam setup and its diagnostic are user friendly and can be performed locally. First tests also showed both high quality of the beam and stability of the beam-line settings. It should assure reliable exposures and large number of users tests.

Fig. 1: Location of the PIF facility at PROSCAN.

and positioning of the user device under test DUT with the XY-table are remotely controlled from the PIF measurement barrack that is located on the roof of the experimental area. Calibrations of the beam intensity measured by the ionization chambers are performed using small plastic scintillator detectors of precisely know area. The detectors are mounted exactly at the position of DUT and count single protons passing through the scintillator – see Fig. 3. Calibration runs are performed before starting the DUT exposures at low beam intensity for all energies used in the experiment. Further verification of the proton flux is possible with a Single Event Upset SEU Monitor based on the SRAM memory. The SUE monitor was

LOW ENERGY ELECTRON DETECTOR FOR STUDIES OF THE PARTICLE ENVIRONMENT IN SPACE

W. Hajdas, F. Burri, K. Egl,i Ch. Eggel, St. Scherrer, N. Schlumpf, B. Schmitt (PSI),
A. Mohammadzadeh (ESA-ESTEC)

Low Energy Electron Detector LEED is a miniature particle monitor for measurements in space. It is based on the MYTHEN Si-microstrip instrument made at PSI for X-ray detection at SLS. The space version will measure electrons with energies from few keV up to few hundred keV at very high fluxes and harsh radiation environments. The device aims to study hot plasmas and particle acceleration, monitor Space Weather and map planetary Radiation Belts.

Low Energy Electron Detector LEED was designed in collaboration with the European Space Agency in order to provide the instrument that covers an unexplored energy range of space electrons below few tens keV. The device shall also demonstrate the technological readiness to develop miniature, cost effective space radiation monitors. The requirements put on such monitors are tough and often conflicting. Firstly it should be of low mass, size and with minimized power consumption. Simultaneously it should detect very high fluxes with good energy resolution and efficient background suppression. Its radiation harness should be at least 100 krad for Earth orbiting missions and of about 1 Mrads for flights to Jupiter (comparable with LHC demands).

As result of our initial studies we based LEED on the Microstrip System For Time-resolved Experiment MYTHEN Si-microstrip instrument made at PSI for the synchrotron X-ray detection at SLS – see Fig. 1.

Fig. 1: Test structure with the Si-microstrip detector bonded to the MYTHEN readout ASIC.

MYTHEN utilizes PSI designed ASIC coupled with a microstrip SI-detector. The fast, low noise (below 200 e-) and radiation hard (better than 1 Mrad) ASIC works at the room temperature, serving simultaneously for 128 channels.

Fig. 2: CAD model of the LEED prototype.

Each channel is equipped with a preamplifier and shaping electronics, energy discriminator and 24 bit long counter. Connection with the detector is made using a wire-bonding. LEED specifications rely in large on the ASIC parameters and will allow for an efficient and undisturbed operation is space. The instrument should be able to deal with particle fluxes up to 10^9 /cm^2/s (ca. 1 MHz channel) and have small power consumption of few hundreds mW. The total mass of about 200 g and the size of ca. 5x5x3 cm^3 (see Fig. 2) show a major reduction comparing with its predecessors (e.g. SREM mass was 2.5 kg). The first version aims for overall radiation hardness level of at least 300 krads allowing even for far planetary missions. The detector energy range spans between 10 and 250 keV with the energy resolution of ca. 3 keV. Currently available novel Si-diodes with negligible dead layer thickness on the surface should make it possible to reduce the low energy threshold down to ca. 3 keV.

The LEED was extensively modeled using GEANT4 package from CERN. Its response matrix to mono-energetic electrons coming from all direction is showed in Fig. 3. The fully functional prototype is at present under construction.
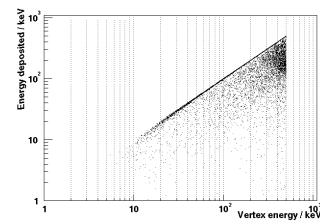
Fig. 3: LEED response matrix for electrons.

All electronic components have been ordered and mechanical prototype is fabricated. In the first step the standard MYTHEN sensors (width of 50 μm) will be used. Next versions will have larger stripe widths to minimize the multiple strips response caused by a charge deposition from a single electron – see Fig. 4 for widths of 250 μm.
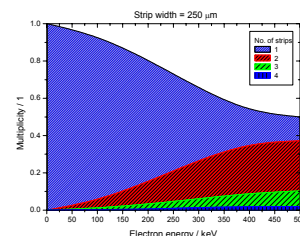
Fig. 4: Number of strips responding to single electron.

MONTE CARLO SIMULATIONS FOR POLAR

E. Suarez-Garcia, W. Hajdas, A. Mtchedlishvili, U. Hartmann, I. Herda, M. Jaworski (PSI), T.J.L. Courvoisier,
N. Produit, D. Haas, R. Walter (ISDC), M. Pohl, C. Leluc, D. Rapin (Uni Genf), M. Gierlik, R. Marcinkowski,
G. Wrochna (IPJ), Ch. Tao (CPPM), G. Lamanna, J.-P. Vialle (LAPP), B. Wu, S. Xiang, S.N. Zhang (IHEP)

Having in mind the importance of X- and γ-ray polarization information for understanding of many astrophysical objects we are developing a novel polarimeter: POLAR. High-precision Monte Carlo simulations of POLAR that we are performing, has already demonstrated the usefulness in finalizing the design of the instrument, understanding the laboratory results, and predicting the influence of different sources of background. Ultimately, our modeling will be of crucial importance for the characterization of POLAR and a proper interpretation of its future measurements.

The nature of gamma ray bursts (GRB), the brightest events in the universe, is still a mystery almost forty years after their discovery. One of the crucial and not-yet-determined parameters is their level of linear polarization. This quantity, intimately related with their emission mechanism, can provide vital information on the origin of GRBs. Thus we are building the novel hard X-ray polarimeter POLAR. It will measure polarization of photons with energy 50-500keV and consists of an array of 40x40 low-Z plastic scintillators (6x6x200mm^3 each). A POLAR engineering-qualification model (EQM) will be ready in 2010.

Using the GEANT4 code developed by CERN, Monte Carlo simulations of POLAR are carried out to predict the polarimeter capabilities and determine materials providing the best instrument performance. In the actual mass model, the 1600 scintillators wrapped with aluminium foil have been implemented. The size, material, and spatial distribution of the bars were precisely taken into account. To simulate the polarimeter response to different particles, a realistic particle gun has been defined. Selected particles can come from any predefined direction and a specific input spectrum can be generated following the user instructions. As an example, POLAR response to polarized photons with energies of 5, 50, and 250 keV was studied, producing the spectra of energy depositions and the 100% modulation curves. In Fig. 1, the result obtained with an ideal POLAR is compared with the same data after applying the energy resolution of the scintillator and taking into account the non-uniformity of the PM-anode from Hamamatsu data-sheet. It is clearly seen that while the energy smearing does not diminish the POLAR performance, it is crucial to calibrate each channel to correct for sensitivity differences.
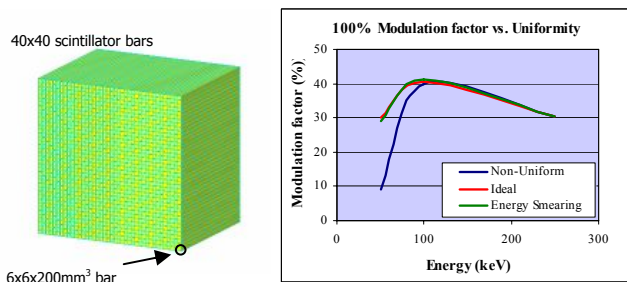
In another series of simulations the light collection of a scintillation element has been studied using the optical photon tools provided by GEANT4. A single scintillator bar was implemented with different wrapping materials applied to it: air (no-wrapping), refractive paint, Teflon, Teflon with a thin air gap between it and the scintillator, and aluminium with the same air gap. In all cases both the optical properties of the materials and of the contact surfaces were accurately described. Monochromatic flux of photons was shot at three different positions: bottom (close to the PM), middle, and top of the bar. The light collection was studied calculating the ratio between the number of optical photons that were registered at the PM position and the total number of optical photons that had been initially produced by the interacting gamma. The best results (see figure 2) were achieved when the scintillator bar was wrapped with aluminium, leaving an air gap between the foil and the scintillator surface. It this case, more than a 40% of the optical photons are detected even when their initial point of interaction is far away from the PM. The air gap warranties total reflexion for all angles below 68 degrees due to its lower refractive index, and the aluminium contributes by reflecting back into the scintillator some of the optical photons that were refracted. Using the same simulation we also studied the influence of the scintillator surface roughness on the collection efficiency. It was found that the number of optical photons arriving to the PM largely decrease when the surface of the scintillator loses its smoothness. Both results (wrapping materials and surface smoothness) were confirmed with laboratory experiments.

Fig. 1: Left: view of POLAR mass model. Right: dependence of the 100% modulation factor on the photon energy. The effect of the scintillator energy resolution and the readout un-uniformity of the PM anode array are shown together with the ideal case.
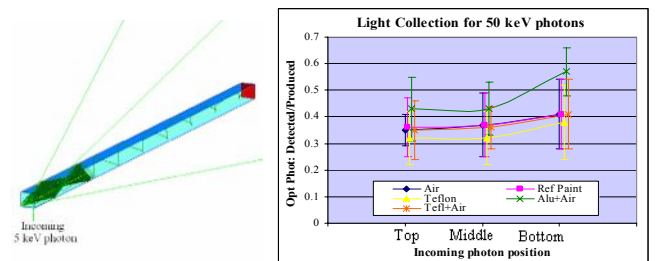
Fig. 2: Light collection simulations. Left: visualization with a 5 keV incoming photon and the optical photons tracked inside of the scintillator. Right: light collection results for five types of bar wrapping at three different incoming positions.

New simulations are planned with Al replaced by the high reflectivity Wikuity™ tape. It should improve the linearity and increase the number of collected optical photons.

DEMO MODEL AND READOUT ELECTRONICS OF POLAR

W. Hajdas, A. Mtchedlishvili, U. Hartmann, I. Herda (PSI), U. Ammann (PIE), T.J.–L. Courvoisier, N. Produit,
D. Haas, R. Walter (ISDC), M. Pohl, E. Suarez-Garcia, C. Leluc, D. Rapin (Uni Genf), M. Gierlik, R. Marcinkowski,
G. Wrochna (IPJ), Ch. Tao (CPPM), G. Lamanna, J.-P. Vialle (LAPP), B. Wu, S. Xiang, S.N. Zhang (IHEP)

Polarization measurement in the prompt emission of Gamma Ray Bursts (GRB) is an ultimate tool in understanding their nature. To provide a large set of precise data a novel γ-ray polarimeter POLAR is proposed. Its demonstration model (DM) was developed by PSI and PIE. It consists of 128 scintillators arranged into two 8x8 arrays. Signals are processed by two ASICs with digital and analogue outputs. Data flow is controlled by fast FPGA.

Measurements of the polarization in γ-rays are to date generally neglected mainly due to serious experimental difficulties in construction of reliable and efficient space instruments. Few recent measurements are inconclusive and still impeded by large uncertainties. Nonetheless, polarization of γ-rays from the GRBs prompt emission is an ultimate observable needed to find the true nature of these biggest explosions in the universe. Moreover, systematic and accurate polarization measurements will allows for:
1. probing magnetic fields during creation of Black Holes
2. verification of several Quantum Gravity theories
3. testing of fundamental physics e.g. the Lorenz invariance
4. looking into the features of the Dark Age Universe
POLAR instrument was proposed by a team of several Swiss institutes in order to address above issues and unravel the GRB mystery. It is based on Compton scattering and consists of a uniform 40x40 array of low-Z, fast plastic scintillators with the size 6x6x200 mm^3. The energy range is between 5 and 500 keV. POLAR main features are: large active area ($\sim$ 400 cm^2), large modulation factor ($\sim$ 40%) and large field of view (> 1/3 of the sky).
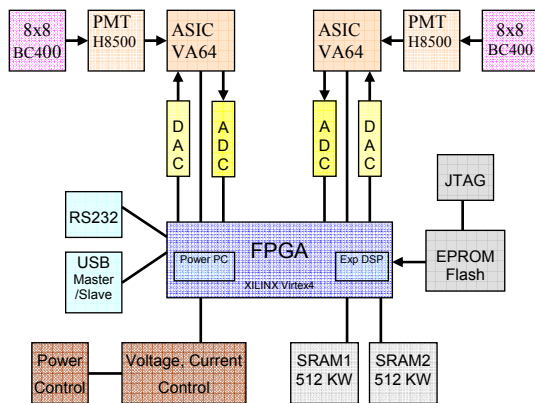
Fig. 1: Scheme of the POLAR Demo Model electronics.

The instrumental novelty of POLAR is that it utilizes two highest energy depositions from scatterings in the uniform detector material. This concept will be tested with the POLAR Demo Model developed at PSI with help of the PI Electronics – see Fig. 1. DM utilizes only 2x64 channels and its plastic detectors (BC400) are wrapped with a high reflectivity foil (3M) and are coupled to two multi-anode photomultipliers PMT (H85000 HAMAMATSU) – see Fig. 2-left. Signals from PMTs are delivered to the ASICs (VA64MAPMT IDEAS) mounted on the separate PCBs – see Fig. 2-right. VA64 has 64 discriminators connected with parallel digital trigger outputs. The analogue signals after shapers are connected to the multiplexer. Its readout is

realized using an external S/H signal The ASIC analogue electronics is tuned by 8 DACs. The whole DM is controlled by a fast logic unit - XILINX Virtex4 FPGA, programmed through the EPROM. The unit allows for monitoring of all A/D currents and voltages (16 ADCs), optimizing of ASIC parameters and data taking and storage.
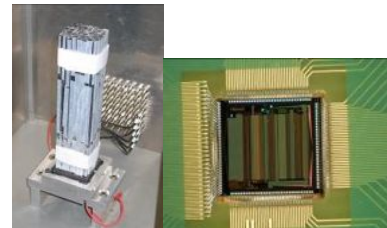
Fig. 2: Array of 8x8 plastic scintillators on the PMT (left). VA64 ASIC bonded to the PCB interface (right).

The device operates at 100 MHz major clock frequency. DM is also equipped with two fast, low power SRAMs, (512 KWords) and low power, 65 MSPC ADCs. The link to the PC is possible with both USB and RS232 protocols. The DAQ software uses CVI/LabWindows package. The POLAR DM populated board is showed in Fig. 3.
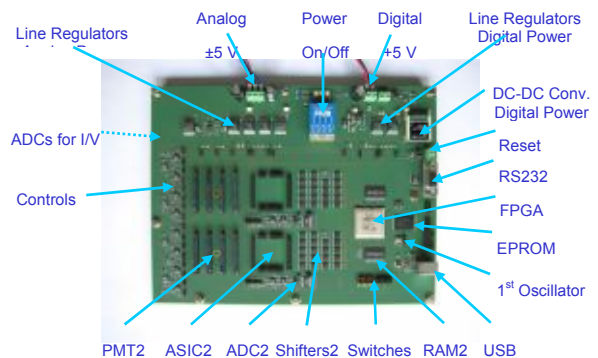
Fig. 3: POLAR DM printed circuit board.

Currently the DM undergoes first tests and adjustments at PSI. In the next step the input signals characterization and data flow studies will be performed. Final qualification runs with polarized γ- and X-rays from sources and PSI SLS are planned for winter/spring 2008.

PREDICTIONS OF THE GRB POLARIZATION DETECIONS BASED ON BATSE DB

W. Hajdas, M. Jaworski, I. Herda (PSI), E. Suarez-Garcia (PSI, UNI Ge), N. Produit (ISDC)

Polarization measurements of γ-rays and hard X-rays in space are still very scarce and imprecise. They are, however indispensable to solve the mystery of Gamma Ray Bursts GRBs – the biggest explosions in the universe. POLAR instrument has been proposed to provide polarization data from the GRB prompt emissions. Using the BATSE GRB database DB we estimated the distribution of the minimum detectable polarizations to be measured by POLAR.

Despite of more than 30 years after the discovery of GRBs, we still cannot elucidate their true nature. Future measurements of the γ-ray polarization from the GRBs prompt emission should clarify their mechanisms. Thus, the University of Geneva with the Integral Science Data Center and PSI proposed an original γ–ray polarimeter POLAR.
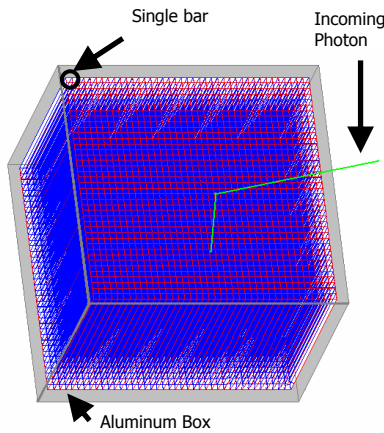
Fig. 1: GEANT4 model of POLAR instrument.

The polarimeter is based on the fully uniform detector system. It consists of 1600 fast plastic scintillators $(6 \times 6 \times 200 \text{ mm}^3)$ – see Fig. 1, and is able to detect incoming bursts from at least a third of the sky. For polarization determination one uses Compton scattering between two plastics. The signal - modulation curve is shown in Fig. 2.
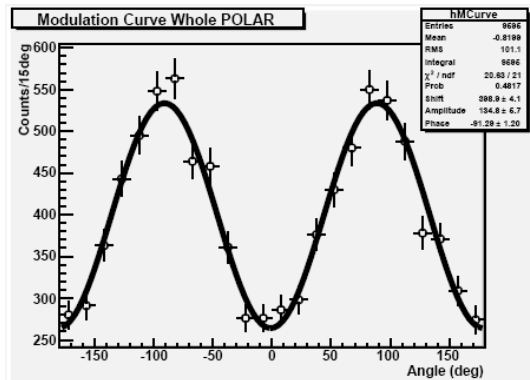
Fig. 2: Modulation curve for 100% polarized photons.

The energy range of incoming photons extends from 50 to 500 keV. A precise Monte Carlo model of POLAR was constructed at PSI using the GEANT4 package (CERN). It allows exposing of POLAR to the γ-ray fluxes coming from any direction and with a predefined polarization degree. For this work the energy spectrum of photons is described with the Band function normally used by the GRB community.
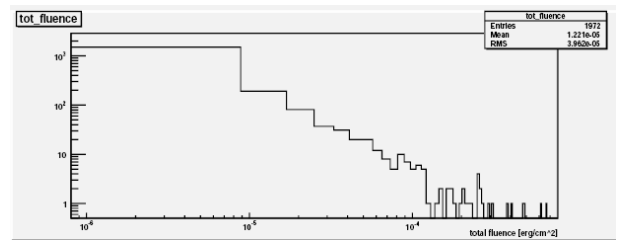
Fig. 3: GRB energy distribution in BATSE catalogue.

Parameters of the GRBs to be seen by POLAR are taken from the BATSE catalog. This instrument flew on the CGRO mission and detected between 1991 and 2000 about 3000 bursts. Distribution of their total energy is shown in the Fig. 3. Most of the bursts emit total energy below 10^{-5} erg/cm^2. Spectral parameters are computed for the 350 strongest bursts with 93 described by the Band model.
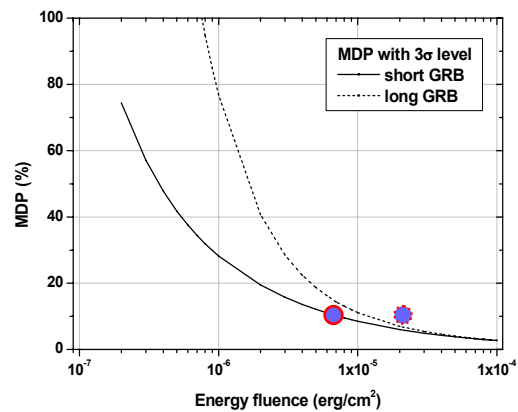
Fig. 4: MDP sensitivity curves with two BATSE GRBs.

The minimum detectable polarization MDP of POLAR was computed as a function of the burst energy fluence – see Fig. 4. Two curves show the MDP values for the short and long bursts. We also determined that POLAR will observe ca. 12 strong GRBs (energy fluence above 10^{-5} erg/cm^2) during one year. Using realistic Band parameters we confirmed the MDP curves with two BATSE triggers: 5563 – short and 6763 – long GRBs. It promises a large GRB sample with the MDP of ca. 10% and achievement of the POLAR scientific goals within two years of the mission.

RHESSI TESTS GAMMA-RAY BURST THEORIES

C. Wigger (PSI), O. Wigger, E. Bellm (UCB), W. Hajdas (PSI)

GRB021206 is one of the brightest Gamma Ray Bursts GRBs ever observed. Its prompt emission, as measured by RHESSI satellite, shows an unexpected spectral hardening around 5 MeV. Below this energy, the spectrum is well described by the usual Band function with the peak energy of about 700 keV. However, using the full RHESSI energy range up to 17 MeV, the spectrum can not be fitted with a Band function. The alternative Cannonball Model predicts such a spectral hardening, and we found that it fits the spectrum of GRB021206 perfectly.

Gamma-ray bursts (GRB) are highly energetic outbursts in the cosmos, occurring on a weekly timescale. The standard theory of GRBs, the fire-ball model, explains most properties of long GRBs satisfactorily, but not all. One of the alternative theories of GRBs, the cannonball model (CBM), makes predictions about the shape of the prompt - ray spectrum.

NASA with UC Berkeley and PSI built the Reuven Ramaty High Energy Solar Spectroscopic Imager RHESSI. This solar observatory [1] is equipped with the spectrometer having the broadest coverage of the photon spectrum currently in operation (together with Konus-Wind). It is located in a low Earth orbit and its telescope is always pointed at the Sun. However, photons above 60 keV can enter the detector from any direction, enabling RHESSI to be used for non-solar observations as well. The energy resolution is 3 keV at 1 MeV, and the time resolution is 1 μs. RHESSI is capable to see photons at energies above 4 MeV where other instruments' sensitivity falls off, thereby enabling us to test the CBM.

GRB021206 was detected on 6th December 2002 and is one of the brightest GRBs ever observed. We measured its fluence in the $0.1 - 10$ MeV band as $4.9 \ 10^{-4}$ erg/cm^2. The raw spectrum as observed in the rear segments of RHESSI Ge-spectrometer after background subtraction is shown in Fig. 1.

The standard GRB spectral model (Band function) fits the spectrum of GRB021206 only up to 4.5 MeV (purple line in the Fig. 1). At higher energies, the extrapolated Band function deviates from the data points. The spectral hardening around 5 MeV is significant (the purple residuals are not compatible with zero).

In the CBM theory [2], the spectral shape of the burst contains an additional term that makes the spectrum harder at high energies. Indeed, CBM fits the observed spectrum perfectly (blue line in the Fig. 1).

Since most GRB spectra suffer from low statistics at high energies and therefore large observational errors, the Band and CBM functions fit equally well in most cases. We analyzed seven other bright RHESSI GRBs detected from 2002 and 2003 and found that they all can be fit equally well with both functions.
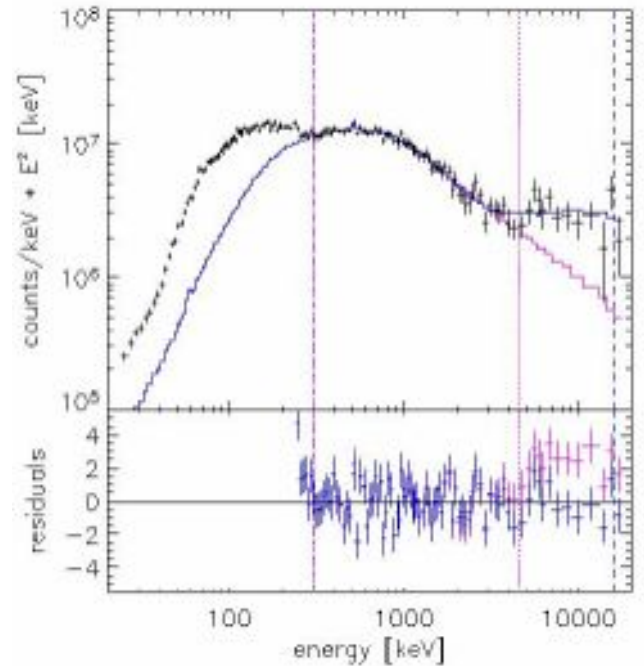
Fig. 1: Spectrum of GRB021206 observed by RHESSI. Black: observation, blue: fit to CBM function, purple: fit to Band function. The fit ranges are indicated by the vertical lines. The excess counts below 300 keV are due to Earth backscatter.

We therefore conclude that the Cannonball Model of Gamma-Ray Bursts is not ruled out by observations and should be considered for fitting GRB spectra. For full details of the analysis see [3].

REFERENCES

[1] R.P. Lin et al. Solar Physics, 210:3, 2002.

[2] A. Dar and A de R´ujula. Physics Reports, 405:203, 2004.

[3] C. Wigger, O. Wigger, E. Bellm, and W. Hajdas. ApJ, 675, 2008.

RHESSI INSTRUMENTAL LIMITS IN MEASUREMENTS OF THE GAMMA-RAY POLARIZATION FROM GRBS, SGRS AND SFS

W. Hajdas, E. Suares-Garcia, A. Mtchedlishvili, C. Wigger, A. Zehnder (PSI)

The Reuven Ramaty High Energy Solar Spectroscopic Imager RHESSI satellite with its 9 large Ge detectors may be used as a rotating gamma ray polarimeter. The polarimetric performance of RHESSI is analyzed below for the coincidence mode applicable at energies above 120 keV. The results are based both on the real RHESSI data and detailed Monte Carlo simulations. We found that despite of the RHESSI large modulation factor, other parameters like the effective area and background substantially limit its minimum detectable polarization MDP.

RHESSI was launched on the 5th Feb 2002 as the NASA SMEX mission into a circular Low Earth Orbit. The satellite points to the Sun and rotates with a period of 4 sec. Its instrumentation consists of the imager and Germanium spectrometer. The primary goal of the mission is to provide high resolution images and spectra from the Solar Flares SF in X-rays and γ-rays. The RHESSI spectrometer consists of 9 cylindrically shaped ultra high purity Ge-detectors – see Fig. 1. It covers a wide energy range from 3 keV up to 20 MeV. The data are stored using the event-by-event mode and for each event the photon energy, its arrival time and detector number are saved onboard for further downlink.
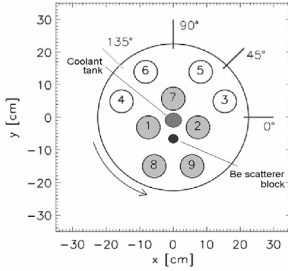
Fig. 1: Arrangement of RHESSI detectors. All nearby pairs are used for coincidence measurements.

A large field of view of up to 2π as well as a big detector volume also enables RHESSI for effective detection of Gamma Ray Bursts GRBs and Soft Gamma Repeaters SGRs. Typical detection rate of GRBs is 1-2 per week.
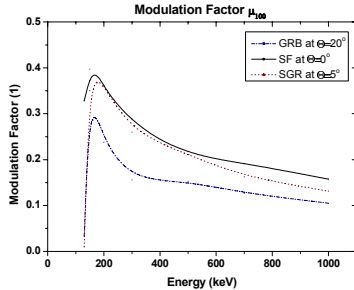
Fig. 2: Modulation factor of the RHESSI polarimeter.

Polarization measurements with RHESSI are possible for events coming at angles θ close to the rotation axis using coincidences of two close detectors at energies above 120 keV. The method utilizes Compton scattering. Spacecraft rotation provides sampling of the scatter distribution between two detectors and is used to construct modulation curves and extract polarization signals. Modulation factors

μ_{100} of the RHESSI polarimeter are determined for each type of event using GEANT3 Monte Carlo simulations – see Fig. 2. The values are relatively high reaching levels of 20-40%. In addition, we determined the RHESSI effective area A_{eff} for the polarimeter coincidence mode. The results are plotted in Fig. 3. It is seen that even at high energies A_{eff} reaches a few square cm only. The ultimate parameter of
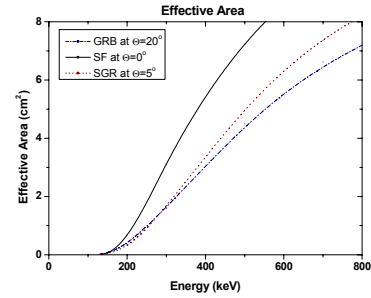
Fig. 3: Effective area of RHESSI polarimeter vs. energy.

the polarimeter is the Minimum Detectable Polarization MDP. It is defined in terms of the source and background rates. For RHESSI the event signal rate depends on the small effective area (≈ 1 cm^2) for detection of coincidences. The background rate is a sum of the real and accidental events, both proportional to the large effective area of the spectrometer for detection of single photons. Using μ_{100} and A_{eff} values as well as typical parameters for SFs, GRBs and SGRs like duration, energy fluence and spectral index we calculated MDPs of the device. As it is seen in table 1, even

Table 1: Description of polarization characteristics.

Event type	GRB	SF	SGR
Energy (keV)	100-1000	100-350	100-350
Power index (1)	2	3	6
Fluence(erg/cm^2)	$2.0\cdot10^{-4}$	$1.2\cdot10^{-3}$	$9.9\cdot10^{-5}$
Duration (sec)	1	200	400
Area single (cm^2)	177	282	82.2
Area coinc. (cm^2)	2.19	0.698	0.061
Mod. Factor (%)	14.6	31.7	45.7
Signal events (1)	1308	4165	36.3
Background (1)	64	4420	8840
Accidentals (1)	180	512	1
MDP-1σ (%)	35.	10.	700.

for the best polarization candidates either low signal rates or high background severely limit the MDP. Improvement by a factor of more than 10 is needed to pin down physical processes and mechanisms involved in the energy release.

SOLAR FLARE POLARIZATION MEASUREMENTS WITH RHESSI

E. Suarez-Garcia, W. Hajdas, C. Wigger, K. Arzner, M. Guedel, A. Zehnder (PSI), P. Grigis (ETHZ)

The degree of linear polarization in solar flares has not yet been precisely determined despite multiple attempts to measure it with different missions. The high energy range in particular has very rarely been explored, due to its greater instrumental difficulties. We approached the subject using the Reuven Ramaty High Energy Spectroscopic Imager (RHESSI) satellite to study 6 X-class and 1 M-class flares in the energy range between 100 keV and 350 keV.

To understand the acceleration and transport of particles in flaring regions, it is necessary to know both the angular and the energy distribution of energetic particles as they interact in the solar material. Attempts to measure the angular distribution of the accelerated electrons rely on the fact that an anisotropic ensemble of Bremsstrahlung-producing electrons will generate a radiation field that is both polarized and anisotropic. But to date, the level of linear polarization for the high energy emission of solar flares remains a variable extremely difficult to determine.

The RHESSI satellite enables polarization measurements in a wide range of energies from 20 keV to 1 MeV. Its spectrometer consists of 9 cylindrical (7.1 cm diameter) coaxial germanium detectors [3]. The satellite rotates with period of 4 sec continuously pointing at the Sun. It allows taking the images of the flares and determining location of the signal. It also reduces systematic effects in the polarization measurements. For photons between 20 and 100 keV, polarization can be measured using Be block as scatterer (see Fig. 1). [2]. For energies above 100 keV, polarization measurements are performed using the "coincidence mode" with photons that Compton-scatter from one Ge detector into another. The degree and orientation of the polarization are calculated from the modulation curve constructed for neighbour detector-pairs after taking into account the satellite rotation.
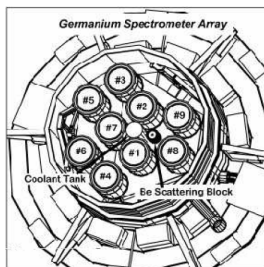
Fig. 1: Layout of RHESSI spectrometer.

We selected 6 X-class and 1 M-class flares with strong high energy emission and measured their linear polarization using the "coincidence mode". Flares located close to the solar limb are expected to present higher levels of polarization. Therefore, we selected flares that appeared in the outer part of the solar disk. We performed spectral fits to determine the energy regions of different emission mechanisms and we selected the non-thermal Bremsstrahlung part of the spectrum in the energy band from 100 to 350 keV. RHESSI data are store in the event-list. For every photon that RHESSI detected, the list gives its time of arrival, the detector it hit, and the deposited energy. Most of photons are completely absorbed in the first interaction, or are lost after it. Only about 0.1% of

them experience Compton scattering between two of germanium detectors of RHESSI. To select them we applied to the event-list strict cuts in energy, time, and geometry. Subsequently we subtracted accidental and background coincidences. Comparing the distribution of scattering directions with the Monte Carlo simulation of a 100% polarized photon flux the degree of linear polarization was obtained. The photons scattered in the Earth atmosphere were also simulated in detail to determine their influence on the results. It was found that they do not affect as they are mostly rejected by the selection cuts.

Only two studies on X-ray polarization of solar flares have been published to date, both of them using RHESSI in the "coincidence mode" [1, 4]. All together eight flares were measured. Results on the level of polarization are between 2% and 54%, with errors ranging from 5% to 26% in 1σ level (see Fig. 2). Regarding the angles of polarization, [1] found a correlation between the position of the flare in the solar disk and the orientation of the polarization vector for the two flares that they studied. We however, could not confirm this result. In contrary, we measured scattered values between 35° and 85°, which were independent on the flare location. Attempts to correlate them with different parameters were also inconclusive.
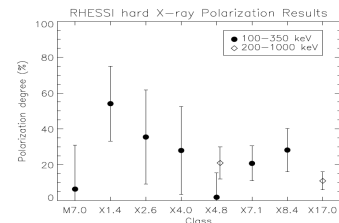
Fig. 1: Levels of linear polarization in hard X-ray energies vs. flare class. Filled dots – [4], diamonds – [1].

The currently available data are not sensitive enough to provide conclusive results on the polarization of the hard X-ray emission of solar flares. The RHESSI design is not optimized for polarization studies and the results obtained with it have been hampered by the small effective area and the high background contribution. Future progress will require a polarimeter able to measure polarization with errors on the level of 1 to 2%.

REFERENCES
[1] Boggs et al, ApJ, 638, 1129.
[2] McConnel et al, Solar Physics, 210, p. 125 (2002).
[3] Smith et al., Solar Physics, 210, p. 33 (2002).
[4] Suarez-Garcia et al., Solar Physics, 239, pp. 149 (2006).

DETERMINATION OF BIOGENIC AND FOSSIL CO_2 EMITTED BY WASTE INCINERATION BASED ON $^{14}CO_2$

S. Szidat (Univ. Bern), J. Mohn (EMPA)

Important industries, such as waste incinerators, co-incineration plants or cement kilns burn a mixture of biogenic and fossil fuel. The quantification of their respective contribution is highly relevant for emission budgets and emission trading. We developed a field application of the radiocarbon (^{14}C) method for the determination of biogenic vs. fossil CO_2 emissions at waste-to-energy plants (WTE).

1 INTRODUCTION

In Switzerland, over 99 % of combustible waste is currently incinerated. Although waste incineration is superior to landfilling regarding its overall environmental impact, it leads to significant CO_2 emissions which have to be considered in the national greenhouse gas inventory. While CO_2 emission factors per ton of waste are quite readily available, its fossil vs. biogenic distribution is usually only a rough estimate. Here, the ^{14}C method [1] enables a distinction of fossil carbon, in which the originally existing ^{14}C is completely decayed, and modern (biogenic) carbon, which exhibits the current ^{14}C level [2]. In the present study, we implemented the ^{14}C method for field measurements at three WTE plants. Additionally, an intercomparison measurement was performed using a completely independent approach (balance method), which is based on operation data of the incineration plants [3].

2 SAMPLING AND MEASUREMENT

Three waste incinerators (A – C) in the vicinity of Zurich (Switzerland) were investigated from October 2006 to February 2007. On-site sampling at all three WTE plants was done by collecting CO_2 samples integrating over several days. A constant flow of 10 mL of flue gas was sucked through two consecutive washing bottles (4 M aqueous KOH solution). CO_2 was released in the laboratory by acidification of <1 ml solution with 1 ml 4 M phosphoric acid. After removal of water vapour, CO_2 was isolated for ^{14}C determination.

REFERENCE VALUE OF BIOGENIC WASTE

For the correct calculation of the fossil CO_2 emissions of the incineration plants, the ^{14}C content of the pure biogenic fraction of the waste is needed as a reference. Due to the ^{14}C excess of the nuclear bomb tests [3], this value depends on the ^{14}C content of atmospheric CO_2 during tree growth and thus mainly on its age and felling year. Using Monte Carlo simulation, the ^{14}C content of the pure biogenic fraction was established as 113 ± 4 pMC by determination of the relative contribution for the main biogenic waste fractions (wood, paper and fresh biomass) and evaluation of the age distribution for each waste fraction.

3 RESULTS AND DISCUSSION

The ^{14}C method was successfully applied at three different WTE plants in Switzerland (Fig. 1). For every WTE plant, six time intervals of 3 to 4 days were selected.
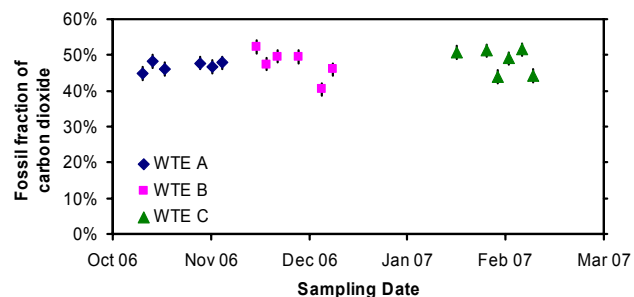
Fig. 1: Fractions of fossil CO_2 emissions for three WTE plants in Switzerland determined by the ^{14}C with 95% confidence intervals.

Excellent agreement between the ^{14}C method and the independent balance method [3] was observed with respect to the average fossil CO_2 emissions of all WTE plants (Tab. 1).

Tab. 1: Average fossil fractions by two independent methods with 95% confidence intervals.

Plant	^{14}C method	Balance method
WTE A	47.3 ± 2.6	48.1 ± 2.6
WTE B	47.9 ± 8.2	48.2 ± 2.8
WTE C	48.8 ± 6.9	50.3 ± 3.6

For all WTE plants, the fossil CO_2 fraction was >47%. It was thus distinctly higher than 40%, which is used in the current Swiss greenhouse gas inventory [4]. However, the emphasis of our study was on the method development. Seasonal variations in waste composition would have to be taken into consideration to obtain a reliable annual average.

4 ACKNOWLEGDEMENT

REFERENCES

[1] J. Mohn et al., Bioresour. Technol., in press, doi:10.1016/j.biortech.2007.11.042 (2007).
[2] I. Levin et al., Geophys. Res. Lett., **30**, 2194 (2003).
[3] J. Fellner et al., Environ. Sci. Technol., **41**, 2579 (2007).
[4] Federal Office for the Environment, Switzerland's greenhouse gas inventory 1990-2005, 58 (2007).

.

COMPOUND-SPECIFIC RADIOCARBON MEASUREMENTS OF AEROSOL COMPONENTS

S. Fahrni, H.W. Gäggeler, M. Ruff (Univ. Bern & PSI), S. Szidat (Univ.Bern), L. Wacker (ETHZ)

In order to gain better understanding of sources of carbonaceous aerosols, compound-specific radiocarbon analysis of the organic components is the technique of choice. Radiocarbon measurements are used to distinguish between contemporary and fossil sources and can thus help to explain emission and formation processes.

1   INTRODUCTION

Carbonaceous particles are of great interest in the environmental sciences and are therefore investigated intensively. About one third of the aerosol mass is made up from the carbonaceous fraction which consists of ~80% organic carbon (OC) and ~20% elemental carbon (EC). Since EC is a heterogeneous and high-molecular fraction, its isotope characterization is restricted to the overall material. In contrast to EC, OC consists of lower-molecular organic substances which can be separated by HPLC with an appropriate method. This procedure allows measuring the content of radiocarbon in single compound fractions. These measurements may give further insight into formation processes of secondary organic aerosols (SOA), and furthermore provide a powerful tool to assess sources of air pollution.

Radiocarbon measurements are carried out at the AMS facility at ETH/PSI, where it is possible to measure very small samples in the range of ~10 μg carbon, as necessary for compound-specific analysis [1]. In our study, we mainly focus on C_2-C_5 dicarboxylic acids, since they are part of the SOA fraction and their sources are not yet well understood. However, the applied technique is not restricted to aerosol studies, but also enables source apportionment in other compartments, such as soil.

2   EXPERIMENTAL

The aerosol filter material is cut into pieces and is put into a tube with about 15 ml water. Water extraction takes place in a sonication bath during 30 min. Thereupon, the aqueous solution is pressed through a filter (0.45 μm pore size) in order to remove the undissolved particles. The purified solution is frozen at -20 °C and lyophilized. The remaining yellowish, solid residue is dissolved in water and injected into a 50 μl injection loop of the HPLC.

The separation is conducted on an Acclaim OA column with an isocratic run (eluent: aqueous HCl, 5 mM, pH 2.3) within 15 min. The signal is detected with a light scattering detector. Fractions are collected automatically in suitable PFA vials and dried at 40 °C under a stream of nitrogen. For convenient handling, the dried fractions are redissolved in 20 μl water and injected into tin capsules which are closed by cold-welding. These capsules can be stored for weeks until they are combusted in the elemental analyzer (EA). The CO_2 produced in the EA is trapped and fed into the gas ion source of the AMS [1].

3   FIRST RESULTS

The chromatogram shown in Figure 1 features four organic acids, which are separated by HPLC. The chromatogram was obtained upon injection of an artificial mixture of the main carboxylic acids present in carbonaceous aerosols [2]. Since every filter sample contains other water-soluble components besides the carboxylic acids, overloading of the column is a problem.

In order to allow the combustion of aqueous samples in the elemental analyzer, an appropriate method was developed and tested.
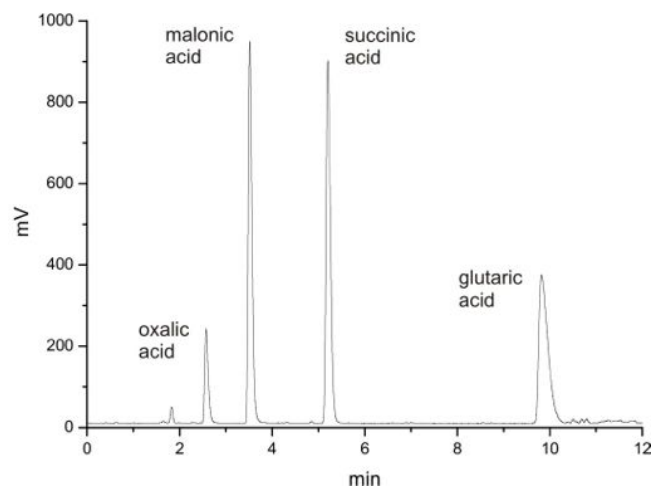
Fig. 1: Chromatogram of an artificial mix of C_2-C_5 dicarboxylic acids.

4   OUTLOOK

Overloading of the column lowers the separation capacity and disables the collection of single compounds. Therefore, overloading has to be avoided by means of a pre-separation or 2D chromatography. To provide a good separation from those compounds, their composition has to be identified by mass spectrometry. Further steps include testing the new coupling of the elemental analyzer and the CO_2 trap with the AMS facility.

REFERENCES

[1]   M. Ruff et al., Radiocarbon, **49**, 307-314 (2007).
[2]   C. Lund et al., Atmos. Chem. Phys., **4**, 1759-1769 (2004).

VALIDATION OF GASEOUS RADIOCARBON MEASUREMENTS USING A SEMIAUTOMATED SAMPLE AMPOULE CRACKER

M. Ruff, S. Fahrni, H.W. Gäggeler (Univ. Bern & PSI), S. Szidat (Univ. Bern),
H.-A. Synal (ETHZ & PSI), L. Wacker, M. Suter (ETHZ)

A gas inlet system for the measurement of radiocarbon in gaseous samples was installed at the Mini Radiocarbon Dating System (MICADAS), the smallest accelerator of the PSI/ETH AMS group in Zürich. The system is constructed for semi-automated measurements of small samples containing 1-50 µg carbon. The quality of the measurements has been determined by measuring certified reference materials.

1 INTRODUCTION

Direct radiocarbon measurements with gaseous samples are one possibility to get along with the strong demand on measuring small samples in the range of $1 - 50$ µg carbon. Especially in the wide field of environmental and geological research, the interest of measuring those small samples as precise as possible increase more and more. For this reason a hybrid cesium sputter source was build at the smallest accelerator mass spectrometer at PSI/ETH Zurich (MICADAS, 200 kV). The ion source is able to measure carbon dioxide in addition to graphite targets without requiring any rebuilding at the machine. The gaseous CO_2 samples are supplied in glass ampoules. A gas inlet system was constructed [1] for releasing the small amounts of CO_2 and mixing it with helium for better handling. The whole system is now running for more than 15 months and used for routine operation. To determine the quality of the measurements, a number of 14 samples of different certified reference materials were measured.

2 SAMPLE PREPARATION AND MEASUREMENT

For sample preparation, the reference materials IAEA C5 (wood), IAEA C6 (sucrose) and IAEA C7 (oxalic acid) have been combusted as described in [2]. The released carbon dioxide was subdivided in 3-5 glass ampoules in the range of 3-23 µg carbon content each. 2-3 samples of each approach have been measured. The reference material IAEA C8 (oxalic acid) has been combusted using the sample preparation line of the radiocarbon laboratory of ETH Zurich. Only one sample ampoule containing 32 µg carbon was measured.

The 4 % CO_2 in helium mixture is transferred by a stepping motor continuously into the ion source via a 2 m fused silica capillary connected to the centre of the cathode target. All samples were measured during 2 days of operation at the ETH/PSI MICADAS system. The OXA I standard (oxalic acid) was used for calibration; ^{14}C-free blanks were prepared using carbon dioxide from a common pressure gas bottle.

3 RESULTS

The contribution of the measured samples with their nominal value is shown in Fig. 1. The values are split in two groups: samples with an amount of carbon between 15 and 32 µg carbon and samples containing less than 10 µg carbon. According to the counting statistic, which is the main source for the deviation, the different uncertainties of
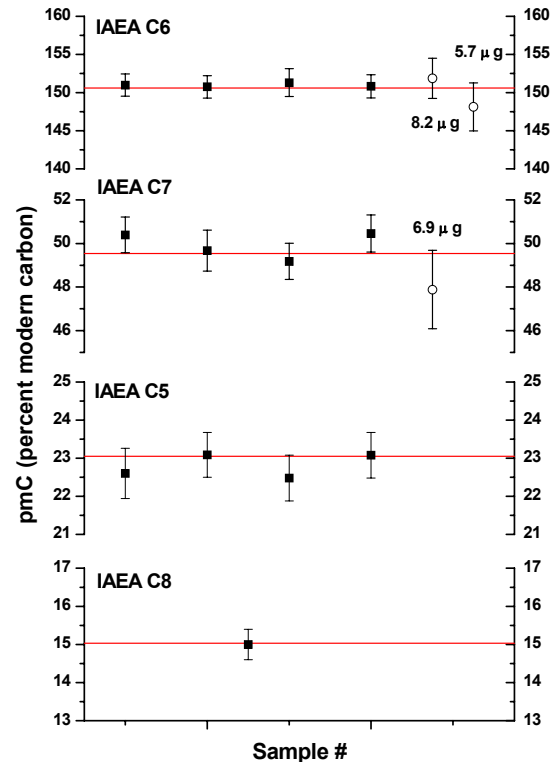
Fig. 1: Measured values for the reference materials with 1σ uncertainties. The red lines mark the nominal value, the closed dots the samples in the range of 15-32 µg C and the open dots represent the samples smaller than 10 µg C.

the samples depend on the sample size and the age of the used materials. The blank value was 0.7 ± 0.2 pmC (~40'000 years old). All results are in perfect agreement with the nominal value and no trend is visible during the measurements.

4 ACKNOWLEDEGMENT

We thank Edith Vogel (Bern University) for preparing standard and blank samples for the gas measurements.

REFERENCES

[1] M. Ruff et al., Radiocarbon, **49**(2), 307 (2007).
[2] S. Szidat et al., Nucl. Instr. and Meth. in Phys. Res. B, **223-224**, 829 (2004).

AUTOMATION OF RADIOCARBON MEASUREMENTS USING AN ONLINE COUPLED ELEMENTAL ANALYSER

M. Ruff, S. Fahrni, H.W. Gäggeler (Univ. Bern & PSI), S. Szidat (Univ. Bern),
H.-A. Synal (ETHZ & PSI), L. Wacker, M. Suter (ETHZ)

For a complete automation of radiocarbon measurements, an elemental analyser (EA) as an automatic combustion unit was connected to the gas inlet system described before. A first online system was built up and first measurements have been done.

1   INTRODUCTION

Radiocarbon measurements with gaseous samples supported in glass ampoules [1] are time consuming and require much manpower, as the ampoule cracker is difficult to automate. Hence, this method is only useful for samples which need a special treatment for combustion like the separation of organic and elemental carbon in environmental samples. With the combination of an elemental analyser and the gas inlet system, online radiocarbon measurements from combustion to detection can be realised [2]. An elemental analyser has the advantage that combustion as well as gas separation are automated and can be optimised. The samples are stored in tin capsules in the auto sampler. After combustion, the amount of carbon dioxide is determined by a thermal conductivity detector. As the combustion gases leave the elemental analyser in a high stream of helium, the goal is to transfer the carbon dioxide into the syringe of the gas inlet system described earlier in this annual report. [3]

2   INSTRUMENTAL SETUP

A schematic picture of the setup is shown in Fig.1. During combustion, the elemental analyser (Elementar, Hanau, Germany) produces nitrogen, carbon dioxide and water. These gases are separated by an internal adsorption trap. The machine is permanently flushed with a helium flow of 80 ml/min. The gas flow is always directed via valve 1 to the atmosphere. As the concentration of carbon dioxide is much too low for direct measurements, it has to be enriched on an external trap. This is realised by switching valve 1: the gas streams through a chemical trap filled with a zeolite material. While the carbon dioxide keeps on the trap, helium runs straight to the atmosphere. The external trap can be heated up to 500 °C. The carbon dioxide is released and can be flushed with helium into the existing syringe of the gas inlet system used for the ampoule cracker. The whole gas leading system is optimised for short pathways and small dead volumes. All connecting tubes are made of stainless steel capillaries with only 0.5 mm inner diameter.

3   RESULTS

Some measurements with standards and blanks have been made. The blank is ~1.6 pmC (~35.000 a), which is higher compared to the measurements with the ampoule cracker [3]. This increased value mainly comes from the tin capsules used for the samples which contain up to 0.2 μg carbon.

First tests indicated that no cross contamination was caused by the external zeolite trap: the blank value measured directly after a standard sample (OXA II with 135 pmC) was not significantly increased. Two samples with certified reference material IAEA C7 with a nominal value of 49.54 pmC have been measured. Both results (50.36 ± 1.46 and 50.29 ± 1.10 pmC) are in good agreement with the nominal value.
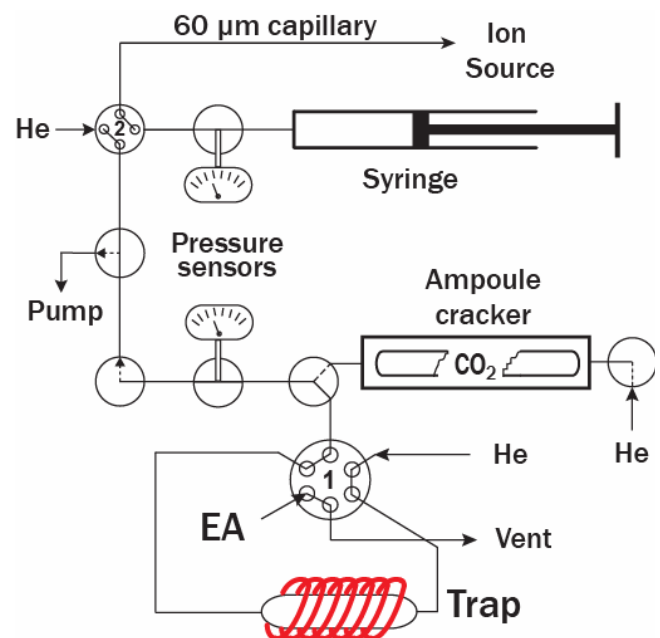
Fig. 1: Scheme of the online system with elemental analyser (EA) and gas inlet.

4   OUTLOOK

The system will be rebuilt to combine both methods within one system, measurements with the elemental analyser and the ampoule cracker. A LabView-controlled software program is in progress. Further investigations aim at the reduction of the increased blank value.

REFERENCES

[1] M. Ruff et al., Radiocarbon, **49**(2), 307 (2007).
[2] T. Uhl et al., Radiocarbon, **46**(1), 65 (2004).
[3] M. Ruff et al., Ann. Rep. Labor für Radio- und Umweltchemie, this report p. 50.

INVESTIGATION OF I-129 IN LAKE THUN

K. Li, E. Vogel, U. Krähenbühl (Univ. Bern), V. Alfimov (ETH)

Increased level of ^{129}I and the powerful technique highlight the feasibility of applying ^{129}I as an environmental tracer in studying geochemical or hydrodynamic process of a specified system. The study presented here utilizes Accelerator Mass Spectrometry (AMS) to investigate the distribution of ^{129}I in the system of Lake Thun, between stratified layers, and between water and suspended particles. The possible relations between the water mixing process and the distribution of ^{129}I in the lake are examined preliminarily.

1 INTRODUCTION

The increased content of long-lived radionuclide ^{129}I ($T_{1/2} = 1.57E7$ y) in environmental samples from air, water and soil has been reported for European area due to anthropogenic input. Data shows a spatial and temporal variation clearly related to the distance and the ^{129}I releasing schedule from the source, e.g. the two noticeable nuclear fuel reprocessing plants at Sellafield (Great Britain) and La Hague (France). This highlights the feasibility of applying ^{129}I as a environmental tracer in the investigations of hydrosphere, e.g. as oceanographic tracer to study the transport, the circulation and the exchange of the water mass in the area of North Atlantic, North sea and Baltic sea[1]. Besides the spatial variation in global scale, local discrepancy has also been shown in some studies when comparisons were made between surface and deep water for a lake[2]. Given the specified input pattern, this discrepancy could be related to the mixing process of the lake itself, which is important for assessment of pollutant fate in a lake system.

This project is intended to find out whether ^{129}I can be an alternative indicator, beside the temperature, oxygen or concentrations of nutrients, to study the mixing process of the lake. For this purpose, the contents of ^{129}I at different depth of water as well as ^{129}I bonded on suspended particles are investigated on a monthly time scale.

2 EXPERIMENT

Lake Thun is in the middle of Europe, without direct influence from any noticeable nuclear fuel reprocessing plants. Origin of ^{129}I attributes to wet/dry precipitation, either directly into the lake or into the rivers and their catchment area and transport into the lake along with the water flow. About 40L of water from the lake were taken monthly from the surface and 100m depth, respectively, at the position (+46°40'30.27"N, +7°44' 32.73"E), for which the temperature profile is available from GSA (Amt für Gewässerschutz und Abfallwirtschaft), Canton Bern.

Original samples are filtered through 0.45μm membrane filters for collecting ≥10mg of particular matter and 2L water samples, respectively. The particles (with filter) are digested by microwave oven in TMAH (tetramethylammonium hydroxide) matrix. After filtration, ^{127}I carrier is added. $NaHSO_3$ is used to reduce all iodine species to I^-. By addition of HNO_3/H_2O_2, I_2 is formed, which is extracted into toluene and back-extracted as I^- by an aqueous solution of ascorbic acid. AgI is formed by addition of $AgNO_3$ in to the ascorbic acid solution. The 2L water collected after filtration are processed following the procedure described by Szidat[3]. All AgI samples are washed by MQ water, separated by centrifugation, and dried at 60°C overnight before being measured by AMS. A small fraction of each sample is measured by ICP-MS prior to the addition of ^{127}I carrier to get the original concentration of ^{127}I in the sample.

Ratio of ^{129}I/^{127}I is measured by AMS at ETH/PSI (0.5MV tandem accelerator "Tandy"[4]). Two charge states, +3 and +4, are used with total energies of 2 and 2.5 MeV, respectively. The main interferences are $^{97}Mo^{3+}$ for +4 state, and $^{43}Ca^+$, $^{86}Sr^{2+}$, or molecular ions with same m/z values for +3 state. For usual samples, the achieved ^{129}I/^{127}I backgrounds are 3E-13 for +4 state and 1E-13 for +3 state.

3 PRELIMINARY RESULTS

Filtered water samples collected in the months of Jun. to Aug. have been measured as showed in table 1. The ratio of ^{129}I/^{127}I varied between 1.9-6.8 ×10^{-8}. The highest value was found in July when the highest water level happened due to heavy precipitation. This indicates that the main source of ^{129}I in Lake Thun is from the precipitation. In addition, a trend of higher ratio of ^{129}I/^{127}I in deep water comparing to the surface water exist throughout these three months. Taking into account the flow direction and the temperature profile within the lake as well as the temperatures of the two dominating contributors, i.e. river Aare and river Kander, the discrepancy with depth is not likely due to the different concentrations of ^{129}I in the sources. The higher values of ^{129}I/^{127}I in 100m depth probably come from the former higher input of ^{129}I which has been evenly distributed in whole water column due to the last overturn. The thermal stratification effect in the summer prevents the mixing and equal distribution of the fresh input water containing ^{129}I. Further test for particles should provide more detailed information about the ^{129}I distribution along with the lake mixing process.

Table 1 Ratio of ^{129}I/^{127}I in water of Lake Thun

	Water of surface (×10^{-8})	Water of 100m depth(×10^{-8})
June	2.91 ± 0.19*	3.15 ± 0.22
July	5.65 ± 0.29	6.83 ± 0.34
August	1.92 ± 0.15	2.24 ± 0.15

*the uncertainties for all values are calculated based on the measured results from ICP-MS and AMS with 1σ.

REFERENCES

[1] X. Hou, Journal of Radioanalytical and nuclear Chemistry 262-1, 67-75(2004).
[2] P. H. Santschi, et al, Science of the total Environment 321, 257-271 (2004).
[3] S. Szidat, Thesis, (2002).
[4] M. Stocker, et al, Nuclear Instruments and Methods in Physics Research B 240, 483–489 (2005).

RADIOCARBON-SUPPORTED SOURCE APPORTIONMENT OF PM10 CARBONACEOUS AEROSOL ALONG THE SWISS RHONE VALLEY

N. Perron, A. Prévôt, U. Baltensperger (PSI LAC), S. Szidat, M. Ruff (Univ. Bern & PSI), L. Wacker (ETHZ)

The PM10 compositions of carbonaceous aerosol were investigated at five different sites along the Swiss Rhone Valley in November-December 2006. The radiocarbon content of daily filters was analysed so as to assess the influence of fossil and non-fossil contributions to the PM10 burden at these location. We found a significantly lower fossil contribution on Sunday compared to weekdays, probably resulting from the influence of the Sunday truck ban in Switzerland.

1 MOTIVATIONS

PM10 (particulate matter with an aerodynamic diameter below 10μm) in the Swiss Canton of Valais has been a matter of growing concern over the last years. In 2006, almost all the measuring sites along the Rhone valley recorded PM10 yearly concentrations exceeding the Swiss legal threshold of 20μg/m^3 [1]. Understanding this pollution phenomenon to undertake efficient abatement strategies requires source apportionment of the carbonaceous contribution since these aerosols are one of the main components of PM10. Radiocarbon, which enables to discriminate between fossil and contemporary sources of carbonaceous aerosol, is a very well suited tracer to achieve this goal [2].

2 METHODS

During a winter campaign in November-December 2006, daily PM10 samples were collected on pre-heated quartz-fibre filters at five stations along the Swiss Rhone valley: two sites with industrial proximity, one rural site on the valley-floor, one rural site at more elevated altitude and one site in a town centre. The organic carbon (OC) and elemental carbon (EC) contents of the filters were separated using the THEODORE system, as described by Szidat et al. [2], and transformed into CO_2 for later ^{14}C-analyses by accelerator mass spectrometry (AMS) at PSI/ETH Zürich.

3 RESULTS AND DISCUSSION

In the weekdays (excluding Saturday), the average EC fossil contributions range from 12% for the elevated rural site of Eggerberg to 25% for the town-centre, traffic-influenced site of Sion. The two industrial-proximity sites exhibit very different patterns. Massongex is comparable to the rural site of Saxon on the valley floor whereas the profile of Brigerbad is much closer to that of Sion. Since traffic in Brigerbad is very unlikely to be as high as in Sion, this reveals possibly a higher influence of the industrial activities than in Massongex, at least under the then prevailing meteorological conditions.

Furthermore, all sites (except Eggerberg, for which too few ^{14}C analyses could be performed due to the low concentrations) show a clear reduction of fossil emissions on Sunday compared to the weekdays, revealing a significant decrease of fossil fuel-emitting activities during the week-end.

4 ACKNOWLEDGEMENT

REFERENCES

[1] Qualité de l'air en Valais – Résival – Rapport 2006.
[2] S. Szidat et al., J. Geophys. Res. **111**, D07206 (2006).
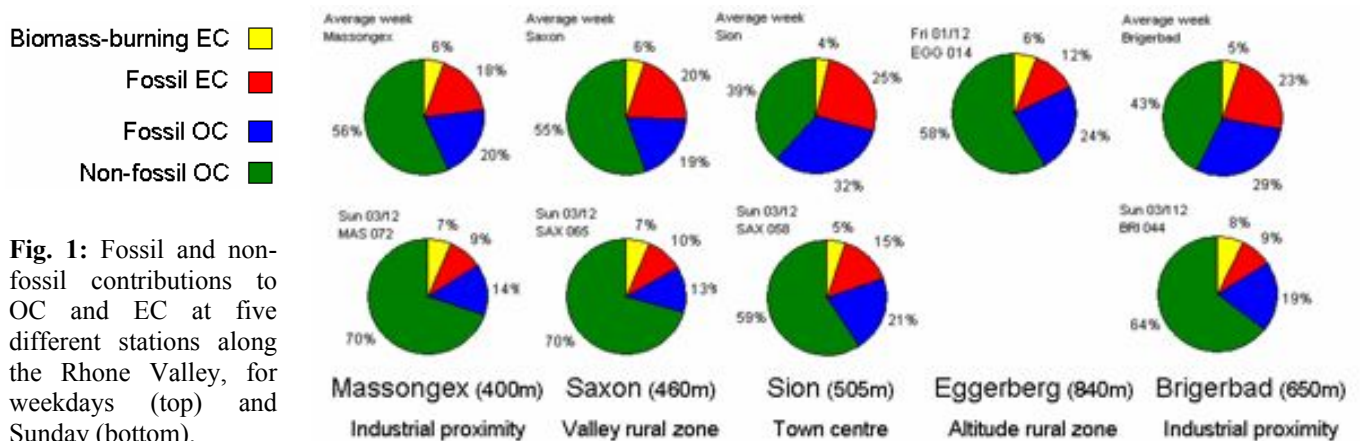
Fig. 1: Fossil and non-fossil contributions to OC and EC at five different stations along the Rhone Valley, for weekdays (top) and Sunday (bottom).

LIST OF PUBLICATIONS

HEAVY ELEMENTS

R. Eichler, N.V. Aksenov, A.V. Belozerov, G.A. Bozhikov, V.I. Chepigin, R. Dressler, S.N. Dmitriev, H.W. Gäggeler, V.A. Gorshkov, F. Haenssler, M.G. Itkis, V.Y. Lebedev, A. Laube, O.N. Malyshev, Yu.Ts. Oganessian, O.V. Petruschkin, D. Piguet, P. Rasmussen, S.V. Shishkin, A.V. Shutov, A.I. Svirikhin, E.E. Tereshatov, G.K. Vostokin, M. Wegrzecki, A.V. Yeremin
Chemical properties of element 112
Nature **447**, 72-75 (2007).

R. Eichler, N.V. Aksenov, A.V. Belozerov, G.A. Bozhikov, V.I. Chepigin, R. Dressler, S.N. Dmitriev, H.W. Gäggeler, V.A. Gorshkov, F. Haenssler, M.G. Itkis, V.Y. Lebedev, A. Laube, O.N. Malyshev, Yu.Ts. Oganessian, O.V. Petruschkin, D. Piguet, P. Rasmussen, S.V. Shishkin, A.V. Shutov, A.I. Svirikhin, E.E. Tereshatov, G.K. Vostokin, M. Wegrzecki, A.V. Yeremin
Confirmation of the decay of ^{283}112 and evidence for Hg-like behavior of element 112
Nucl. Phys. **A787**, 373c-380c (2007).

S. Hofmann, D. Ackermann, S. Antalic, H.G. Burkhard, R. Dressler, F.P. Hessberger, B. Kindler, I. Kojouharov, Kuusiniemi, M. Leino, B. Lommel, R. Mann, G. Munzenberg, K. Nishio, A.G. Popeko, S. Saro, H.J. Schott, B. Streicher, B. Sulignano, J. Uusitalo, A.V. Yeremin
Studies of superheavy elements at SHIP
Int. J.Mod. Phys. **E16**, 937 (2007)   (NSR code: JOUR IMPEE 16 937).

U. Köster, O. Arndt, R. Catherall, J.G. Correia, B. Crepieux, R. Eichler, P. Fernier, L.M. Fraile, S. Hennrich, Johnston, S. Lukic, J. Neuhausen, B.S. Nara Singh, B. Pfeiffer, E. Siesling
ISOL beams of hafnium isotopes and isomers.
Eur. Phys. J. Special Topics **150**, 293–296 (2007).

SURFACE CHEMISTRY

M. Ammann, U. Pöschl
Kinetic model framework for aerosol and cloud surface chemistry and gas-particle interactions: Part 2 - exemplary practical applications and numerical simulations
Atmos. Chem. Phys. **5**, 7, 6025–6045, 2007.

F. Domine, M. Albert, T. Huthwelker, H.-W. Jacobi, A.A. Kokhanovsky, M. Lehning, G. Picard, W.R. Simpson
Snow physics as relevant to snow photochemistry
Atmos. Chem. Phys. Discuss. **7**, 5941-6036, 2007.

A. M. Grannas, A.E. Jones, J. Dibb, M. Ammann, C. Anastasio, H.J. Beine, M. Bergin, J. Bottenheim, C.S. Boxe, G. Carver, G. Chen, J.H. Crawford, F. Dominé, M.M. Frey, M.I. Guzman, D.E. Heard, D. Helmig, M.R. Hoffmann, R.E. Honrath, L.G. Huey, M. Hutterli, H.W. Jacobi, P. Klan, B. Lefer, J. McConnell, J. Plane, R. Sander, J. Savarino, P.B. Shepson, W.R. Simpson, J.R. Sodeau, R. von Glasow, R. Weller, E.W. Wolff, T. Zhu
An overview of snow photochemistry: evidence, mechanisms and impacts
Atmos. Chem. Phys. **7**, 4329-4373, 2007.

M. Hess, U.K. Krieger, C. Marcolli, T. Huthwelker, M. Ammann, W.A. Lanford, Th. Peter
Bromine enrichment in the near-surface region of Br-doped NaCl single crystals diagnosed by rutherford backscattering spectrometry
J. Phys. Chem. A **111**, 4312-4321, 2007.

M. Kerbrat, S. Le Calve, P. Mirabel
Uptake measurements of ethanol on ice surfaces and on supercooled aqueous solutions doped with nitric acid between 213 and 243 K
J. Phys. Chem. A **111**, 925-931, 2007.

M. Kerbrat, B. Pinzer, T. Huthwelker, H.W. Gäggeler, M. Ammann, M. Schneebeli
Measuring specific surface area of snow with X-ray tomography and gas adsorption: comparison and implications for surface smoothness,
Atmos. Chem. Phys. Discuss. **7**, 10287–10322, 2007.

M.J. Krisch, R. D'Auria, M.A. Brown, D.J. Tobias, J.C. Hemminger, M. Ammann, D.E. Starr, H. Bluhm
The effect of an organic surfactant on the liquid-vapor interface of an electrolyte solution
J. Phys. Chem. **111**, 13497-13509, 2007.

U. Pöschl, Y. Rudich, M. Ammann
Kinetic model framework for aerosol and cloud surface chemistry and gas-particle interactions: Part 1 - general equations, parameters, and terminology
Atmos. Chem. Phys., **5**, 7, 5989–6023, 2007.

K. Stemmler, M. Ndour, Y. Elshorbany; J. Kleffmann, B. D'Anna, C. George, B. Bohn, M. Ammann
Light induced conversion of nitrogen dioxide into nitrous acid on submicron humic acid aerosol
Atmos. Chem. Phys. **7**, 4237–4248, 2007.

O. Vesna, S. Sjogren, E. Weingartner, V. Samburova, M. Kalberer, H.W. Gäggeler, M. Ammann
Changes of fatty acid Aerosol hygroscopicity induced by ozonolysis under humid conditions
Atmos. Chem. Phys. Discuss. **7**, 15651-15668, 2007.

ANALYTICAL CHEMISTRY

T.M. Jenk, S. Szidat, M. Schwikowski, H.W. Gäggeler, L. Wacker, H.-A. Synal, M. Saurer
Microgram level radiocarbon (^{14}C) determination on carbonaceous particles in ice
Nucl. Instr. Meth. Phys. Res. B **259**, 518-525, doi:10.1016/j.nimb.2007.01.196 (2007).

M. Luetscher, D. Bolius, M. Schwikowski, U. Schotterer, P.L. Smart
Comparison of techniques for dating of subsurface ice from Monlesi ice cave, Switzerland
J. Glaciology **53**, No. 182, 374-384 (2007).

H. Reithmeier, M. Schwikowski, V. Lazarev, W. Rühm, H.W. Gäggeler, E. Nolte
Increase of ^{129}I in the European environment
Chimia **61** (1/2), 283 (2007).

RADWASTE ANALYTICS

U. Köster, P. Carbonez, A. Dorsival, J. Dvorak, R. Eichler, S. Fernandes, H. Frånberg, J. Neuhausen, Z. Novackova, R. Wilfinger, A. Yakushev
(Im-)possible ISOL beams
Eur. Phys, J. Special Topics **150**, 285-291 (2007).

Y. Nir-El, G. Haquin, Z. Yungreiss, M. Hass, G. Goldring, S.K. Chamoli, B.S. Nara Singh, S. Lakshmi, U. Köster, N. Champault, A. Dorsival, V.N Fedoseyev, G. Georgiev, B.A. Marsh, D. Schumann, G. Heidenreich, S. Teichmann
Precision measurement of the decay rate of ^{7}Be in host materials
Phys. Rev. C**75**, 012801 (R) (2007).

D. Schumann, J. Neuhausen, R. Weinreich, F. Atchison, P. Kubik, H.-A. Synal, G. Korschinek, Th. Faestermann, G. Rugel
Determination of the radionuclide inventory in accelerator waste using calculation and radiochemical analysis
Nucl. Inst. Meth. B **264** (2007) 83-95.

D. Schumann, J. Neuhausen
Accelerator waste as a source for exotic radionuclides
J. Phys. G: Nucl. Part. Phys. **35** (2008) 014046.

PROTON IRRADIATION FACILITY

H. Araújo, C. Boatella, M. Chmeissani, A. Conchillo, E. García-Berro, C. Grimani, W. Hajdas, A. Lobo, L. Martínez, M. Nofrarias, J. A. Ortega, C. Puigdengoles, J. Ramos-Castro, J. Sanjuán, P. Wass, X. Xirgu,
LISA and LISA PathFinder, the endeavour to detect low frequency GWs
Physics: Conference Series, **66** 012003 (2007).

S.E. Boggs, A. Zoglauer, E. Bellm, K. Hurley, R. P. Lin, D. M. Smith, C. Wigger, W. Hajdas
The giant flare of 2004 December 27 from SGR 1806-20
The Astrophysical Journal, **661** 458-467 (2007).

J.M. Edmund, C. E. Andersen, S. Greilich, G. O. Sawakuchi, E. G. Yukihara, M. Jain, W. Hajdas, S. Mattsson,
Optically stimulated luminescence from Al2O3:C irradiated with 10 60 MeV protons
Nucl. Instr. and Meth. in Physics Research Section A, **580** 210-213 (2007).

W. Hajdas, E. Suares-Garcia, A. Mchedlishvili, C. Wigger, A. Zehnder
RHESSI instrumental limits on measurements of the gamma-ray polarization from GRBs, SGRs and SFs
Proceedings of the 6th INTEGRAL Workshop, The Obscured Universe, Space Research Institute (IKI), Moscow, Russia, July 2-8, 2006, ESA's Publications Division Special Publication SP-622.

W. Hajdas, E. Suares-Garica, C. Wigger, O. Bergogne, P. Buehler, A. Mohammadzadeh, F. di Marco, N. Produit, M. Schmidt
Tracking down the spectral data from the SGR1806-20 geant flare with the IREM instrument on INTEGRAL
Proceedings of the 6th INTEGRAL Workshop, The Obscured Universe, Space Research Institute (IKI), Moscow, Russia, July 2-8, 2006, ESA's Publications Division Special Publication SP-622.

M. Jain, C. E. Andersen, W. Hajdas, J. M. Edmund, L. Bøtter-Jensen
OSL response to proton irradiation in some natural dosemeters: Implications for martian sediment dating
Nuclear Instruments and Methods in Physics Research Section A, **580** 652-655 (2007).

C. Wigger, W. Hajdas, A. Zehnder, K. Hurley, E. Bellm, S. Boggs, M. Bandstra, D.M. Smith
Spectral Analysis of GRBs Measured by RHESSI
Nuovo Cimento B, **121,** 1117-1121. (2007).

RADIOCHEMISTRY UNIVERSITÄT BERN

M.R. Alfarra, A.S.H. Prévôt, S. Szidat, J. Sandradewi, S. Weimar, V.A. Lanz, D. Schreiber, M. Mohr, U. Baltensperger
Identification of the mass spectral signature of organic aerosols from wood burning emissions
Environ. Sci. Technol. **41**, 5770-5777, doi:10.1021/es062289b (2007).

O. Eugster, S. Lorenzetti, U. Krähenbühl, K. Marti
Comparison of cosmic-ray exposure ages and trapped noble gases in chondrule and matrix samples of ordinary enstatite and carbonaceous chondrites
Meteoritics & Planet. Sci. **42** 1351-1371 (2007).

N. Homazava, A. Ulrich, M. Trottmann, U. Krähenbühl
Micro-capillary system coupled to ICP-MS as a novel technique for investigation of micro-corrosion processes
J. Anal. At. Spectrom. (2007) **22** 1122-1130.

M. Ruff, L. Wacker, H.W. Gäggeler, M. Suter, H.-A. Synal, S. Szidat
A gas ion source for radiocarbon measurements at 200 kV
Radiocarbon **49**, 307-314 (2007).

S. Szidat, A.S.H. Prévôt, J. Sandradewi, M.R. Alfarra, H.-A. Synal, L. Wacker, U. Baltensperger
Dominant impact of residential wood burning on particulate matter in Alpine valleys during winter
Geophys. Res. Lett. **34**, L05820, doi:10.1029/2006GL028325 (2007).

A. Ulrich, T. Barrelet, U. Krähenbühl
Spatially resolved plant physiologicalaAnalysis using LA-HR-ICP-MS
Chimia, **61** 111 (2007).

Bookchapter

Dr. Wojtek Hajdas
E.P. Kontar, J.C. Brown, A.G. Emslie, W. Hajdas, G.D. Holman, G.J. Hurford, J. Kasparova, P.C.V. Mallik,
A.M. Massone, M.L. McConnell, M. Piana, M. Prato, E.J. Schmall, E. Suarez-Garcia
The RHESSI book:
Angular
Chapter 7.5.5. X-ray polarization and electron angular distribution
2007 Springer Science + Business Media. Printed in the USA

REPORTS

E. Bellm, C. Wigger, M. Bandstra, S. Boggs, W. Hajdas, D.M. Smith, K. Hurley
RHESSI spectrum of GRB070508
GRB Coordinates Network, Circular Service, 6399, 1 (2007).

W. Hajdas
Proton Irradiation Facility Annual Report 2006
European Space Agency Internal Document.

W. Hajdas
POLAR Demo Model Electronics
POLAR Progress Meeting, ISDC, Versouix, 4 April 2007.

W. Hajdas
Test of BC400 responses to gammaand beta sources
POLAR Progress Meeting, PSI, Villigen, 22 May 2007.

W. Hajdas
1. Electronics for POLAR DM
2. Tests of the BC400 scintillator response
POLAR Progress Meeting, DPNC, Geneva, 22 June 2007.

W. Hajdas
POLAR EM – PSI Activities in June – August 2007
POLAR Progress Meeting, DPNC, Geneva, 24 August 2007.

W. Hajdas
1. POLAR Demo Electronics
2. Tests of Plastics from Institute of Nuclear Reactions Warsaw
POLAR Progress Meeting, DPNC, Geneva, 17 December 2007.

S. Hofmann, D. Ackermann, S. Antalic, H.G. Burkhard, V.F. Comas, R. Dressler, Z. Gan, S. Heinz, J.A. Heredia,
G. Munzenberg, K. Nishio, A.G. Popeko, S. Saro, H.J. Schott, B. Streicher, B. Sulignano, J. Uusitalo, A.V. Yeremin
Studies of SHE at SHIP
Proc.Intern.Symposium on Exotic Nuclei, Khanty-Mansiysk, Russia, 17-22 July, 2006, Yu.E.Penionzhkevich,
E.A.Cherepanov, Eds. p.211 (2007); AIP Conf.Proc. 912 (2007)   (NSR code: CONF Khanty-Mansiysk (Exotic Nuclei)
Proc, P211).

M.M. Marin Marmol, J. Neuhausen, S. Lüthi, D. Schumann
Experimental study of Po evaporation from liquid eutectic lead-bismuth alloy in vacuum
TM-18-07-02 Paul Scherrer Institut, Villigen 200.7

J. Neuhausen, R. Dressler, B. Eichler, R. Eichler, D. Schumann
Report on Semi-Empirical Modeling of Thermodynamical Data for the Assessment of the Solubility
and Chemical Behavior of Nuclear Reaction and Corrosion Products in a liquid Lead-Bismuth Spallation Target
EUROTRANS Domain 4 DEMETRA Report D4.32., Paul Scherrer Institut, Villigen 2007.

J. Neuhausen, D. Schumann
Gas phase concentrations of volatile nuclear reaction products in the MEGAPIE expansion tank
TM-18-07-03 Paul Scherrer Institut, Villigen 2007.

F. v. Rohr, J. Neuhausen, D. Schumann, R. Eichler, R. Dressler
Über das Verhalten von ^{210}Po in Blei-Wismut
TM-18-07-01, Paul Scherrer Institut, Villigen 2007.

C. Wigger, E. Bellm, M. Bandstra, S. Boggs, W. Hajdas, D.M. Smith, K. Hurley
RHESSI spectrum of GRB070220
GRB Coordinates Network, Circular Service, 6135, 1 (2007).

CONTRIBUTIONS TO CONFERENCES, WORKSHOPS AND SEMINARS

HEAVY ELEMENTS

S.N. Dmitriev, H.W. Gäggeler et al.
Gas phase chemistry with elements 112 and 114
3-rd International Conference on Chemistry and Physics of Transactinides TAN, Davos, Switzerland,
23-27 September 2007.

R. Dressler for the SHIP* and 112 Chemistry collaborations*
Confirmation of super heavy element production in ^{48}Ca induced fusion reactions a handshake of physics and chemistry for element 112
Frontiers In NUclear STructure, Astrophysics and Reactions, FINUSTAR-2, Agios Nikolaos, Crete, September 10-14, 2007.

*SHIP Collaboration
S. Hofmann, D. Ackermann, S. Antalic, H.G. Burkhard, V.F. Comas, R. Dressler, Z. Gan, S. Heinz, J.A. Heredia, F.P. Heßberger, J. Khuyagbaatar, B. Kindler, I. Kojouharov, P. Kuusiniemi, M. Leino, B. Lommel, R. Mann, G. Münzenberg, K. Nishio, A.G. Popeko, S. Saro, H.J. Schött, B. Streicher, B. Sulignano, J. Uusitalo, M. Venhart, A.V. Yeremin

*112 Chemistry Collaboration
R. Eichler, N.V. Aksenov, A.V. Belozerov, G.A. Bozhikov, V.I. Chepigin, S.N. Dmitriev, R. Dressler, H.W. Gäggeler, V.A. Gorshkov, F. Haenssler, M.G. Itkis, A. Laube, V.Ya. Lebedev, O.N. Malyshev, Yu.Ts. Oganessian, O.V. Petrushkin, D. Piguet, A.G. Popeko, P. Rasmussen, S.V. Shishkin, A.V. Shutov, A.I. Svirikhin, E.E. Tereshatov, G.K. Vostokin, M. Wegrzecki, A.V. Yeremin

R. Eichler
Gas phase chemistry with Transactinides
3-rd International Conference on Chemistry and Physics of Transactinides TAN, Davos, Switzerland,
23-27 September 2007.

R. Eichler
Isothermal VAcuum Chromatography (IVAC) @ TASCA
6-th Workshop on physical recoil separators dedicated for chemical experiments Davos, Switzerland,
23-27 September 2007

R. Eichler
Chemistry enters the island
Seminar, Frankfurt Institute of Advanced Studies, Frankfurt Main, Germany, 28 February 2007.

R. Eichler
Gas phase chemical investigations of Transactinides
Seminar in Anorganischer, Analytischer und Physikalischer Chemie, Departement für Chemie und Biochemie,
Universität Bern, Switzerland, 14 June 2007.

R. Eichler
Gas Phase Chemistry with the elements Hassium and element 112
TEM Kolloquium, Paul Scherrer Institute, Switzerland, 14 December 2007.

H.W. Gäggeler
Recent achievements in the search for superheavy elements
SPS Jahrestagung, Zürich-Irchel,Switzerland, 21-22 February 2007.

H.W. Gäggeler
Chemistry with single atoms of heaviest elements
Journée Mendelejev, Université de Fribourg, Switzerland, 7 March 2007.

H.W. Gäggeler
Gas Phase Chemistry of Heaviest Elements
ACS Spring Meeting, Glenn T. Seaborg Award Session, Chicago,USA, 25-29 March 2007.

H.W. Gäggeler
Chemical studies of transactinides
Int. Symp. on Heavy Ion Physics, FLNR, Dubna, Russia, 24-26 May 2007.

H.W. Gäggeler
Stability and formation of heaviest elements
Texas A&M University, College Station, TX, USA, 5 November 2007.

H.W. Gäggeler
Chemical properties of heaviest elements
Texas A&M University, College Station, TX, USA, 6 November 2007.

H.W. Gäggeler
Recent achievements in the chemical studies of elements Bh, Hs, Z=112 and Z=114
Texas A&M University, College Station, TX, USA, 7 November 2007.

H.W. Gäggeler
Gibt es noch unentdeckte chemische Elemente,
BioChemie am Samstag, Dept. für Chemie und Biochemie, Universität Bern, Switzerland, 24 November 2007.

H.W. Gäggeler
Chemical studies of heaviest elements at the single atom level
Faculty of Physics, University of Vienna, Austria, 10 December 2007.

A. Serov
Chemistry of Element 113: Development of Experimental Techniques
1-st Year PhD Symposium, Bern University, Bern, Switzerland, 17-18 September 2007.

A. Serov
Chemistry of super heavy elements: Development of isothermal vacuum Chromatography (IVAC) Method.
EMPA PhD Symposium 2007, p. 51, EMPA Duebendorf, Germany, 21. November 2007.

A. Serov
Isothermal Vacuum Adsorption Chromatography (IVAC) for Determination of chemical properties of Superheavy Elements (Poster)
3-rd International Conference on Chemistry and Physics of Transactinides TAN, Davos, Switzerland, 23-27 September 2007.

SURFACE CHEMISTRY

M. Ammann
Heterogeneous chemistry of nitrogen oxides at low concentrations
Seminar Labor für Verbrennungsforschung, Paul Scherrer Institute, Switzerland, 1 June 2007.

D.E. Starr, M. Ammann, H. Bluhm
The adsorption and uptake of acetone on ice studied
With ambient pressure photoemission spectroscopy
American Geophysical Union Annual Meeting, San Francisco, USA, 15 December 2007.

O. Vesna, S. Sjogren, E. Weingartner, M. Kalberer, K. Stemmler, H. W. Gäggeler, M. Ammann
The reaction of unsaturated fatty acids aerosol with ozone: product formation and hygroscopic properties of the processed aerosol
European Geophysical Society General Assembly 2007, Vienna, Austria, 17 April 2007.

M. Kerbrat, T. Huthwelker, H.W. Gäggeler, B. Pinzer, M. Schneebeli, M. Ammann
Co-adsorption of nitrous acid and acetic acid on ice
European Geophysical Society General Assembly 2007, Vienna, Austria, 15-20 April 2007.

M. Kerbrat, T. Huthwelker, H.W. Gäggeler, B. Pinzer, M. Schneebeli, M. Ammann
Ice-atmosphere interactions
EMPA PhD Symposium, Dübendorf, Switzerland, 21 November 2007.

M. Kerbrat, T. Huthwelker, H.W. Gäggeler, B. Pinzer, M. Schneebeli, M. Ammann
Evidence of the smoothness of snow crystals under alpine conditions
Seminar at Laboratory for Radio- and Environmental, PSI, Switzerland, 12 January 2007.

M. Kerbrat, T. Huthwelker, H.W. Gäggeler, B. Pinzer, M. Schneebeli, M. Ammann
Experiments and Modelling on ice-air interactions
Seminar at Laboratory for Radio- and Environmental, PSI, Switzerland, 7 December 2007

A. Rouvière and P. Baussand
*Etude des émissions gazeuses de la combustion du bois de chauffage dans les habitations :
recherche de traceurs spécifiques.*
4ème édition des Journées Interdisciplinaires de la Qualité de l'Air (JIQA), Villeneuve d'Ascq.
Université des Sciences et Technologies de Lille, 25 January 2007.

A. Rouvière and P. Baussand
Etude cinétique du créosol, traceur de combustion, en chambre de simulation atmosphérique
Groupe Français de Cinétique et Photochimie, Marseille, France, 4-5 June 2007.

M. Kerbrat, T. Huthwelker, T. Bartels-Rausch, H.W. Gäggeler, B. Pinzer, M. Schneebeli, M. Ammann
Recent Results from Laboratory Studies: Interaction of nitrogen oxides with ice surfaces
SCOUT-O3 Annual Meeting, Heraklion, Greece, 7-11 May 2007.

T. Bartels-Rausch, J. Kleffmann, Y. Elshorbany, C. George, M. Brigante, and Markus Ammann
Sonne, Erde, Schnee und HONO
Seminar at Laboratory for Radio- and Environmental, Univ. Bern, Switzerland, 27 April 2007.

A. Schlierf, T. Bartels-Rausch, M. Ammann, M. Brigante2, A. Jammoul, B. D'Anna, and C. George
Investigation of photosensitized polymerization in organic aerosols
EUCAARI Meeting Helsinki, Finland, 19-23 November 2007.

V. Zelenay, T. Huthwelker, G. Tzvetkov, A. Krepelova, M. Birrer, J. Raabe, M. Ammann
Microspectroscopy of Mixed Phase Aerosols
EMPA PhD Symposium, Dübendorf, Switzerland, 21 November 2007.

V. Zelenay, A. Krepelova, M. Birrer, G. Tzvetkov, J. Raabe, T. Huthwelker, M. Ammann
First results obtained from measurements with the new environmental cell at the POLLUX X-ray microscope
NEADS Meeting, EAWAG Dübendorf, Switzerland, 11 December 2007.

K. Stemmler, A. Vlasenko, M. Birrer, M. Ammann
Influence of surfactant monolayers on the uptake of nitric acid to deliquesced NaCl aerosol
ACCENT Mass accommodation workshop, Galway, Ireland, 11-13 April 2007.

O. Vesna, S. Sjoegren, E. Weingartner, M. Kalberer and M. Ammann
Ozonolysis of condensed phase alkenes: hygroscopic changes and H_2O_2 formation
EUCAARI Meeting Helsinki, Finland, 19–23 November 2007.

T. Huthwelker, G. Tvetkov, J. Raabe, S. Sjögren, E. Weingartner, M. Heuberger-Vernooij, M. Birrer, M. Ammann
*Micro spectroscopy on high vapor pressure condensed matter under controlled gas and temperature environment:
planned experiments and technical developments at POLLUX*
Faraday Discussions 137 'The Spectroscopy and Dynamics of Microparticles', Bristol, United Kingdom, 2–4 July 2007.

M.M. Miedaner, T. Huthwelker, F. Enzmann, M. Kersten, M. Ammann, M. Stampanoni
On the kinetics of trapping air bubbles and salt precipitates during freezing of diluted salt solution droplets
European Geophysical Society General Assembly 2007, Vienna, Austria, 15-20 April 2007.

B. Pinzer, M. Kerbrat, T. Huthwelker, M. Ammann, M. Schneebeli
Is the surface of ice smooth in snow?
European Geophysical Society General Assembly 2007, Vienna, Austria, 15-20 April 2007.

M.A. Hutterli, T. Huthwelker, M. Ammann, M. Miedaner, M. Enzmann, M. Schneebeli, A.E. Jones, E.W. Wolff
Growing individual artificial frost flowers and first results from 3-D X-ray micro computer tomography
European Geophysical Society General Assembly 2007, Vienna, Austria, 15-20 April 2007.

T. Huthwelker, G. Tzvetkov, S. Sjoegren, J. Raabe, M. Ammann
Micro-morphology of artificial mixed organic aerosols studied using X-Ray microscopy
European Geophysical Society General Assembly 2007, Vienna, Austria, 15-20 April 2007.

T. Huthwelker, M. M. Miedaner, M. Hutterli, F. Enzmann, M. Stampanoni, M. Ammann, M. Kersten
Process studies on the impurity trapping in natural and artificial ice assessed by X-ray microtomography
SLS user meeting, PSI, Switzerland, 11 September 2007.

ANALYTICAL CHEMISTRY

G. Casassa, M. Schwikowski, P. Ginot
Ice core records from mid latitudes in South America, a needed link between the Tropics and Antarctica
IUGG XXIV General Assembly, Perugia. Italy, 2-13 July 2007.

A. Ciric, L. Tobler, E. Vogel, M. Schwikowski, H. W. Gäggeler
An ice core record of Mercedario (32°S) in the Central Argentinean Andes
European Research Course on Atmospheres, Grenoble and Forcalquier (Oberservatoire Haute Provence), France, 8 January-10 February 2007.

A. Ciric, L. Tobler, E. Vogel, A. Schwerzmann, G. Casassa, H.W. Gäggeler, M. Schwikowski
An ice core record of Mercedario (32°S) in the Central Argentinean Andes
8th Swiss Global Change Day, Bern, Switzerland, 4 April 2007.

A. Ciric
An ice core record from Mercedario (32°S), Central Argentinean Andes
Seminar Radio- und Umweltchemie, Paul Scherrer Institut, Switzerland, 7 December 2007.

A. Eichler, S. Oliver, K. Henderson, A. Laube, J. Beer, H.W. Gäggeler, T. Papina, M. Schwikowski
Sun-induced climate change during the last millenium recorded in a Siberian ice core
8th Swiss Global Change Day, Bern, Switzerland, 4 April 2007.

A. Eichler
Climate and environmental information from a Central Asian ice core for the last millennium
Seminar Radio- und Umweltchemie, Paul Scherrer Institut, Switzerland, 22 June 2007.

H.W. Gäggeler
Neuere Entwicklungen auf dem Gebiet der Radiocarbonanalytik und einige Anwendungen in der Umweltforschung
Universitätsspital INSEL, Bern, Switzerland, 9 March 2007.

H.W. Gäggeler
Radiocarbon determination with micro amounts of carbon, some applications in environmental research
Department of Oceanography, Texas A&M, Galveston, TX, USA, 9 November 2007.

T. Kellerhals
Trace Element Records from an Andean Ice Core
Seminar Radio- und Umweltchemie, Universität Bern, Switzerland, 2 February 2007.

Ch. Mayer, A. Lambrecht, M. Schwikowski, C. Smiraglia
Accumulation conditions in a high elevated glacier basin in the eastern Karakoram
IUGG XXIV General Assembly, Perugia, Italy, 2-13 July 2007.

M. Schläppi, M. Schwikowski, T. Jenk, B. Rufibach, A. Rivera, M. Rodriguez, G. Casassa
A new ice core from the Southern Patagonian Icefield, first results
8th Swiss Global Change Day, Bern, Switzerland, 4 April 2007.

M. Schläppi
A new ice core from the Southern Patagonian Ice fields – first results
First year graduate symposium, University of Bern, Switzerland, 17-18 September 2007.

M. Schläppi
A new ice core from the Southern Patagonian Ice fields – first results
Seminar Radio- und Umweltchemie, University of Bern, Switzerland, 2 November 2007.

M. Schwikowski
Glaciers as archives of atmospheric pollution and climate
Millennium Subgroup 3 meeting, Cala Millor, Mallorca, Spain, 3-4 February 2007.

M. Schwikowski, M. Sigl, E. Isaksson, D. Divine
European glaciers as archives of atmospheric pollution and climate
Millennium 1st Milestone meeting, Cala Millor, Mallorca, Spain, 5-8 February 2007.

M. Schwikowski
Firn/ice core studies by Paul Scherrer Institut in the Andes
Workshop „Glaciology in the South with a View from the North, sailing on board of the "A.P. Aquiles"
fom Punta Arenas to Puerto Williams, CECS Valdivia, Chile, 14-17 January 2007.

M. Schwikowski
Klimageschichte aus alpinen Eisbohrkernen
Fachtagung „Die Alpen ohne Eis?", Bern, Switzerland, 23 February 2007.

M. Schwikowski
Climate change from Andean ice cores: examples from the North of Chile and Argentina
Seminar on Climate Change and Glaciers: Impacts in Water Resources, Sea Level Rise and Mountain Environments, Rome, Italy, 6-7 July 2007.

M. Schwikowski
Ice coring projects in Chile
Workshop "Chile-Canada collaborative research initiative in glaciology, Valdivia, Chile, 3 September 2007

M. Schwikowski
Palaeo climate reconstructions using ice cores from high-mountain glaciers
Foro Bicentenario "Desafíos de los cambios climáticos para Chile, Antártica y sus Glaciares", Valdivia, Chile, 4 September 2007.

M. Schwikowski
High-alpine glaciers as climate archives
Seminar Ion Beam Physics ETH Zurich, Zurich, Switzerland, 12 December 2007.

M. Sigl, M. Schwikowski, E. Isaksson, T. Martma
100-year palaeo records from European ice cores
Millennium European Climate 1st Milestone Meeting, Cala Millor Mallorca, Spain, 5-8 February 2007.

M. Sigl
Past climate from a high-alpine glacier: new findings from Colle Gnifetti, Switzerland
Seminar Laboratory for Radiochemistry and Environmental Chemistry, Paul Scherrer Institut, Villigen, Switzerland, 23 June 2007.

M. Sigl, D. Bolius, M. Schwikowski, H.W. Gäggeler, T.M. Jenk
Long-term trends of air pollution recorded in an ice-core from Colle Gnifetti, Swiss Alps,
NCCR 6th International NCCR Climate Summer School, Grindelwald, Switzerland, 26-31 August 2007.

M. Sigl
Climate signals stored in Alpine ice
Seminar – WSL Dendro Sciences, Birmensdorf, Switzerland, 19 December 2007.

F. Thevenon, F. S. Anselmetti, S. Bernasconi, M. Sigl, M. Schwikowski
Black carbon aerosol determination from a European high-alpine glacier (Colle Gnifetti, Swizerland)
EGU General Assembly, Vienna, Austria, 15–20 April 2007.

F. Thevenon, F. S. Anselmetti, S. Bernasconi, D. Williamson, M. Sigl, M. Schwikowski
Pyrogenic carbon quantification from lacustrine, oceanic, and glacier records
EGU General Assembly, Vienna, Austria, 15–20 April 2007.

F. Thevenon, F. S. Anselmetti, D. Williamson, S. Bernasconi, M. Schwikowski
Biomass burning and fossil fuel combustion proxies from Lake Lucerne sediments and Glacier Colle Gnifetti ice-core (Switzerland)
4th Int. Limnology Congress (ILIC2007), Barcelona, Spain, 11-14 July 2007.

F. Thevenon, M. Schwikowski, M. Sigl, T. Jenk, S. Szidat, S. Bernasconi, F. S. Anselmetti
Atmospheric aerosols from an Alpine ice core (Glacier Colle Gnifetti), and new developments in image analysis applied in paleoenvironmental studies
5th Swiss Geoscience Meeting, Geneva, Switzerland, 16 November 2007.

L. Tobler
Trace element records in an ice core from the Belukha glacier (Siberian Altai)
Seminar Radio- und Umweltchemie, Paul Scherrer Institut, Switzerland, 23 March 2007.

E. Ziessler
Regional climate and $\delta^{18}O$ signals in glacier ice of the subtropical Andes in „normal"- and ENSO-periods
Seminar Laboratory for Radiochemistry and Environmental Chemistry, Paul Scherrer Institut, Villigen, Switzerland, 23 March, 2007.

RADWASTE ANALYTICS

R. Dressler, D. Schumann, S. Shishkin
Experiments with the descendants of $^{288}115$ revisited from the spectroscopic point of view
TAN07, Davos, Switzerland, 23-27 September 2007.

J. Neuhausen, F. v. Rohr, N. Aksenov
Progress of the investigations on spallation product chemistry in liquid lead-bismuth
EUROTRANS-DM4: WP4.1, WP4.2 and WP4.3 Technical Review Meeting – Forschungszenrum Karlsruhe, Germany, 5-9 March 2007.

J. Neuhausen
Behavior of nuclear reaction products in liquid lead-bismuth
ESS-Scandinavia Workshop, Lund, Sweden, 13 March 2007.

J. Neuhausen, F. v. Rohr, S. Horn, S. Lüthi, D. Schumann
Polonium behavior in eutectic lead bismuth alloy
Fifth International Workshop on the Utilisation and Reliability of High Power Proton Accelerators, HPPA5, SCK·CEN, Mol, Belgium, 6-9 May 2007.

J. Neuhausen, R. Dressler, F. v. Rohr, S. Horn, B. Eichler, S. Lüthi,
D. Schumann, T. Stora, M. Eller
Nuclear reaction product behavior in liquid metal targets
3rd High Power Targetry Workshop, Bad Zurzach, Switzerland, 10-14 September 2007.

D. Schumann
ERAWAST (Exotic radionuclides from Accelerator Waste for Science and Technology)
Seminar at IPN Orsay, France, 22 January 2007.

D. Schumann, J. Neuhausen
Radiochemical separation techniques for the analytics of accelerator waste
NUCAR 07, Vadodara, India, 12-16 February 2007.

D. Schumann
Accelerator waste - a new challenge for the radiochemist
Seminar at SINP, Kolkata, India, 2 March 2007.

D. Schumann, J. Neuhausen
Accelerator waste as a source for exotic radionuclides
Nuclear Physics in Astrophysics III (XXI International Nuclear Physics Divisional Conference of the European Physical Society), Dresden, Germany, 26-30 March 2007.

D. Schumann:
ERAWAST (Exotic radionuclides from Accelerator Waste for Science and Technology)
2nd CARINA workshop, Spa, Belgium, 25-28 April 2007.

D. Schumann, J. Neuhausen
ERAWAST - A new production route for exotic long-lived radionuclides
5th international workshop on "Utilisation and Reliability of High Power Proton Accelerators", Mol, Belgium, 7-9 May 2007.

D. Schumann
Production of radioactive samples at PSI
Workshop on experimental opportunities for nuclear astrophysics at the Frankfurt neutron source of the Stern-Gerlach-Zentrum - The FRANZ Neutron Source, Karlsruhe/Frankfurt, Germany, 21-23 May 2007.

D. Schumann
ERAWAST - a new production route for long-lived radionuclides
TUM, Beschleunigerlabor, München, Germany, 20 June 2007.

D. Schumann
ERAWAST - a new production route for long-lived radionuclides
Institut für Radiochemie, FZ Rossendorf, Dresden, Germany, 13 July 2007.

D. Schumann, J. Neuhausen, M. Wohlmuther
Accelerator waste - a new challenge for radioanalytics
ICEM 07, Brügge, Belgium, 3-7 September 2007.

D. Schumann
Production and separation of long-lived radionuclides for nuclear physics experiments
FINUSTAR II, Aghios Nikoaos, Greece, 10-14 September 2007.

D. Schumann, J. Neuhausen, M. Wohlmuther
Radiochemical characterisation of accelerator waste
ENC2007, Brüssel, Belgium, 17-20 September 2007.

D. Schumann
Accelerator waste as a source for exotic radionuclides
Institut für Kernchemie, Universität Mainz, Germany, 29 October 2007.

M. Wohlmuther, D. Schumann, P. Kubik, H.-A. Synal, V. Alfimov, G. Korschinek, G. Rugel, T. Feastermann
Validation of activation calculations with MCPNX with samples from a copper beam dump
AccApp 07, Pocatello, USA, 30 July - 3 August 2007.

PROTON IRRADIATION FACILITY

E. Bellm
RHESSI spectral fits of swift GRBs
'Gamma Ray Bursts 2007', Santa Fe, New Mexico, 5-9 November 2007.

W. Hajdas
Miniature low energy electron detector for particle environments studies in space
Workshop on Precision Measurements at Low Energy, Paul Scherrer Institut, Villigen, Switzerland, 18/19 January 2007.

W. Hajdas
News from the European Component Irradiation Facilities, PIF, HIF, RADEF & ECF.
8th ESA/ESTEC D/TEC-QCA Final Presentation Day 2007, Université catholique de Louvain, 'Auditoires Sainte-Barbe' hosted by Centre de Recherches du Cyclotron, Louvain-la-Neuve, Belgium, 23/24 January 2007.

W. Hajdas
POLAR Hardware development status
POLAR Beijing Meeting, Institute of High Energy Physics, China, 16-23 September 2007.

W. Hajdas
POLAR Monte Carlo modeling
POLAR Beijing Meeting, Institute of High Energy Physics, China, 6-23 September 2007.

W. Hajdas
Atmospheric scattering background in RHESSI measurements of solar flare polarization
5th SOLAR POLARIZATION WORKSHOP, A workshop in honor of Jan Olof Stenflo, Ascona, Switzerland, 17-21 September 2007.

W.Hajdas
PIF Activities from ground tests to space weather monitoring and biggest cosmic explosions
Seminar at Laboratory for Radio- and Environmental, PSI, Switzerland, 4 October 2007.

W. Hajdas
POLAR project status
CHIPP Plenary Meeting, PSI Villigen, Switzerland, 15/16 October 2007.

W. Hajdas
Standard radiation environment activities at PSI
Ionising Radiation Detection and Data Exploitation Workshop
ESA/ESTEC, Noordwijk, The Netherlands, 17-18 October 2007.

W. Hajdas
Development of the low energy electron detctor
Ionising Radiation Detection and Data Exploitation Workshop
ESA/ESTEC, Noordwijk, The Netherlands, 17-18 October 2007.

W.Hajdas
Demo model and readout electronics of POLAR – New Gamma Ray Burst Polarimeter
The 2007 IEEE Nuclear Science Symposium (NSS) and Medical Imaging Conference (MIC), Honolulu, Hawaii, 27 October -3 November 2007.

W. Hajdas
Irradiation facilities at PSI
6th LHC Radiation Workshop, CERN, Switzerland, 29-30 November 2007.

K. Hurley
Short bursts and giant magnetar flares
'Gamma Ray Bursts 2007', Santa Fe, New Mexico, 5-9 November 2007.

K. Hurley
Short bursts and giant magnetar flares
American Astronomical Society, AAS Meeting 211, Austin, Texas, USA, 04 December 2007.

G. Lamanna
POLAR – an instrument to measure GRB polarization
30th International Cosmic Ray Conference
Merida, Yucatan, Mexico, 3–11 July 2007.

M. McConnell
Rhessi solar flare polarization measurements in the 20-100 keV energy range
American Astronomical Society Meeting 210, Honolulu, Hawai, USA, 01 May 2007.

S. Scheithauer
Irradiation tests of magneto-electrical components for the James Webb Space Telescope.
9th European Conference Radiation and Its Effects on Components and Systems Organized by the Commissariat à l'Energie Atomique, Deauville, France, 10-14 September 2007.

E. Suarez-Garcia
Probing Magnetic fields during black hole creation with the new X-ray polarimeter
Workshop on Precision Measurements at Low Energy, Paul Scherrer Institut, Villigen, Switzerland, 18/19 January 2007.

E. Suarez-Garcia
X-ray polarimetry of solar flares with RHESSI
5th SOLAR POLARIZATION WORKSHOP, A workshop in honor of Jan Olof Stenflo, Ascona, Switzerland
17-21 September 2007.

E. Suarez-Garcia
POLAR: A novel instrument to measure Gamma Ray Bursts polarization
PSI Radiochemistry Seminar, Switzerland, 4 October 2007.

E.Suarez-Garcia
POLAR: A novel instrument to measure Gamma Ray Bursts polarization
DPNC Seminar, University of Geneva, Switzerland, 5 October 2007.

E. Suarez-Garcia
GEANT4 Response calculations and light collection studies for Gamma-Ray Burst Polarimeter - POLAR
The 2007 IEEE Nuclear Science Symposium (NSS) and Medical Imaging Conference (MIC), Honolulu, Hawaii, 27 October–3 November 2007.

C. Wigger
Prompt spectrum of GRB 021206 supports the cannonball model
'Gamma Ray Bursts 2007', Santa Fe, New Mexico, 5-9 November 2007.

RADIOCHEMISTRY UNIVERSITÄT BERN

A.C. Aiken, D. Salcedo, J.A. Huffman, I. Ulbrich, P.F. DeCarlo, M. Cubison, K. Docherty, D. Sueper, D.R. Worsnop, A. Trimborn, M. Northway, A. Prevot, S. Szidat, M.N. Wehrli, C. Wiedinmyer, J. Wang, J. Zheng, E. Fortner, R. Zhang, J.S. Gaffney, N.A. Marley, G.E. Sosa Iglesias, J.L. Jimenez
Aerosol analysis with the high resolution time-of-flight aerosol mass spectrometer at the urban superSite (T0) in Mexico City during MILAGRO
AGU Fall Meeting, San Francisco, USA, 10-14 December 2007.

S. Fahrni, S. Szidat, M. Ruff, L. Wacker, H.W. Gäggeler
Low concentrations of radiocarbon for pharmacokinetic studies
Annual Meeting of the Swiss Society of Pharmacology and Toxicology, Bern, Switzerland, 27-28 September 2007.

M. Furger, N. Bukowiecki, J. Sandradewi, M.R. Alfarra, P. Lienemann, S. Szidat, A.S.H. Prevot, U. Baltensperger
Elemental composition of winter PM10 aerosol at rural and urban sites determined with synchrotron x-ray fluorescence spectrometry
EGU, 4th General Assembly, Vienna, Austria, 10-15 April 2007.

J. Mohn, S. Szidat, L. Emmenegger
Determination of fossil fuel in waste incinerators on the gaseous emission of radioactive CO_2
8th International Conference on Emissions Monitoring, Zürich, Switzerland, 5-6 September 2007.

N. Perron, M.N. Wehrli, S. Szidat, J. Sandradewi, A.S.H. Prévôt, U. Baltensperger
Source apportionment of PM10 carbonaceous aerosols in winter 2005/2006 in Swiss rural and urban sites using radiocarbon analyses of the OC and EC fractions
EGU, 4th General Assembly, Vienna, Austria, 10-15 April 2007.

N. Perron, S. Szidat, J. Sandradewi, A.S.H. Prévôt, U. Baltensperger
Source apportionment study of PM1 and PM10 carbonaceous aerosols in Roveredo and Moleno using ^{14}C analysis
Seminar Laboratory of Atmospheric Chemistry, PSI, Switzerland, 18 June, 2007.

N. Perron, S. Szidat, A.S.H. Prévôt, U. Baltensperger
Source apportionment of carbonaceous aerosols using ^{14}C analyses of the organic and elemental carbon fractions
First year graduate symposium, University of Berne, Switzerland, 17 September 2007.

N. Perron, S. Szidat, A. S. H. Prévôt, U. Baltensperger
Winter 2006 campaign in the Valais: results of the last ^{14}C analyses
Seminar Laboratory of Atmospheric Chemistry, PSI, Switzerland, 12 November 2007.

N. Perron, S. Szidat, A. S. H. Prévôt, U. Baltensperger
^{14}C analyses for source apportionment of carbonaceous aerosol
EUCAARI annual meeting, Helsinki, Finland, 20-23 November 2007.

M. Ruff, H.W. Gäggeler, M. Suter, H.-A. Synal, S. Szidat, L. Wacker
Halbautomatische Messungen mit einer Gasionenquelle
Frühjahrstagung der Deutschen Physikalischen Gesellschaft – Fachverband Massenspektrometie, Düsseldorf, Germany, 19-23 March 2007

M. Ruff
Radiocarbon AMS of CO_2 - further steps towards a fully automated system
Seminar Radio- und Umweltchemie, Bern, Switzerland, 02 November 2007.

J. Sandradewi, M.R. Alfarra, A.S.H. Prévôt, E. Weingartner, M. Gysel, R. Schmidhauser, S. Szidat, U. Baltensperger
Wood burning aerosol during winter in an Alpine valley: Aethalometer and the aerosol mass spectrometer measurements
European Aerosol Conference, Salzburg, Austria, 10-14 September 2007.

S. Szidat, M. Ruff, L. Wacker, N. Perron, J. Sandradewi, M.R. Alfarra, A.S.H. Prévôt, M. Hallquist, A.S. Shannigrahi, U. Baltensperger
Source apportionment of carbonaceous aerosols with radiocarbon
EGU, 4th General Assembly, Vienna, Austria, 10-15 April 2007.

S. Szidat, M.N. Wehrli, M. Ruff, L. Wacker, J. Noda, T. Gustafsson, J. Pettersson, R.M. Volkamer, J.-L. Jimenez, A.S.H. Prévôt, U. Baltensperger
Emission sources of carbonaceous aerosols in Mexico City deduced from radiocarbon analysis
EGU, 4th General Assembly, Vienna, Austria, 10-15 April 2007.

S. Szidat
On the track of environmental carbonaceous aerosols
Seminar at Department of Chemistry and Biochemistry, Universität Bern, Switzerland, 26 April 2007.

S. Szidat, M. Ruff, S. Fahrni, L. Wacker, H.-A. Synal
Ein Kopplungssystem für die automatisierte ^{14}C-Messung mit Beschleunigermassenspektrometrie
GDCh Wissenschaftsforum Chemie 2007, Ulm, Germany, 16-19 September 2007.

S. Szidat, M.N. Wehrli, M. Ruff, N. Perron, J. Sandradewi, M.R. Alfarra, A.S.H. Prevôt, U. Baltensperger, L. Wacker, M. Hallquist
Holzverbrennung: Eine wichtige Quelle von kohlenstoffhaltigem Feinstaub im Winter
GDCh Wissenschaftsforum Chemie 2007, Ulm, Germany, 16-19 September 2007.

S. Szidat
Neueste Resultate der ^{14}C-Analysen in der Schweiz
Wintersmog-Workshop, ETH Zürich, Switzerland, 16 October 2007.

S. Szidat
Potenzial der AMS für die Anwendung kleiner Dosen von ^{14}C in der biomedizinischen Forschung
Seminar Isotope Chemistry & Metabolite Synthesis, Sanofi-Aventis Deutschland GmbH, Frankfurt/Main, Germany, 30 November 2007.

S. Szidat
^{14}C micro-analysis: Applications and challenges of chemical speciation
Seminar Radio- und Umweltchemie, PSI, Switzerland, 7 December 2007.

M. Viana, X. Querol, T.A.J. Kuhlbusch, A. Miranda, M. Vallius, A. Kasper-Giebl, S. Szidat, W. Winiwarter, R.M. Harrison
Overview of source apportionment methods in selected European COST633 action member countries
European Aerosol Conference, Salzburg, Austria, 10-14 September 2007.

PUBLIC RELATIONS

Heavy Elements
Printed media:

- Horizonte, Schweizerischer Nationalfonds
  Bodenprobe von der Insel der Stabilität
  September 2007.

- Naturwissenschaftliche Rundschau
  Chemische Eigenschaften des Elements 112
  60(9), 2007.

- Neue Züricher Zeitung
  Hassium-270 – superschwer und doch langlebig
  3 January 2007.

- *NEWS & VIEWS*, Nature 447
  "Panning for Ununbium" by A. Türler
  47-48 (2007).

- Nature 447
  Abstractions „First Author (R. Eichler)"
  3 May 2007.

- The Economist
  It's a gas
  3 May 2007.

- SCIENTIFIC AMERICAN
  Superheavy Element "Ununbium" Has Ordinary Chemistry
  3 May 2007.

- Chemical & Engineering News
  Probing Element 112's Chemistry,
  7 May 2007.

- Chemistry World, News
  Chemists arrive at the island of stability
  2 May 2007.

- Softpedia, SoftNews NET SRL
  Superheavy Element "Ununbium" Actually Has Ordinary Chemistry - Element 112 and its chemical reactivity
  4 May 2007.

- Spektrum Direkt 3
  Superschwere Eigenschaften
  http://www.wissenschaft-online.de/artikel/872810
  May 2007.

- WebElements
  Element 112 ununbium similar to mercury
  http://www.webelements.com/nexus/node/1195
  3 May 2007.

Analytical Chemistry

Broacast:

- Radio DRS 2
  Domino: Margit Schwikowski, Gletscherforscherin
  18 August 2007.

Demonstration and presentation:
- 1. Nationales Klimaforum der Schweiz in Thun
  Demonstration Eisbohrung
  6 September 2007.

- Besuchstag Schülerinnen/Schüler Kanti Wettingen
  Vortrag M. Schwikowski: Gletscher als Klimaarchive, Laborbesuch und Demonstration:
  S. Biner, A. Ciric, A. Eichler, A.-L. Grauel, M. Schläppi, M. Schwikowski, M. Sigl, T. Kellerhals
  31 October 2007.

- Nationaler Tochtertag am PSI
  Vortrag M. Schwikowski: Chemie im Schnee von gestern: Gletscher als Umweltarchive
  A. Ciric: Einblick in den Berufsalltag einer Chemikerin
  8 November 2007.

Radwaste

Printed media:

- Alexander Murphy, University of Edinburgh
  Exotic Radionuclides for Science and Technology
  Nuclear Physics News, Vol. 17, No 3, 2007, p. 31-33.

LECTURES AND COURSES

Prof. Dr. H.W. Gäggeler
Universität Bern, SS2007:
Bachelor
- Instrumentalanalytik II (with others) (3 ECTS)
- Allgemeine Chemie (Einführung Radioaktivität) (with others) (4 ECTS)

Master
- Kolloquium Radio- und Umweltchemie in collaboration with the Paul Scherrer Institut (organized by Dr. R. Eichler)

Universität Bern, HS2007:
Bachelor
- Physikalische Chemie IV (with Prof. H. Siegenthaler) (3 ECTS)
- Praktikum Phys. Chemie II (with others) (4 ECTS)
- Biochemische Methoden I (with others) (3 ECTS)
- Biochemische Methoden (Übungen) (with others)

Master
- Nuclear and Radiochemistry (3 ECTS)
- Lab course Nuclear and Radiochemistry (with others) (4 ECTS)
- Lab course Paul Scherrer Institut (with others) (4 ECTS)
- Environmental Radionuclides and Nuclear Dating (with Dr. S. Szidat) (1.5 ECTS)
- Kolloquium Radio- und Umweltchemie in collaboration with the Paul Scherrer Institut (organized by Dr. D. Schumann)

Prof. Dr. U. Krähenbühl
Universität Bern, SS2007:
- Analytische Ergänzungen für Pharmazeuten
- Analytisches Praktikum für Pharmazeuten
- Praktikum Physikalische Chemie II

Universität Bern, HS 2007:
- Allgemeine Chemie für Veterinär Mediziner
- Umweltchemie
- Praktikum Physikalische Chemie II
- Radiochemiepraktikum Master Kurs

PD Dr. M. Schwikowski
Universität Bern, SS2007:
- Instrumentalanalytik II (with others) (3ECTS)

Universität Bern, HS2007:
- Atmospheric and Aerosol Chemistry (3ECTS)

Dr. R. Eichler
Universität Bern, HS2007:
- Kolloquium Radio- und Umweltchemie in collaboration with Paul Scherrer Institut
- Praktikum Phys. Chemie II (with Prof. H.W. Gäggeler)
- Lab course Nuclear and Radiochemistry (with Prof. H.W. Gäggeler)
- Lab course Paul Scherrer Institut (with Prof. H.W. Gäggeler)

Dr. S. Szidat
Universität Bern, HS2007:
- Environmental Radionuclides and Nuclear Dating (with Prof. H.W. Gäggeler)
- Lab course Nuclear and Radiochemistry (with Prof. H.W. Gäggeler and Dr. R. Eichler)

MEMBERS OF SCIENTIFIC COMMITTEES
EXTERNAL ACTIVITIES

Dr. Markus Ammann:
- PSI internal research commission (FoKo), member
- Atmospheric Chemistry and Physics, editor
- IUPAC Subcommitte for Gas Kinetic Data Evaluation, member
- AICI (Air - ice chemical interactions, a task of IGAC and SOLAS), steering committee member

Dr. Robert Eichler:
- PSI internal research commission (FoKo), member

Prof. Dr. Heinz W. Gäggeler:
- Nuklearforum Schweiz, Member of the Executive Board and Member of the Science Board
- Schweizerische Kommission für die hochalpine Forschungsstation Jungfraujoch der SANW (Mitglied)
- Astronomische Kommission der Stiftung Jungfraujoch und Gornergrat (Member)
- Joint IUPAC/IUPAP Working Party (JWP) on the discovery of new elements (Member)
- International Union of Pure and Applied Chemistry (IUPAC) (Fellow)
- Steering Committee of EURISOL (Member)
- TAN'07 Conference, 23 – 28 Sept. 2007, Davos (Chairman)
- Division of Nuclear and Radiochemistry, European Association for Chemical and Molecular Sciences (EuCheMS) (Chairman)

Dr. Wojtek Hajdas:
- Official Reviewer for the 9th European Conference Radiation and Its Effects
  on Components and Systems Organized RADECS by the Commissariat à l'Energie Atomique,
  September 10-14, 2007 - Deauville, France
- Swiss Representative of the Space Environments and Effects Network of Technical Centers SEENoC

Prof. Dr. Urs Krähenbühl:
- Member of the Meteoritical Society.
- Meteoritics & Planetary Science; associate editor.
- Eidgenössische Kommission für Strahlenschutz und Überwachung der Radioaktivität.

PD Dr. Margit Schwikowski:
- Expert of the Matura Examination of Kantonsschule Baden.
- Member of the Coordinating Committee of the Pages/IGBP initiative LOTRED SA
  (Long-Term climate Reconstruction and Diagnosis of (southern) South America).
- Schweizerische Gesellschaft für Schnee, Eis und Permafrost (SEP), board member.
- Member of the University of Maine Graduate Faculty

Leonhard Tobler:
- Experte Neutronenaktivierungsanalyse, Workshop Schweizer Jugend forscht, Zürich, 24 November 2007.

BACHELOR THESIS

Cédéric Clivaz

*Bestimmung des terrestischen Alters von Meteoriten
über die Messung der Oberflächenurankonzentration mittels ICP-MS*

Prof. Dr. U. Krähenbühl / Uni Bern
May 2007

Stefan Schmoker

Untersuchung zweier Megacryometeoren von Habsburg (AG) und Alberswil (LU)

PD Dr. M. Schwikowski / PSI
Prof. Dr. H. W. Gäggeler / PSI & Uni Bern
June 2007

Barbara Leder

Ultratrace determination of palladium in environmental samples by CRI-ICP-MS

Prof. Dr. U. Krähenbühl / Uni Bern
June 2007

MASTER / DIPLOMA THESIS

Meena Zala

Möglichkeiten und Grenzen der CRI Technik in der Massenspektrometrie
(*CRI Collision Reaction Interface)*

Prof. Dr. U. Krähenbühl / Uni Bern
March 2007

Elisabeth Dietze

Das Regionalklima und die Isotopensignale von Eisbohrkernen der subtropischen Anden in Normal- und ENSO-Zeiten

Prof. Dr. A. Kleber/TU Dresden / PD Dr. M. Schwikowski/PSI
May 2007

Sarah Biner

Investigation of mercury (Hg) behaviour in seasonal snow cover at the Jungfraujoch

PD Dr. M. Schwikowski / PSI
Prof. Dr. H. W. Gäggeler / PSI & Uni Bern
December 2007

HONORY DEGREE

On 26 May 2007 **Heinz W. Gäggeler** received a honory doctoral degree
from the Joint Institute of Nuclear Research (JINR) in Dubna in
recognition of his seminal contribution to the chemistry of heavy elements.

SUMMER STUDENTS

Graell Josep
Development of a coated wall flow tube experiment to investigate the interaction of HNO$_4$ with ice surfaces
University of Barcelona
August – October 2007

Grauel Anna-Lena
Aufbereitung und IC-Messungen eines Eisbohrkernteilstücks vom Pio XI, Patagonien
Universität Zürich
August – November 2007

Heinitz Stephan
Verhalten von Polonium in eutektischer Blei-Wismut-Legierung
Universität Leipzig
September – December 2007

Herda Irena
POLAR DEMO model: DAQ, Quick Look and Diagnostic mode
Jagiellonian University, Cracow
July – September 2007

Jaworski Marciej
Minimum Detectable Polarization Distribution for POLAR based on BATSE GRB Catalog
Jagiellonian University, Cracow
August – September 2007

Kälin Sarah
Chemical analysis of a segment from an ice core stemming from Glaciar La Ollada in the Argentinian Andes
Tufts University, USA
May - August 2007

Marin Marmol Maria Mercedes
Experimental study of Po evaporation from liquid eutectic lead-bismuth alloy in vacuum
University of Murcia, Spain
May – August 2007

Wittwer David
Thallium Abtrennung von Blei, Legierungsbildung zwischen einem Lanthanoid und einem Edelmetall
Universität Bern
July – September 2007

Dujmovic Hrvoje
3-wöchiges Berufspraktikum zur Analyse von Gletschereis mit ICP-MS
Kantonsschule Wettingen
October 2007

VISITING GUESTS AT PSI 2007

08-10 January:
E. Hiltbrunner, Institute of Botany, University of Basel, Switzerland
Ion chromatographic analysis of water samples

12 January:
A. Semchenkov, GSI, Darmstadt, Germany
TASCA - the new gas-filled separator at the GSI: present status and future plans

02 February:
M. Wohlmuther, PSI, Switzerland
Characterisation of radioactive waste at PSI

02 February:
F. Preusser, University Bern, Switzerland
Luminescence dating: Basics, methods and application

13 February:
J. Gabrieli, University of Venice Ca' Foscari, Italy
Ice core analysis with CIM-ICP-MS

09-10 March:
G. Casassa, Centro de Estudios Científicos, Valdivia, Chile
Flow modelling of La Ollada glacier, Mercedario

02-24 April:
C. George, University Lyon, France M. Brigante CNRS/Uni Lyon, Lyon, France
Collaboration experiment: Photosensitized reaction of nitrogen oxide on humic acid containing ice

02-26 April:
Y. Elshorbany, University of Wuppertal, Germany
Collaboration experiment: Photosensitized reaction of nitrogen oxide on humic acid containing ice

02 April–02 Mai:
J. Kleffmann, Y. Elshorbani, University of Wuppertal, Germany;
C. George, M. Brigante, CNRS and University Lyon, France
Collaboration experiment: Photosensitized reaction of nitrogen oxide on humic acid containing ice

12-13 April:
M. Chiari, S. Nava, G. Calzolai, National Institute of Nuclear Physics, Florence, Italy
Sample pretreatment and measurement for ^{14}C analysis of carbonaceous aerosols

27 April:
N.V. Homazava, EMPA, Dübendorf, Switzerland
Element-specific investigation of localized corrosion processes in Al alloys by ICP-MS

27 April:
F. Thevenon, ETHZ Zürich, Switzerland
A new approach for determining biomass burning and fossil fuel combustion products from sediment and ice core records

30 April, 29-30 August:
E. Dietze, Institut für Geographie, Technische Universität Dresden, Germany
Response of regional climate and glacier ice proxies to El Niño-Southern Oscillation (ENSO) in the subtropical Andes

15 June-06 July:
P. Santibañez, Centro de Estudios Científicos, Valdivia, Chile
Preparation of ice samples from Pio XI glacier for analysis of algal biovolume

22 June:
F. Vimeux, LSCE, France
Past climate variability in tropical South America from the isotopic composition of Andean ice cores

15 August:
T. Papina, Institute for Water and Environmental Problems SB RAS, Barnaul, Russia
Preparation of Swiss-Russian Seminar on reconstruction of past climate variability in Siberia from natural archives

19-22 September:
K. E. Gregorich, Lawrence Berkeley National Laboratory, Berkeley, USA
Collaboration talks regarding: Charge State measurements of Heavy Ions traveling in Gases

22 September:
Yu.Ts. Oganessian, Flerov Laboratory for Nuclear Reactions, Dubna, Russia
Visit of large facilities at PSI

01-02 October:
P. Schwerdtfeger, Massey University, Auckland, New Zealand.
Left or Right in Nature? That is the Question.

07-22 October:
N.A. Aksenov, G. A. Bozhikov, V. Ya. Lebedev , E. Tereshatov
Joint Institute for Nuclear Research, Dubna, Russia
Participation at beam time experiments at the PSI Philips Cyclotron:

08-10 October, 18 December:
D. Fischer, Institute of Geography, University of Bern, Switzerland
Analysis of biogenic Si in lake sediment cores

02 November:
J. Mohn, EMPA, Dübendorf, Switzerland
Discrimination of fossil and biogenic CO_2 from waste incineration based on radiocarbon measurements and mass balances

5 November:
B. Pinzer, M. Schneebeli, WSL/SLF Davos, Switzerland
Project meeting 'Microchemistry of snow under non-equilibrium conditions'

12 November:
D.J. Donaldson, University of Toronto, Canada
New spectroscopic tools for investigating surface premelting on ice

25 November-8 December:
O. V. Petrushkin, S. V. Shishkin
Joint Institute for Nuclear Research, Dubna, Russia
Participation at beam time experiments at the PSI Philips Cyclotron:

06-15 December:
M. Hutterli, British Antarctic Survey, United Kingdom
Beamtime at SLS: X-ray tomography of frost flowers and frozen sea water

19 December:
B. Pinzer, WSL/SLF Davos, Switzerland
Beamtime at PROTRAC: Migration of HONO through snow under temperature gradient conditions

PAUL SCHERRER INSTITUT

LABOR FÜR RADIO- UND UMWELTCHEMIE
DES PAUL SCHERRER INSTITUTS UND DER UNIVERSITÄT BERN
31. 12. 2007

u^b

UNIVERSITÄT
BERN

PSI   **Prof. Dr. Heinz W. Gäggeler**   **Uni Bern**

Angela Blattmann (Secretary / 80 %)   Catrina Veraguth (Secretary / 40 %)

PD Dr. Margit Schwikowski (Deputy)

SURFACE CHEMISTRY
Dr. Markus Ammann (80 %)
Dr. Thorsten Bartels-Rausch
Dr. Aurélie Rouviere
Dr. Adèla Krepelovà
Mario Birrer (80 %)
Olga Vesna [1]
Michael Kerbrat [1]
Yulia Sosedova [1]
Andrea Schlierf [1]
Veronika Zelenay [1]

ANALYTICAL CHEMISTRY
PD Dr. Margit Schwikowski
Leonhard Tobler
Dr. Anja Eichler (50%)
Thomas Aemmer
Sabina Brütsch   Silvia Köchli
Michael Sigl [1]   *Thomas Kellerhals* [1]
Anita Ciric [1]   *Christian Stenger* [1]
Manuel Schläppi [1]
Sarah Biner [2]

RADIOCHEMISTRY
Dr. Sönke Szidat
Matthias Ruff [1]
Simon Fahrni [1]

GEOCHEMISTRY
Prof. Dr. Urs Krähenbühl
Edith Vogel
Gisela Weibel
Martin Rauber
Kaizhen Li [1]

HEAVY ELEMENTS
Dr. Robert Eichler
Dr. Rugard Dressler
Dave Piguet
Andreas Laube
Alexey Serov [1]
Beat Muther [2]

RADWASTE ANALYTICS
Dr. Dorothea Schumann
Dr. Jörg Neuhausen
Susanne Horn 50 %
Sabrina Lüthi 80 %

PROTON IRRADIATION FACILITY
Dr. Wojtek Hajdas
Ken Egli
Stephan Scherrer

[1] Graduate student
[2] Master student

AUTHOR INDEX

AFFILIATION INDEX

ATOMKI Debrecen	Institute of Nuclear Research of the Hungarian Academy of Sciences, Debrecen, Bem ter 18/C, H-4026, Hungary
BAS	British Antarctic Survey, High Cross, Madingley Road, Cambridge CB3 0ET, United Kingdom
CEA-Saclay	DSM/DAPNIA/SPhN, Bat.703, CEA-Saclay, 91191 Gif-sur-Yvette cedex, France
CERN (ISOLDE/CERN)	Organisation (Conseil) Européenne pour la Recherche Nucléaire, CH-1211 Genève 23
CECS	Centro de Estudios Cientificos, Valdivia, Chile
CG BAdW	Commission for Glaciology, Bavarian Academy of Sciences, Alfons-Goppel Str. 11, D-80539 Munich, Germany
EAWAG Dübendorf	Eidgen. Anstalt für Wasserversorgung, Abwasserreinigung und Gewässerschutz, Überlandstrasse 133, 8600 Dübendorf, Switzerland
ETHZ	Eidgen. Technische Hochschule Zentrum, CH-8092 Zürich, Switzerland
FLNR Dubna	Flerov Laboratory of Nuclear Reactions, Joliot Curie 6, 141980 Dubna, Russia
EMPA	Forschungsinstitution im ETH-Bereich, Überlandstrasse 129, Dübendorf, 8600 Dübendorf, Switzerland
FZ Jülich	Forschungszentrum Jülich GmbH, Leo-Brandt-Str., D-52428 Jülich, Germany
FZ Karlsruhe	Forschungszentrum Karlsruhe, Hermann-von-Helmholtz-Platz 1, D-76344 Eggenstein-Leopoldshafen, Germany
ILL, Grenoble	Institut Laue-Langevin, 6, Rue Jules Horowitz, BP 156 - 38042 Grenoble Cedex 9, France
ITE	Instytut Technologii Elektronowej, al. Lotnikow 32,46, 02-668 Warszawa, Poland
IWEP	Institute for Water and Environmental Problems, Siberian Branch of the Russian Academy of Sciences, 105 Papanintsev Str., RU-Barnaul 656099, Russia
JINR	Joint Institute for Nuclear Research, Joliot-Curie 6, 141980 Dubna, Moscow region, Russia
KUP	Climate and Environmental Physics, Physics Institute, University of Bern, Sidlerstrasse 5, 3012 Bern, Switzerland
LBNL	Lawrence Berkeley National Laboratory, Berkeley, CA 94720, USA
LGGE	Laboratoire de Glaciologie et Geophysique de l'Environnement, 38402 Saint Marin d'Hère, Cedex, France
NCCR Climate	NCCR Climate Management Centre, University of Bern, Erlachstrasse 9a, CH-3012 Bern, Switzerland
Niels Bohr Inst.	Centre for Ice and Climate, Niels Bohr Institute, Copenhagen University, Juliane Maries Vej 30, DK-2100 København Ø, Denmark
PSI	Paul Scherrer Institut, CH-5232 Villigen PSI, Switzerland
SLF	Institut für Schnee- und Lawinenforschung, Flüelastr. 11, CH-7260 Davos, Switzerland
Tokyo Institute of Technology	Department of Biological Sciences, Graduate School of Bioscience and Biotechnology, Tokyo Institute of Technology, 2-12-1-W3-43 Ookayama Meguro-ku, Tokyo 152-8551, Japan
TU Dresden,	Technische Universität Dresden Institut für Geographie, Helmholtzstr. 10, HÜL O 262, 01069 Dresden, Germany
TU / TUM	Technische Universität München, Physik Department E 15, James-Franck-Strasse, D-85748 Garching, Germany
UCI	University of California, Chemistry Departement, Irvine, CA 92697, USA

Univ. Bergen	Geofysisk Institutt, (124400) Allegt. 70, N-5007 BERGEN, Norway
Univ. Bern	Departement für Chemie und Biochemie, Universität Bern, Freiestr. 3, CH-3012 Bern, Switzerland
Univ. Erlangen	Friedrich-Alexander Universität Erlangen-Nürnberg, Physikalische Chemie II, Egerlandstrasse 3, D-91058 Erlangen, Germany
Univ. Lyon	IRCELYON - Institut de Recherches sur la Catalyse et l'Environnement de Lyon UMR5256 CNRS-Université LYON 1, Domaine Scientifique de la Doua, Batiment J. Raulin - 4eme Etage, 43 Bd du 11 Novembre 1918, F-69622 Villeurbanne Cedex, France
Univ. Mainz	Universität Johann Gutenberg, Institut für Kernchemie, 55128 Mainz, Germany
VAW ETHZ	Versuchsanstalt für Wasserbau Hydrologie und Glaziologie, ETH Zürich, 8092 Zürich, Switzerland
Universidad Austral de Chile	Instituto de Botanica, Facultad de Ciencias, Universidad Austral de Chile, Valdivia, Chile.
Univ. Venice	University of Venice, 30123 Venice, Italy
Univ. Wuppertal	Physikalische Chemie/FB C, Bergische Universität Wuppertal, 42097 Wuppertal, Germany
ZSR Hannover	Zentrum für Strahlenschutz und Radioökologie, Universität Hannover, Hannover, Germany

PAUL SCHERRER INSTITUT

PSI